Spring 2012

Application of First Principle Modeling in Combination with Empirical Design of Experiments and Real-Time Data Management for the Automated Control of Pharmaceutical Unit Operations

Brian Zacour

THE APPLICATION OF FIRST PRINCIPLE MODELING IN COMBINATION WITH EMPIRICAL DESIGN OF EXPERIMENTS AND REAL-TIME DATA MANAGEMENT FOR THE AUTOMATED CONTROL OF PHARMACEUTICAL UNIT OPERATIONS

A Dissertation

Submitted to the Graduate School of Pharmaceutical Sciences

Duquesne University

In partial fulfillment of the requirements for

the degree of Doctor of Philosophy

By

Brian M. Zacour

May 2012

THE APPLICATION OF FIRST PRINCIPLE MODELING IN COMBINATION WITH EMPIRICAL DESIGN OF EXPERIMENTS AND REAL-TIME DATA MANAGEMENT FOR THE AUTOMATED CONTROL OF PHARMACEUTICAL UNIT OPERATIONS

By

Brian M. Zacour

Approved March 22, 2012

Carl A. Anderson, Ph.D. Associate Professor of Pharmaceutics Graduate School of Pharmaceutical Sciences (Committee Chair)	James K. Drennen, III, Ph.D. Associate Professor of Pharmaceutics Associate Dean for Graduate Programs and Research Mylan School of Pharmacy (Committee Member)
Peter L.D. Wildfong, Ph.D. Assistant Professor of Pharmaceutics Graduate School of Pharmaceutical Sciences (Committee Member)	Ira S. Buckner, Ph.D. Assistant Professor of Pharmaceutics Graduate School of Pharmaceutical Sciences (Committee Member)
Tzuchi Ju, Ph.D. Associate Research Fellow Head, NCE-Formulation Sciences II Global Pharmaceutical Sciences Abbott Laboratories (Committee Member)	J. Douglas Bricker, Ph.D. Dean, Mylan School of Pharmacy and the Graduate School of Pharmaceutical Sciences

ABSTRACT

THE APPLICATION OF FIRST PRINCIPLE MODELING IN COMBINATION WITH EMPIRICAL DESIGN OF EXPERIMENTS AND REAL-TIME DATA MANAGEMENT FOR THE AUTOMATED CONTROL OF PHARMACEUTICAL UNIT OPERATIONS

By

Brian M. Zacour

May 2012

Dissertation supervised by Carl A. Anderson, Ph.D.

The U.S. Food and Drug Administration has accepted the guidelines put forth by the International Conference on Harmonization (ICH-Q8) that allow for operational flexibility within a validated design space. These Quality by Design initiatives have allowed drug manufacturers to incorporate more rigorous scientific controls into their production streams.

Fully automated control systems can incorporate information about a process back into the system to adjust process variables to consistently hit product quality targets (feedback control), or monitor variability in raw materials or intermediate products to adjust downstream manufacturing operations (feedforward control). These controls enable increased process understanding, continuous process and product improvement,

assurance of product quality, and the possibility of real-time release. Control systems require significant planning and an initial investment, but the improved product quality and manufacturing efficiency provide ample incentive for the expense.

The fluid bed granulation and drying unit operation was an excellent case study for control systems implementation because it is a complex unit operation with dynamic powder movement, high energy input, solid-liquid-gas interactions, and difficulty with scale-up development. Traditionally, fluid bed control systems have either used first principle calculations to control the internal process environment or purely empirical methods that incorporate online process measurements with process models. This dissertation was predicated on the development of a novel hybrid control system that combines the two traditional approaches.

The hybrid controls reduced the number of input factors for the creation of efficient experimental designs, reduced the variability between batches, enabled control of the drying process for a sensitive active pharmaceutical ingredient, rendered preconditioned air systems unnecessary, and facilitated the collection of data for the development of process models and the rigorous calculation of design spaces. Significant variably in the inlet airstream was able to be mitigated using feedforward controls, while process analytical technology provided immediate feedback about the process for strict control of process inputs. Tolerance surfaces provided the ideal tool for determining design spaces that assured the reduction of manufacturing risk among all future batches, and the information gained using small scale experimentation was leveraged to provide efficient scale-up, making these control systems feasible for consistent use.

DEDICATION

This dissertation is dedicated to my wife, Nicole, my parents, Sam and Pat, and my brother, Matt. All of my family members have always been there to support me and believe in me, and for that I am deeply indebted.

ACKNOWLEDGEMENTS

Graduate school is an undertaking that cannot be completed alone. Guidance, tutelage, support, coordination, and encouragement from many are necessary to come through successfully. I would like to take this opportunity to recognize the people who have helped make this journey a success.

I am extremely grateful to my academic advisor, Dr. Carl. A Anderson, for giving me the opportunity to attend graduate school and work in his laboratory. His guidance, training, challenges, opportunities, and support were instrumental in my development as a scientist. His work as my advisor and connections within the pharmaceutical industry have provided me with the experiences needed to be successful in my budding career. Dr. Anderson and his family accepted us all as friends to create an environment that challenged us, but was also welcoming. I always enjoyed coming to work.

I am also indebted to my committee member, Dr. James K. Drennen, III, who acted as a second advisor to me. His vast experiences, scientific background, and kindness helped make the graduate experience something that I will always look back on fondly. There were always opportunities in our laboratory to expand our scientific knowledge, gain industrial experience, and hone our skills as researchers, and for that I am grateful.

The remainder of my dissertation committee, Dr. Peter L.D. Wildfong, Dr. Ira S. Buckner, and Dr. Tzuchi (Rob) Ju, were critical in my graduate training and the progress of my research project. I am thankful for the time and effort that they expended on my

behalf. I would like to thank Dr. Wildfong for his efforts in getting me my first opportunity to begin my career within the pharmaceutical industry.

The laboratory environment at Duquesne University and our lab in particular offered a unique setting that was both scientifically challenging and very supportive. The friendships that I made during my graduate career will be cherished forever. I would like to specifically thank my graduate colleagues, Dr. Steven M. Short, Dr. Michael D. Moore, Dr. Zhenqi (Pete) Shi, Dr. Benoit Igne, Dr. Robert P. Cogdill, Dr. Hua (May) Ma, Ryanne Palermo, Robert W. Bondi, Jr., Sameer Talwar, and Jeffrey Katz for helping me through the graduate school process.

The National Institute for Pharmaceutical Technology and Education (NIPTE), the United States Food and Drug Administration (FDA), Abbott Laboratories, and Pfizer were critical contributors to the research in this dissertation. I would like to thank the research groups within NIPTE and Dr. Ju at Abbott Laboratories for their contributions to my research.

I would not be the person that I am today without the love and support of my parents, Samuel and Patricia, and my brother, Matthew. My parents provided an amazing upbringing that helped me be successful, and their support throughout graduate school and extreme generosity helped make everything so much easier. My brother has always been an unbelievable friend and was always there to make me happy.

Finally, I don't know how I could ever express my love and gratitude for my wife, Nicole. She provided love and support from the beginning, and her patience with me throughout this journey has been awesome. She always knew when I needed support or

when I needed a push. Nicole is truly my best friend and I could never have come close to getting through everything without her.

TABLE OF CONTENTS

Page

LIST OF TABLES

Page

LIST OF FIGURES

Page

LIST OF ABBREVIATIONS

ACLS	Augmented Classical Least-Squares
ACLS/PLS	Augmented Classical Least-Squares/Partial Least-Squares
AEDs	Antiepileptic Drugs
ANACOVA	Analysis of Covariance
ANN	Artificial Neural Networks
ANOVA	Analysis of Variance
API	Active Pharmaceutical Ingredient
BS	Batch Size
CCD	Charged-Coupled Device
cGMP	Current Good Manufacturing Practice
CLS	Classical Least-Squares
CLS/PLS	Classical Least-Squares/Partial Least-Squares
CMAs	Critical Material Attributes
CNS	Central Nervous System
CPPs	Critical Process Parameters
CQAs	Critical Quality Attributes
CSF	Cerebrospinal Fluid
DCPT	Duquesne Center for Pharmaceutical Technology
d_m10	Mass Fraction Under 10%
d_m50	Mass Fraction Under 50%
d_m90	Mass Fraction Under 90%
DOE	Design of Experiments

DRESS	Drug Reaction with Eosinophilia and Systemic Symptoms
DS	Direct Standardization
EEF	Environmental Equivalency Factor
EMT	End Moisture Target
EPTT	End Product Temperature Target
FBD	Fluid Bed Dryer
FBP	Fluid Bed Processor
FDA	The United States Food and Drug Administration
GABA	γ-Aminobutyric Acid
HPC	Hydroxypropyl Cellulose
HPLC	High Pressure Liquid Chromatography
HPMC	Hydroxypropyl Mellylcellulose
HVAC	Heating, Ventilation, and Air Conditioning
ICH	International Conference on Harmonisation
InGaAs	Indium Gallium Arsenide
IS	Intermediate Scale
LOD	Loss on Drying
LS	Lab Scale
LSSVM	Least-Squares Support Vector Machines
Mg St.	Magnesium Stearate
MCC	Microcrystalline Cellulose
NAS	Net Analyte Signal
NIPTE	The National Institute for Pharmaceutical Technology and Education

NIR	Near Infrared
NIRS	Near Infrared Spectroscopy
OPC	Open Process Control
PACLS	Prediction Augmented Classical Least-Squares
PAT	Process Analytical Technology
PCA	Principal Component Analysis
PDS	Piecewise Direct Standardization
PID	Proportional-Integral-Derivative Controller
PLC	Programmable Logic Controller
PLS	Partial Least-Squares
PS	Pilot Scale
PSI	Pounds per Square Inch
QbD	Quality by Design
R^2	Coefficient of Determination
RMSE	Root Mean Squared Error
RMSEC	Root Mean Squared Error of Calibration
RMSECV	Root Mean Squared Error of Cross Validation
RMSEP	Root Mean Squared Error of Prediction
RPM	Revolutions per Minute
RTO	Real-Time Optimization
RTR	Real-Time Release
SCADA	Supervisory Control and Data Acquisition

S.E.	Standard Error
SEC	Standard Error of Calibration
SEP	Standard Error of Prediction
SNV	Standard Normal Variate
S-T	Side Sensor to Top Sensor Transfer
SVM	Support Vector Machines
SVR	Support Vector Regression
T-S	Top Sensor to Side Sensor Transfer
US	United States
USP	United States Pharmacopeia

Chapter 1: Introduction

1.1 Statement of the Problem

Throughout its history, the pharmaceutical industry has relied upon traditional batch manufacturing processes for the production of solid dosage forms. In these processes, raw materials are processed through several separate unit operations to create the final product. Unit operations for pharmaceutical tablets include particle size enlargement (granulation), drying, particle size reduction (comminution), powder blending, compaction, and coating among several others. Most pharmaceutical production lines are still predicated on these same systems.

Typically, each unit operation is considered independently, with the product of each unit operation analyzed for quality by several measurements of material attributes that are believed to indicate future product performance. Specifications are defined that are believed to represent product quality. These specifications put limits on product measurements, but the link between the specification limits and product performance is not often explicitly defined. Inappropriately defined specifications have the potential to allow unsatisfactory materials to be distributed to the public which could have severe health consequences. Conversely, specifications that are too stringent put an unnecessary economical burden on the manufacturing company, which is then shifted to the public via increased medical costs. Therefore, it is crucial that the impact of process parameters are related to meaningful measures of product performance, which allows specifications to guarantee product quality.

Well developed controls of manufacturing unit operations are also necessary to increase process understanding and limit batch failures. Without measurements on the process or integrated control systems, batch failures require extensive investigations to determine the root cause of failure. While major advancements have been achieved in drug molecules, drug delivery systems, and drug targeting, very little innovation has occurred in manufacturing development to improve efficiency and quality.

Other industries are well ahead of the pharmaceutical industry in terms of manufacturing quality and efficiency. A study published in 2007 reported that the pharmaceutical industry operates at approximately 35,000 defect units per 1,000,000 produced,[1] while the semiconductor industry and a number of chemical companies achieve Six Sigma production (3.4 defects per 1,000,000 units). The United States Food and Drug Administration (FDA) openly acknowledge this shortcoming and have recently encouraged use of the guidelines put forth by the International Conference on Harmonisation (ICH-Q8(R2))[2] that allow for operational flexibility within a validated design space. This allows fully automated control systems that incorporate real-time data management to be feasible. These systems offer the opportunity for continuous improvement of the process and resulting drug product by allowing information gained during manufacturing through online process measurements to inform the process to ensure constant product quality (Feedback Control).[3] Conversely, incoming variability from raw materials, environmental factors, or intermediate products can be identified using process analytical technology (PAT) and the downstream manufacturing parameters can be adjusted accordingly to assure quality in the final product (Feedforward Control).

The FDA Quality by Design (QbD) initiatives are risk based, meaning a company that rigorously defines the unit operations or product properties that most significantly impact product quality and demonstrates sufficient scientific knowledge to control this critical variability will be granted greater regulatory flexibility. The unit operations that comprise batch manufacturing depend on a number of critical process, environmental, and material parameters whose effects and interactions must be understood to establish control. Well executed design of experiments, online process measurements, data management, and control software to create feedback and feedforward models that can predict and control the critical quality attributes (CQAs) of the final product are required to enable successful implementation of control systems. Rigorous statistical analyses are needed to identify the significant factors and interaction terms and to determine meaningful specifications or a design space that guarantees future product quality.

Control systems, especially those that can provide economic incentives for the pharmaceutical company over time, are universally desirable. Consumers are afforded low risk product at reduced costs, regulatory agencies can assess product safety and efficacy using scientific methods, and pharmaceutical companies are able to produce quality product efficiently, and may even achieve real-time release (RTR). Initial implementation can seem daunting and requires a substantial investment, but if developed correctly, automated control systems provide a significant return on investment.

Automated control systems must be developed to meet the specific needs of a given product or unit operation. Quantitative risk management is defined and optimized for each system, independently. For this reason, this dissertation will consider two unit operations, fluid bed processing and powder blending, and two different product

formulations to demonstrate the unique development required for each system. Fluid bed processing of pharmaceutical powders is typically more complicated than powder blending and has more factors that can potentially affect product quality, so the development of a control system for fluid bed processing requires more complicated models and communication systems to mitigate the increased risk. Conversely, additional expenses devoted to the powder blending unit operation beyond those needed to mitigate risk to the final product are wasted expenditures that a pharmaceutical company can avoid. The specific risks of the drug product must be considered simultaneously, as well. This dissertation aims to provide a blueprint for identification and management of critical factors in developing design spaces and automation systems for pharmaceutical unit operations.

First principle calculations are a tool that can be used to increase development efficiency while still providing the necessary control of the major mechanisms by which unit operations effect product quality. They reduce the dimensions of DOE, account for external fluctuations by adjusting process parameters in real time, and enable direct scale-up of first principle variables. Fluid bed processing of pharmaceutical powders is affected by the properties of the air used to fluidize the solid powders, so first principle controls are particularly advantageous for this unit operation. Fluctuations in the inlet air properties can be measured and used to inform process parameter adjustments to maintain consistent product quality. This can eliminate large systems that precondition inlet airstreams, control laboratory environments, or narrow incoming variability. These advantages allow systems to be developed more efficiently while providing benefits to product quality.

Statistical design of experiments (DOE) is another tool that can be valuable in terms of maximizing the value of the development process. Experimentation relies on empirical models to quantify the relationship between important factors of the manufacturing operation and final product characteristics, but designs that are created to satisfy the needs of the system can provide valuable process understanding in an efficient manner. Interactions between independent variables can have a substantial impact on the response variables, and they must be identified through empirical modeling. This information can be used to create feedback control where specifications can be placed on the response factors and maintained by adjusting the input variables.

The process understanding gained by online process monitoring through spectroscopy and other methods is invaluable. Use of such systems lowers the risk of batch failures and thereby eliminates the need for expensive investigations. They allow the immediate identification and correction of deviations in product quality attributes. Online measurements also allow for RTR in well developed systems, which reduces the burden of end product testing and reduces the queue time for batches between unit operations. This can lead to efficient supply chains and better control of inventory, providing an economic incentive for pharmaceutical manufacturing companies. Further, these economic benefits can also be extended to consumers through reduced medical costs. The advantages offered by online PAT systems can be beneficial to both fluid bed processing and powder blending.

Automation systems require the incorporation of myriad models, all of which include error and uncertainty. Rigorous statistical analyses are needed to account for these uncertainties to define meaningful boundaries, so a design space can assure product

quality in future batches. These models must also be robust so that they may function for extended periods of time and be easily transferred to different systems or larger scales, and can be easily updated. Failure in scale-up, transfer, or update may cause the initial investment to be lost, which would make these systems infeasible. Therefore, the process understanding gained during initial development must be leveraged to provide maximum value in future use.

To date, drug manufacturing has not improved at the same rate as comparable industries, leaving a weakness that must be addressed to achieve satisfactory levels of pharmaceutical quality and efficiency. This dissertation demonstrates how automated control systems can be developed using efficient techniques to adjust process parameters in real time to ensure product quality while providing scientific justification of a design space to satisfy regulatory concerns.

1.2 Hypothesis and Objectives

This dissertation is based on the central hypothesis that the integration of first principle calculations with empirical modeling and real-time data management enables a control system to provide a high standard of product quality with economic efficiency that mitigates the risk identified for a specific formulation and manufacturing combination.

Given the central hypothesis, the objectives of this dissertation were to:

1. Develop a fully automated, hybrid control system for the fluid bed drying of a model drug formulation with stability considerations using efficient methods.
2. Develop a model for the prediction of downstream product properties from the reduced variables that are the process factors of the hybrid controls, for the creation of a design space that assures future product quality.
3. Utilize the hybrid control system to facilitate scale-up experimentation.
4. Extend the control system to include fluid bed wet granulation and drying and demonstrate the development of a design space that incorporates both formulation and process factors within a single design space model.
5. Develop an efficient and optimized blending control system using multiple NIR sensors, efficient calibration techniques, and blending homogeneity algorithms.

The results of the objectives provide a blueprint for the development of automated control systems that offer improved product quality with efficient experimental designs. This dissertation provides a clear demonstration to the pharmaceutical industry that a high degree of product quality is possible in an economically feasible system.

1.3 Literature Survey

1.3.1 Fluid Bed Granulation and Drying

1.3.1.1 General Fluid Bed Properties

Fluid bed processing of pharmaceutical powders is an excellent case study for the development of a fully automated control system because of its complexity and the multiple phases typically utilized during processing.[4,5] A single fluid bed unit operation can take raw powders through blending, wet granulation, drying, and cooling. A fully automated control system must be able to define the process at any point during the progression, define meaningful end points of each phase before moving into the next phase, and incorporate information from process measurements back into the process so that the manufacturing parameters can be adjusted to control the process trajectory. This requires a well developed communication system that can synchronize multiple process measurements and organize data for analytical and process models. The models typically require comprehensive experimental designs to be performed so that prediction results maximize user confidence. Development of these systems require a substantial initial investment, but the rewards in product quality and efficiency can lead to a significant return on the investments due to removing batch failures, reduced inventory and storage, and real-time release.

Fluid bed processing is also important because of the significant advantages that can be realized when processing solid powder systems. Fluidization is the operation by which solid particles are transformed into a fluid-like state through suspension in a gas or liquid.[6] For the manufacturing of solid dosage forms in the pharmaceutical industry,

fluidization is almost exclusively solid powders suspended in a flowing gas, which is usually air. This dissertation considers this as the operating definition for fluidization.

Fluidized beds with gases and solids have unusual properties that are useful for industrial applications. Fluidized beds appear as a boiling liquid-like material and exhibit liquid-like behavior. These properties include flow properties, nearly isothermal conditions due to rapid mixing, a resistance to rapid temperature changes due to efficient heat exchange which makes a large magnitude of heat transport possible.[6] Many of these advantages reduce the risk of hot spots or thermal gradients in high energy drying processes while reducing the time needed to dry large batches of moist powders. These properties allow processing at large scales.

At a certain minimum airflow velocity the frictional forces between the fluid and solid particles counterbalance the weight of the particles, the vertical component of the compressive force between adjacent particles disappears, and all particles are suspended by the fluid. This is considered incipiently fluidized or at minimum fluidization.[6] The minimum fluidization velocity for a system can be calculated if the material and equipment have been adequately characterized,[7] but it is typically much easier and more practical to determine empirically. With an increase in flow rate beyond minimum fluidization, large instabilities within the bed are observed creating bubbling and the channeling of gas. The volume of the bed does not expand much beyond its volume of minimum fluidization, but agitation becomes more violent and the movement of solids becomes more vigorous as the airflow rate is increased.

In gas/solid systems, gas bubbles coalesce and grow as they rise. Fine particles flow smoothly down the wall around the rising gas voids, while coarse particles are

pushed upward and rain down from the slug when the gas void finally disintegrates. The range and magnitude of optimum operating conditions depends on particle characteristics including size distribution, shape, and density,[8-10] as well as equipment properties including geometry, bed depth, and distributor plate arrangement.[6] Careful planning and design of the equipment and operating conditions for a given system of particulates is crucial for robust processing at multiple scales.

Different regimes of fluidizations are displayed in Figure 1.1, which is reproduced from Kunii and Levenspiel.[7] Low airflow velocities increase the risk of losing the fluidized bed during processing, while high airflow velocities increase the probability of exceeding the terminal velocity of fine particles, causing entrainment in the filter bags. The mixing or segregation tendencies of a given system are an equilibrium process that depends on processing conditions. Fluidization velocities near the minimum for a given particle size increase the probability of high density particles separating to the bottom of the bed. However, in high velocities the mixing resulting from bubbling and circulation dominate.[11] This mixing is more efficient in larger systems. The range of possible fluidization regimes highlights the importance of controlling the application using first principle controls from the beginning of use.

Industrial applications for physical operations in batch processes in the pharmaceutical industry, such as granulation and drying, are typically performed in the bubbling or turbulent bed regimes.[7,12] In the bubbling or turbulent regimes, temperature is nearly constant throughout the bed due to efficient heat exchange, and a wide size distribution of particles is possible for these applications. These advantages facilitate scale-up. Conversely, a high pressure drop across the distributor plate is necessary to

assure uniform gas flow and uniform fluidization of particles. This leads to large power consumption. This dissertation optimizes the fluidization within the bubbling bed regime.[7]

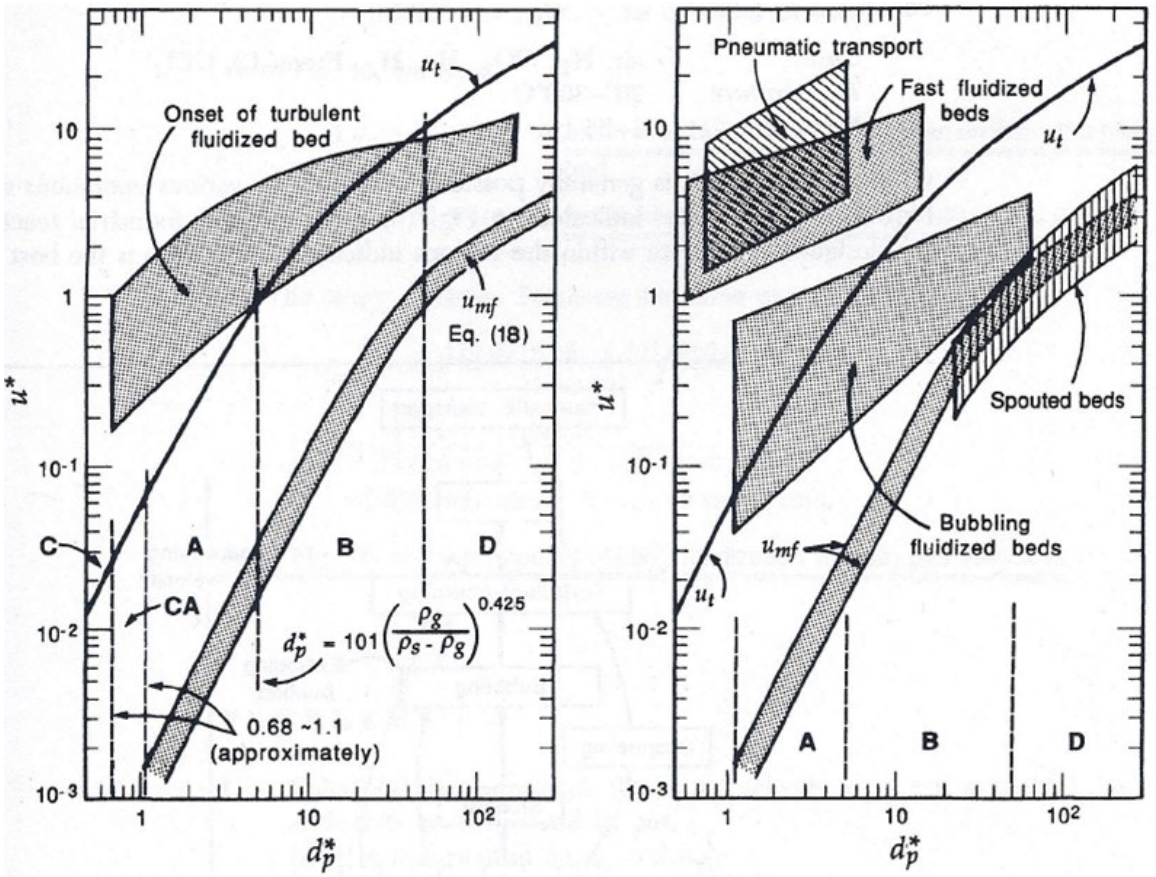

Figure 1.1. A general flow regime diagram reproduced from Kunii and Levenspiel[4] for the whole range of gas-solid contacting, from percolating packed beds to lean pneumatic transport of solids; letters C, A, B, and D refer to the Geldart classifications of solids. The abscissa (d_p^*) is a dimensionless measure of particle diameter, while the ordinate (u^*) is a dimensionless measure of particle velocity.

1.3.1.2 Fluidization of Solid Powders

The particle size distribution of the solid system is a strong factor in determining the fluidization velocities necessary for robust processing. Fine particles tend to clump and agglomerate in the presence of adsorbed moisture, requiring higher airflow velocities

and increased particle entrainment/elutriation. Large, uniform particles fluidize poorly with bumping, spouting, and slugging common. Addition of fines to large particle systems act as a lubricant, allowing for easier fluidization. Due to this lubrication, wide particle size distributions increase the range of possible fluidization velocities, increasing the robustness of the operation.[6] Extensive work is required to characterize and optimize a given system.

The bubbling bed occurs at fluidization velocities between the minimum fluidization velocity and ten times the minimum velocity. The actual magnitude depends on the powder properties and bed geometries, and strongly depends on the fraction of particles less than 45 μm.[7] When the minimum bubbling velocity is exceeded, the bed height decreases slightly and bubbles become visible. The rising bubbles cause the observed churning, mixing, and flow of solids, which provides the desired mixing and contacting properties. Professor D. Geldart characterized particles into four groups based on particle size and density that are very useful in determining fluidization behavior.[9,10] While most pharmaceutical or industrial applications contain particles from several or all groups, Geldart B or A particles are the most common encountered and their characteristics can be used to predict fluidization properties.

Geldart B particles are considered sand-like, with median particle sizes between 40-500 μm and densities between 1.4-4 g/mL. These particles fluidize well with vigorous bubbling action and bubbles that grow large. Bubbles form as soon as the gas velocity exceeds the minimum fluidization velocity. Bubbles grow and coalesce as they rise and their size is independent of the particle size and roughly linearly related to the distance from the distributor plate.

Geldart A particles are considered aerotable, and have small particle sizes and low densities. They fluidized smoothly at low velocities and display controlled bubbling at higher velocities. The bed expands considerably before bubbling occurs with the fines acting as a lubricant to the other particles. In Figure 1.1b, it can be seen that bubbling beds can be operated stably over a wide range of conditions for Geldart A or B particles.

For all particle groups, when the fluidization velocity exceeds ten times the minimum fluidization velocity, particles are projected into the freeboard above the bed, and the amount of particles lost is significantly increased. To minimize loss of powder, the working fluidization velocity should be maintained below the terminal velocity of the smallest size particles in a significant fraction of the bed.[7] The terminal velocity of particles is the velocity a particle falls through a fluid (free-fall velocity). It is inversely proportional to particle size and can be expressed by:

$$u_t^* = \left[\frac{18}{(d_p^*)^2} + \frac{2.335 - 1.744\phi_s}{(d_p^*)^{0.5}} \right]^{-1}, 0.5 < \phi_s < 1 \qquad (1.1)$$

where u_t^* is the terminal velocity, d_p^* is a dimensionless particle size,[7] ϕ_s is the sphericity of the particles, and sphericity must be between 0.5 and 1. This information can be used to reduce the experimental space explored during process development and can be used to guide scale-up efforts.

1.3.1.3 Mixing in a Fluidized Bed

The performance of the fluidized bed operation depends on the bubbling behavior. Control and improvement of performance can only be attained after the gas/solid contacting is understood. The bubbling bed behaves like a bubbling liquid of low

viscosity.[13] Bubbles of similar sizes have similar shapes, small bubbles rise slowly compared to large bubbles, a train of bubbles may coalesce to give larger bubbles, and the rise velocities can be described by the same expressions. Unlike the liquid-gas system, however, there is an interchange of gas between a rising bubble and the dense (emulsion) phase in a fluidized bed.

Bubbling behavior, the movement of gas and solids, and the pressure distribution of rising bubbles has been model by Davidson.[14] The pressure in the lower portion of a rising bubble is lower than in higher portions, so gas enters the bubble from the bottom and leaves from the top. Bubbles circulate three times the amount of gas processed by the equivalent section of emulsion phase gas, giving rise to dynamic mixing. The flow of gas through the emulsion phase far from any bubbles is essentially laminar.

Solids move out of the way as bubbles rise except for the small fraction (0.2-1.0%) caught inside bubbles. Solids, however, are caught in the wake of the rising bubble and are drawn upward behind the bubble. They slowly leak from this wake and fall back into the general bed, meaning there is a continuous interchange of solids between the wake and emulsion regions. This leads to an increase in turbulent mixing.

The wake of a rising bubble is also used to explain why trailing bubbles are drawn into the leading bubble and coalesce. The size of bubbles increases with gas velocity and with distance from the distributor plate, but varies widely between systems due to changes in geometry and particle properties. Smaller particles (Geldart A) tend to have smaller maximum bubble sizes than larger particle system at comparable velocities. There are many different methods to calculate an average bubble size for a given system

using particle property estimates, initial bubble sizes, and distance from the distributor plate.[15]

Early attempts at modeling the bubbling bed as a whole used the simple two phase model. This expression assumed that once bubbling began all gas in excess of the minimum fluidization velocity pass through the bed in bubbles.[15] Numerous examples have shown that empirical results are more complex than the two phase model indicates. The conceptual model developed by Kunii and Levenspiel[15] for the bubbling bed was aimed at estimating features or properties of the bed such as contacting regimes and volume fraction of phases using only a few measurements or correlations. Some of the general findings are presented below.

For typical Geldart B and A particle systems, the bubble gas is less than the difference between the fluidization velocity and the minimum fluidization velocity. The emulsion voidage increases with airflow velocity, and the emulsion phase is not stagnant. Distinct flow patterns, called gulf streaming, occur. Figure 1.2, reproduced from Kunii and Levenspiel,[15] displays typical flow patterns in the emulsion phase of a bubbling bed. The upflow emulsion regions should be rich in bubbles, and the downflow regions should have few, if any, rising bubbles. This dynamic movement, combined with the vigorous mixing from the rising bubbles, creates excellent circulation systems that increase the probability of uniform processing of powders. It should be noted, however, that there is an order of magnitude difference in mixing in the vertical and horizontal directions. Vertical mixing is significantly more efficient, but the duration of normal batch operations still allows for adequate horizontal distribution of materials. Horizontal

mixing is strongly affected by solids ejected into the free board (gas section above the bubbling bed) and mixing in the wake of rising bubbles.

The gulf stream behavior is increased in larger systems because the surface area of walls and equipment is decreased in relation to the bed volume. Walls and equipment provide frictional resistance to flow. As a result, mixing characteristics may change with changes in scale, with more efficient mixing present in larger systems. Internal structures may be added to larger fluidization systems to increase the frictional resistance, slow bubble rise velocities, and decrease bubble size to promote better gas solid contacting and more efficient drying in a pharmaceutical operation. Scaling factors have been proposed by Horio et al.[16] and Fitzgerald and Crane,[17,18] which have shown some success in simple systems, but the authors agree that much more work is needed in the area of fluid bed scale-up, scale-down, and hydrodynamic similarity for practical applications.[15]

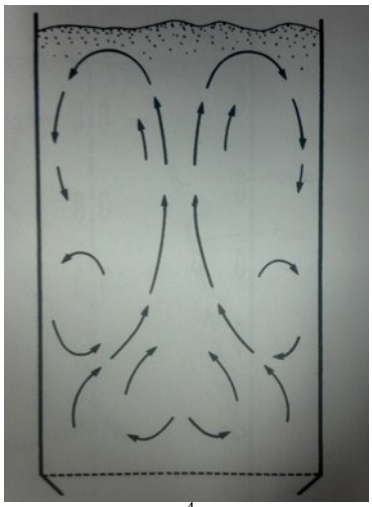

Figure 1.2. Reproduced from Kunii and Levenspiel.[4] The movement of solids within the emulsion phase of bubbling fluidized beds.

The choice of distributor plates at the bottom of the bed and placement of the spray nozzle can significantly impact fluidization behavior and granulation properties.[19]

Contacting between gas and solids is most efficient directly above the distributor plate, so this region significantly affects the efficiency of the overall process. Perforated plates with a uniform distribution of circular openings are the most common plates because they are the least expensive. The plate must provide a significant pressure drop to allow uniform gas flow into the powder bed and to prevent channeling or gas jets. A large pressure drop minimizes the effect that the distributor plate has on gas-solid contacting, which is then dependent on the hydrodynamic properties of the bed itself. This is desirable and increases the probability of uniform processing. While larger pressure drops benefit gas distribution, increased pumping power is required for increases in pressure drop. To maximize contacting uniformity, the fraction of open area in the distributor plate should be less than 10%.

Top spray systems that spray binder solution onto the top of the powder bed can also promote uniform flow and improved mixing. Any spray or fluid movement against the direction of bulk flow breaks up large bubbles and causes better distribution of bubbles within the fluidized bed. Breaking of large bubbles also reduces the fraction of solids that is ejected into the freeboard, thus reducing entrainment and elutriation. This dissertation only considers a top spray granulation system.

1.3.1.4 Fluidized Bed Granulation and Drying

The energy requirement to do work in the fluid bed is provided by the heated airstream. In pharmaceutical operations where the addition and removal of water to a fluidized bed is the primary mechanism of action (the situation investigated in this dissertation), the work can be accomplished via heat or mass transfer between the

fluidized solids and the airstream. Therefore, the contacting of the gas and solid is critical in determining the progress of the unit operation.

This dissertation considers the fluidized bed granulation and drying of pharmaceutical powders using water as the solvent. Therefore, the heat and mass transfer occurs between the solids and surrounding gas to provide the energy for the evaporation of water. The bulk of mass transfer occurs in the emulsion phase of the fluidized bed (outside of bubbles), while the bulk of the air that passes through the bed are in bubbles. As a result, water must travel from particles to the emulsion gas, emulsion gas to cloud gas surrounding bubbles, and finally to bubble gas before leaving the system.[20] This is especially true in fine particle systems where the fraction of gas passing through the bed in bubbles increases. This leads to the conclusion that mass transfer in a given system is governed by the type of particles being fluidized and the diffusion between emulsion gas and bubble gas. These properties remain relatively constant for a given formulation, except for changes due to inlet air humidity and airflow velocity. The major source of control in terms of energy input comes from the heat transfer mechanism.

The heat transfer mechanism has virtually the same contacting properties as described by the mass transfer mechanism, but the driving force (difference in temperature between airstream and particles) is generally much larger and is easily controlled. From the previous discussions it can be concluded that there is not efficient mixing of gas in fine particle systems fluidized in the bubbling bed regime. This leads to inefficient gas/solid contacting. There is efficient mixing of solid particles, however, and the expense of air is low, so fluidized beds still provide advantageous properties for pharmaceutical granulation and drying.

In the drying phase, fluidized beds have large capacities at relatively low cost, high thermal efficiency, and uniform temperature distribution.[12] This is combined with the cooling effect of evaporative drying to reduce the risk of temperature excursions experienced by solid particles.[21] The uniformity of temperature within a fluidized bed exists both in the radial and axial direction, even in large systems.[22] An equilibrium is reached very rapidly, so hot air that contacts cold solids reaches the temperature of the solids before moving more than 2-3 cm into the bed.[23]

Each particle goes through two drying regimes during a drying process: the constant rate and the falling rate drying periods. The constant rate drying regime removes the free moisture on the surface and in the pores of fluidized solids, and is limited by heat transfer. Therefore, the moisture carrying capacity of the airstream limits the drying rate, which varies proportionately with gas velocity and temperature, and inversely with bed height. In this period, the approach to equilibrium is rapid for both heat and mass transfer, so the bed and the leaving gas will remain close to the adiabatic saturation temperature (web-bulb temperature) of the entering gas stream.[23]

After the critical moisture content is reached, the drying rate begins to fall because of diffusional effects. The remainder of the water is bound within the solid particles and the diffusion of moisture to the surface is slow enough to control the overall drying rate. The moisture loss is close to exponential with time. The critical moisture content is reached when the moisture on the surface of solids is in equilibrium with the gas bathing the particle. The vapor pressure at the surface of the solid particles drops below the vapor pressure of the pure liquid at the drying conditions of the inlet gas

stream. The critical moisture content is small for small particle systems and slower overall drying rates.[23]

The high heat capacity of the fluidized bed and the rapid mixing of solids assure that the temperature of solids is mostly independent of location in the bed and at any instant the solids are all at the same stage of drying. This means there is very little interaction between particles in the bed with respect to drying. The overall heating of solids is determined by the heat capacity of the entering hot gas, not by the kinetics of the process, and the time needed to heat a bed of dried solids is proportional to the static bed height and inversely proportional to the gas velocity. The temperature of dried solids changes exponentially with time, and the effect of evaporative cooling during the drying phase keeps the temperature of solids low.[23]

These properties allow for strict temperature control and simple scale-up of the temperature control system. A possible source of error in the temperature control is the heat transfer between the bed and the walls of the equipment, which can be significantly higher than for the gas (air) itself.[22] Heat loss to the surrounding environment is more significant at smaller scales due to the increase in surface area per unit volume. The heat loss in a commercial system is typically a few percent. The error term can be measured simply by running a trial system at several temperatures and calculating the heat transfer coefficient.

In the spray granulation phase, there is a combination of three sets of rate processes: wetting and nucleation, consolidation and growth, and attrition and breakage.[5] Fluid bed granulation has properties that can be advantageous for all of these processes. The efficient and complete solid mixing that takes place in the fluid bed distributes water

or binder solution throughout the bed quickly, which leads to uniform wetting and nucleation. The airstream removes large droplets of water that build up unevenly on a few particles, and reduces the risk of forming large particles that must be milled later. The efficiency with which nucleation and further coalescence occurs is dependent on the wetting properties of the solid material, the water additional/removal rate, and the size of the water droplets in the spray solution.

The mechanisms by which coalescence, attrition, and elutriation occur create a process where small particles agglomerate with a higher probability than larger particles, thereby narrowing the final particle size distribution achieved.[4] The force of particle collisions is proportional to the mass of the particles, so collisions between smaller particles exhibit less force and increase the probability of coalescence in the presence of moisture on the surface of the particles. Smaller particles also heat up faster than larger particles, increasing the probability of evaporating binding solutions on small agglomerates to create solid bridges. Conversely, collisions between larger particles have a greater force, which increases the probability of breakage or attrition. Therefore, precise and narrow particle size distributions are possible in well controlled systems.

Despite the advantages of fluidized beds, their use for industrial applications has not been popular outside of simple drying processes. This is due to the complexity and sensitivity of some systems which leads to problems with control, difficulty in scale-up,[24, 25] and the lack of useful scientific models.[6] In addition, batch processes are not steady state experiments, so the optimum fluidization parameters must be constantly varied as the total mass and particle properties change. As a result, the use of fluidized beds have traditionally been approached as an art, and due to the significant difference in behavior

of large beds compared to small beds, extrapolation to a commercial scale has been unreliable. Development beginning with first principle theory is uncommon. This dissertation attempts to address these shortcomings for the pharmaceutical scientist.

Two separate approaches have been attempted in previous studies to model or control the fluid bed unit operation. The first approach uses first principle calculations based on thermodynamic, heat, and mass balance equations to define and control the environment inside the fluid bed chamber. The second approach is purely empirical and uses online process measurements, spectroscopy, design of experiments (DOE), and process modeling to control the unit operation. Each method has benefits and disadvantages, many of which are complementary, but they have never been used together to their full extent in a single system. This dissertation demonstrates the development and implementation of a hybrid control system that uses both first principle calculations and empirical data management to limit the drawbacks of each method to manufacture pharmaceutical granules within tight specifications.

1.3.2. First Principle Control Systems for Fluid Bed Processing

First principle calculations have been used to model drying, aqueous film coating, and fluid bed processes. However, they are not used frequently except for very simple approximations. Examples of the controls for this approach are the simple temperature difference method,[26-28] complex thermodynamic environment controls,[29-31] fluidization regimes,[4,7-10,15] computational fluid dynamics,[32-36] and transport phenomena.[37, 38] All of these methods use material properties, fluid dynamics, and simple measurements of mass, humidity, airflow, and heat at different points of the process to define the thermodynamic condition of the bulk gas-solid suspension or surrounding environment.

The approach taken in this dissertation utilizes the thermodynamic calculations developed by Ebey and referred to as the environmental equivalency factor (EFF).[29,31] These calculations were established in 1987 to define the aqueous film coating process. The same evaporative drying mechanisms control spray granulation and drying in aqueous fluid bed processing. The derivation of the EEF calculation for a specific fluid bed system and the feedback/feedforward mechanism of control will be addressed in significant detail in chapter 2.

First principle controls offer several advantages that are essential for robust and efficient processing. By definition the calculations are based on material and environmental properties, so the calculations are universal for all systems. Separate calibrations for new or adjusted formulations are unnecessary. Only the optimum set points must be defined independently for new systems. The equations are also independent of scale or specific equipment, meaning all controls based in first principles are directly scalable and transferable. Scaling up processes from lab scales to full manufacturing scales has traditionally been a major hurdle for pharmaceutical processes, in particular, for fluid bed systems.[24, 25] Therefore, eliminating any variables that need to be adjusted between scales is a major advantage.

First principle calculations establish control by quantifying the scientific mechanisms by which the process performs work. In the fluid bed example, the internal environment, which controls the evaporative drying mechanism and the rate of water addition or removal, can be defined to allow the final granule properties to be controlled more precisely. Property fluctuations or failure during development can be explained using scientific principles, leading to easier interpretation and greater process

understanding. Complex interactions between processing parameters can be accounted for by simply understanding their impact on simpler first principle mechanisms.

Mechanistic control offers improved performance in terms of inter-batch product variability. Traditional cookbook and even empirical control systems do not account for many sources of variability that have the possibility to impact final product properties. Even if all process parameters remain constant, small fluctuations in the external environment will affect the incoming airstream, thus altering the drying mechanism or drying rate without additional controls. If the mechanism of action in a given system is known and quantified, the impact that external variability has on the mechanisms can be defined, and process parameters can be adjusted to ensure constant product quality.

The only alternative for achieving the highest degree of product control is to implement systems that assure constant properties for all variables that may impact future product quality (raw materials, air, etc.). While this is impractical, it is common within the pharmaceutical industry to reduce environmental or raw material variability instead of adjusting the process to account for the variability. Preconditioning systems that maintain constant air temperature and humidity within current good manufacturing practice (cGMP) facilities are a standard practice.[39] These systems are expensive, especially for large, commercial facilities, and still do not remove all variability. Large gradients with respect to temperature and humidity are common within large manufacturing spaces, especially in the presence of a large work force. Additionally, purchasing raw materials with reduced variability can be expensive or even impossible. These are expenses that are unnecessary if the investment into a rigorous first principle control system is made.

The final and most substantial economic advantage offered by first principle controls is variable reduction. The amount of development and experimentation can be reduced exponentially by reducing the number of process variables investigated. This is again achieved by quantifying the actual mechanisms of action. As an example, the EEF calculation that will be used in this dissertation takes nine measurements – inlet air temperature, inlet air humidity, heated air temperature, product temperature, outlet air temperature, exhaust air temperature, exhaust air humidity, airflow velocity, and spray rate – and calculates a single reduced variable. Of the nine measurements, four – inlet air humidity, heated air temperature, airflow velocity, and spray rate - are factors that would typically be altered independently in a purely empirical DOE. By reducing the number of input factors to be explored in a DOE by three, the cost of development can be reduced from 128 (2^7) experiments to 16 (2^4) experiments (1/8 costs). While a full factorial design would not be practical for a system with 7 variables, it can be seen that the benefits of a full factorial design can be realized when the number of variables is reduced to 4 without compromising the degree of process understanding acquired.

There are several challenges to first principle controls, however. The calculations in this dissertation assume an adiabatic system, which is not rigorously correct. There is heat exchange from the equipment walls to the surrounding environment. Additionally, first principle controls do not typically account for the effects of atomizing air, changes in the droplet size of the spray, and changes in the kinetic energy of process air and water vapor. Typically, these are minor factors, but can have more serious effects in sensitive processes.

The error term associated with the adiabatic assumption can be measured by running trial systems, so the drying rate and heating effects on the solid can be controlled precisely. A general heat exchange profile can be determined by running an empty system at different airflow velocities and temperatures. More precise profiles can be determined by using trial batches of a given formulation because the heat exchange depends on the solid particles colliding against the inside wall of the equipment. This measured error term can then be added to the feedback control system to adjust the process parameters accordingly.

The droplet size of the spray rate has been shown to significantly affect the granulation regime,[5,25,40] which can impact the final particle size distribution and granule porosity. These are often critical quality attributes (CQAs) of the granulation process, so additional considerations may be necessary. The droplet size variable is often treated as a nuisance variable and held constant. This works well to reduce variability between batches of a given system, but is problematic for transfer and scale-up.[25] It is very difficult to match spray droplet sizes at different scales while keeping processing time constant. This can only be accomplished by using multiple spray nozzles at different locations.

While first principle calculations provide a quantitative and intuitive description of the processing mechanisms, they provide no feedback on actual product properties in real time. First principle control systems do not measure the moisture or chemical concentrations in the product, nor do they provide estimates of particle size. Therefore, the definitions of phase and batch end points are difficult to determine and are not intuitive. Additionally, the first principle calculations describe the batch as a bulk system

and provide no information on the spread of batch properties. There is also no access to additional information such as material phase changes or chemical decomposition. This information can be critical to optimizing a process, increasing process understanding, or identifying a batch trending toward failure.

The measurements typical of a first principle control system (temperature, humidity, etc.) often have slow response times when compared to online spectroscopic methods.[41] As a result, excursions from the process trajectory may be detected after a finite time lag. This can have devastating consequences for a sensitive process. The risk of batch failure may be substantially increased if information about the process lags even 30 seconds behind the process.

While the EEF calculations provide an excellent strategy for controlling the drying mechanism and rate, which is the single most impactful mechanism in a physical fluid bed operation with regards to the final product properties, additional calculations are needed to understand and control airflow dynamics and mixing mechanisms. When controlled, these properties limit the amount of solid entrainment/elutriation, narrow the final particle size distribution, reduce the risk of uneven processing or temperature excursions, and provide insight into potential problems in scale-up and transfer. Due to the complexity of these phenomena, they are addressed through simulation using the bubbling bed model,[4] or through computational fluid dynamics.[32-36] Both methods incorporate material and air properties into simplified expressions for complicated heat and mass transfer models, hydrodynamic expressions, and kinetic theory. The results of the simulation are then compared to empirical results, and the assumptions and input properties are adjusted accordingly. This information can provide knowledge about

potential problems with dead spots in certain fluid bed geometries or distributor plate designs, which is invaluable for initial process design, scale-up, and transfer applications.

Even in the most rigorous first principle control systems, some amount of empirical modeling is necessary to define the optimum set points for the first principle variables and to predict downstream product properties using critical material attributes (CMAs) and critical process parameters (CPPs). Expanding on these models and including process analytical technology (PAT)[41] into the control system can reduce the risk associated with the shortcomings of purely first principle systems. Statistical treatments of development data also quantify future uncertainty to reduce the risk of future batch failures. This dissertation aims to demonstrate the feasibility of a hybrid control system.

1.3.3 Empirical Control Systems for Fluid Bed Processing

The concept of complete empirical controls for fluid bed processors in the pharmaceutical industry are more recent than the first principle controls and became possible with the success of online spectroscopy, multivariate modeling, and complex communication and data management systems. These systems began with traditional DOE studies of fluid bed process factors,[40,42-45] expanded to include online measurements of product properties using spectroscopy,[46-49] imaging systems,[50,51] and other probes,[52,53] to finally creating fully automated supervisory control and data acquisition (SCADA) systems[54,55] with limited complexity.

Empirical control systems are based on experimentation, observation, and statistical modeling. Well designed experimental plans are needed to produce reliable data for modeling. These controls are completely defined through empirical data

analysis. This usually requires a stochastic experimental approach to limit the number of experiments and developmental costs. Screening designs[56] are used to identify significant variables from a large pool of variables using a small number of experiments. Selected variables from the screening design are then investigated in more comprehensive designs such as factorial designs,[57] response surface designs,[58] mixture designs,[59] Bayesian designs,[60, 61] or computer-aided designs[62] to more adequately probe the experimental space. The observed data is then related to the necessary response factors using regression analysis,[63] analysis of variance (ANOVA),[63] analysis of covariance (ANACOVA),[64] or nonlinear methods.[65] Augmentation of the second design or a third design may be required to increase model performance in a local region of the investigated space. Finally, response surface methodologies[66] and estimates of model uncertainty and future performance[67] are often needed to describe the complex behavior and interactions of the most significant variables with respect to product quality, and all models must be validated with independent batches.[2] The combination of these designs creates a large amount of experimentation, but it is absolutely necessary because empirical models are only as good as the variance space from which they are derived.

The advantages of empirical controls complement those of the first principle controls. Online sensors provide direct moisture,[46,47] particle size,[50,68] or other measurements of the product in real time for immediate CQA information and the simple and intuitive definition of phase end points. For single wavelength, diode array, or CCD detector based instruments, which are commonly selected for online applications, measurement and response times can be as short as milliseconds. Predictions can then be generated for the acquired spectra from a previously calculated calibration in a matter of

seconds. This allows the process to be ended or adjusted accordingly prior to significantly changing. The immediate feedback and control action provided by PAT is crucial for robust processing and for reducing the risk of negative batch excursions.

It is also simple to define a phase or batch end point using a meaningful property measurement of the product (e.g. moisture content). This simple and immediate feedback reduces end point variability and improves product precision. Fluid bed drying processes have an increased risk of overdrying when NIRS is not used to monitor moisture content in real time. This can lead to unnecessary heating of the granules, which may impact chemical or physical stability.[21]

The information contained in near infrared (NIR) or Raman spectra, common online techniques, also includes chemical[69] and physical phase information to give insight into the water-solid interactions for improved process understanding.[70-72] For example, an active pharmaceutical ingredient's (API) crystalline phase or percent purity can be monitored in real time. If an API is marketed as an anhydrous crystalline form, conversion to a more stable hydrate may be thermodynamically favorable, which could lead to severe deficiencies with regard to final product dissolution.[71,72,21] This increased process understanding can provide insight into batch failures. The information can also be used to create more robust processes using feedback control to limit the amount of phase conversion during processing.

Online spectroscopic methods typically have small sample volumes in a single measurement. Modern data management systems have very good computational power, so large amounts of data are able to be analyzed with ease. As a result, online methods are usually set to sample the system at high frequencies. This increases the overall

sample size interrogated per unit time, and provides valuable information about process trends, variability, and the breadth of material properties. First principle calculations consider the system as a single unit, so the data afforded by online methods can be used to calculate the precision of product CQAs, for better control of downstream performance.

Finally, every robust control system requires some form of empirical modeling for the optimization of CMAs and CPPs, identification of process interactions, the prediction of downstream performance attributes, and the calculation of a final design space. Even if all process set points can be described using first principle calculations, which is rare, DOE is necessary to efficiently optimize the values for maximum performance and identify interactions between parameters. Additionally, it is likely that empirical models are necessary to quantify the relationship between a unit operation's CPPs and downstream/clinical product performance attributes, which are the only quality metrics that are rigorously meaningful. Well constructed DOE and statistical treatments can provide this information, enabling the identification of a meaningful design space that allows for operational flexibility and corrective action, to assure final product performance. A manufacturing system that attempts to produce downstream CQAs within specifications by maintaining constant CPPs is not a control system unless it can be assured that there is no input variability that will impact performance, which is not practically feasible.

Disadvantages of empirical controls essentially all relate to cost concerns. All online methods require calibration building, and robust process models require large experimental designs. Spectroscopic calibrations are formulation, equipment, and scale

specific, so a new calibration must be created for each system or a rigorous transfer technique[73-75] must be applied. Multiple sensors are necessary in large systems because of sampling concerns and batch uniformity questions, so it can be expensive to calibrate each instrument independently. These costs can make development of purely empirical controls economically infeasible.

Process DOE are large, especially when considering external environment factors. Including any variable that could potentially affect the process creates unreasonably large designs. Designs to investigate a large number of parameters can be cost prohibitive. Adding to this problem, empirical process models are system dependent and not directly scalable. Therefore, the DOE must be repeated for new equipment, scale-up, or formulation adjustments. These factors make the variable reduction capabilities of first principle controls desirable.

A final disadvantage of the empirical approach deals with the sampling interface. Online measurements must be integrated into the process. This can be accomplished by submerging a probe into the process or monitoring the process through a viewing window. The windows can become obstructed by sample build-up, rendering the measurement irrelevant, with possible product quality consequences. This requires a number of sensors, so that the process can be managed without one or several measurements. First principle calculations may also be used to continue a process along the desired trajectory until a sampling interface can be cleared.

This dissertation aims to combine empirical controls with first principle controls in a single hybrid system to eliminate some of the disadvantages and mitigate the risk associated with each control methodology. The first principle calculations are

hypothesized to reduce the variability associated with processing mechanisms, while reducing the experimental burden during development and scale-up. The empirical models are hypothesized to reduce the variability associated with end point criteria, while providing immediate process feedback and increased process understanding. The hybrid control system will provide the most efficient and rigorous automation system for pharmaceutical batch manufacturing to date.

1.3.4 Automated Data Management and Control Systems

A control system is a set of devices, communication systems, and software designed to regulate the manufacturing output of a product to consistently meet product specifications. The purpose is to operate the manufacturing system so that the net return is maximized in the presence of disturbances and uncertainties, rather than the often cited advantage of controlling variables at their set points or to track dynamic set point changes.[76] This is accomplished by scientific design, statistical modeling, and by exploiting available online measurements of the system to implement a control strategy, which is a planned set of controls, derived from current product understanding that assures process performance and product quality.[77]

Prior to 2004, full control systems were difficult to implement in the pharmaceutical industry due to regulatory constraints. Manufacturing processes were approved based on a validated combination of process parameters and had to remain fixed, so the process could not be adjusted to mitigate measured input disturbances. However, the process analytical technology (PAT)[41] and quality by design (QbD)[2] initiatives from the FDA (and recently, other regulatory agencies) allow operational flexibility within a validated design space. These guidelines have made possible

automated control systems that incorporate information about a process back into the system to adjust process variables to consistently hit product quality targets, or feedback control.[76] These systems offer continuous improvement of the process as additional information is gained throughout production life, which provides companies improvements in quality and efficiency,[1,78-80] and the possibility of real-time release.[41]

In the pharmaceutical industry a control strategy seeks to link the attributes of the product that are important to the patient, to the controls in the manufacturing process that are needed to deliver those attributes.[81] This is the main tenet of the QbD initiative, and the effort to describe how the manufacturing operations affect CQAs is a major determinate in the amount of regulatory flexibility afforded to the pharmaceutical manufacturer. It is the responsibility of the pharmaceutical company to relate all variables that are included in the validated design space to a meaningful metric of product risk. The control strategy's objective is to then minimize the quantified risk.

Feedback control is necessary to handle the variability, inaccuracies, and uncertainties present in the design process, and to make full use of the capacity of the equipment and measurement systems. There are two options for feedback: negative feedback or positive feedback. In positive feedback, the measured value is added with the set point, and in negative feedback the difference between the measured value and the set point (system error) is calculated. Negative feedback is the more popular control mechanism because it is more stable and less affected by random variation and error in the measurement.[82] Negative feedback will be considered in all cases in this dissertation.

Feedback control systems are designed so that certain designated signals (errors) do not exceed predetermined levels (specifications). Making this more difficult is that

the mathematical models that are used in representing real systems have uncertainty and the measurements that are used to inform the models contain errors. Rigorous review of all issues of control system design has been covered extensively.[82, 83]

The specific design of a control system should be developed based on the needs of the process that it is controlling. The process to be controlled should be studied and the types of sensors and actuators that are necessary for the requirements must be selected. The system must be adequately modeled and simplified if necessary, and the properties of the final model must be determined. Once the properties are determined, performance specifications can be implemented to ensure the required product quality. Finally, the type of controller can be selected that will ensure production within the defined specifications. It is important that a theory of feedback not only leads to good designs when possible, but also indicates directly and unambiguously when performance objectives cannot be met.[83]

The current dissertation will use a combination of first principle calculations and online process measurements in a combination feedforward/feedback (multicomponent) control system with real-time optimization (RTO).[84] An RTO system is a model based, upper-level control systems in a closed loop that provides set points to lower-level control systems to maintain the process at its optimum state.[76] At the lowest level, simple logic, linear loops, and proportional-integral-derivative controllers (PID) adjust manufacturing controls based on the needs of the upper level models. The system is illustrated in chapter 2.

A PID controller is a control loop feedback mechanism that is the most common for industrial applications. The controller attempts to minimize the error between a

measured process variable and the desired set point. There are three separate calculations that are used to adjust the process variable toward the set point. The first calculation (proportional) depends on the current error, the second (integral) on the accumulation of past errors, and the third (derivative) on the prediction of future errors. The weighted sum of these three calculations is used to adjust the process parameter to minimize error from the set point.[84]

$$u = K_p e + K_i \int e dt + K_d \left(\frac{de}{dt} \right) \tag{1.2}$$

In equation 1.2, u is the control variable value, e is the error, and K is the weight for each of the three calculations. The weights of these can be adjusted for the needs of a given control loop, with the derivative calculation often down-weighted because it is significantly affected by process noise. The final equation for manipulating the control variable to approach the set point is called the transfer function. The PID controller is a basic form of feedback control, and is crucial for the automated control of manufacturing processes.

Higher level control loops are needed to determine the values of the set points to be passed to the lower level PID controls. Real-time optimization is the feedback control strategy that enables these optimum set points to be calculated. Traditional RTO required the system to reach a steady state before any adjustments were implemented, resulting in very long response times. Recent applications have used high frequency RTO to perform real-time evolution, so that the process can be adjusted toward the optimum state continuously before a system steady state is reached.[76] These principles are incorporated into the control system described in this dissertation, and the models that are developed within these control strategies will be discussed in detail in later sections.

Well characterized systems (which often incorporate first principle controls) can be improved when feedback control is combined with a feedforward function. The feedforward function is basically an inverse model of the process, and can be used to inform the process of variability with respect to incoming material or process factors. The advantage of feedforward control is that corrective action is taken for a change in a disturbance input before it affects the control parameter. For example, the heated air temperature can be adjusted to maintain a constant drying rate in a fluid bed dryer based on a measurement of a change in input air humidity. Even when there are modeling errors, feedfoward control can often reduce the effect of the measured disturbance on the output better than feedback control alone. This leads to more stable processes.

Feedforward control is always used in combination with feedback control because feedback control is always required to track set point changes and suppress unmeasured disturbances that are always present in real processes. Process analytical technology is crucial for the successful implementation of either control strategy because it is these online measurements of the process or raw materials that provide all of the information needed for adjustments. Without PAT, process or material disturbances could not be identified and process improvement would be impossible.

The system described in this dissertation will use a combination of engineering process control and statistical process control. Engineering process control is applied to processes in which successive observations are related over time and where the mean drifts dynamically. It seeks to minimize variability by transferring it from the output variable to a related process input.[85] This is the overall control strategy in the proposed multicomponent control system, but statistical process control, which seeks to minimize

variability by detecting and eliminating assignable causes of variation on processes that vary about a fixed mean, is used to reduce variability within local control loops of process inputs at the lowest levels of control loops.

All extensive control systems for dynamic processes use a hierarchical system of control loops of different kinds to achieve full automation.[81] At the highest level, complex models relate product quality measurements to process parameter inputs to control the actual manufacturing process. These controls are called process or engineering controls. An example of these controls is the final moisture content of a pharmaceutical granulation that provides the optimum granule properties, and the process parameters that are required to reach the optimum moisture content. These process controls are the most difficult to develop and require extensive DOE. They often include complex interactions between process factors in real manufacturing examples, and may contain large amounts of uncertainty. The largest investment is made for development of this layer of controls.

Below the process controls are the analytical controls, which relate spectroscopic or process measurements to individual markers of the process trajectory. Analytical models produce the data about product quality that is used to inform the process controls to adjust the manufacturing process. Using the same example, the analytical model would be the model that generates a moisture prediction from an online spectroscopic measurement. The complexity of an analytical model depends on the measurement. Simple univariate models can be used to predict airflow from pressure differential measurements, but more commonly, complex multivariate and chemometric treatments are necessary for spectroscopic data. The investment required for an analytical model

should be proportional to the risk or importance associated with the property measurement. If the measurement is informing the process models for the most important quality metric, then a high degree of model performance is required. Each analytical model must be validated and maintained to assure future performance.

Still below the analytical models are the simple ladder logic or PID loops. These loops are used by the control software to maintain the process parameters at their given set points. For example, they inform the heater when to pulse on or cycle off to maintain a temperature at a given set point. The transfer functions associated with PID loops are optimized to either reduce the risk of over-adjusting a process measurement, or to reduce the time associated with reaching a desired set point. In most practical systems, the control software will optimize the PID loops based on default settings, and must be changed by the user if a different performance criterion is required.

All levels of the control strategy require a maintenance system to assure model robustness over time. The maintenance system is crucial for long term feasibility because all systems drift. Machine parts and motors age, causing them to respond differently to process adjustments, so the transfer functions must be updated to maintain performance. Additionally, the responses of instruments and sensors drift, requiring model update for prediction of product properties.[86] Finally, new variability that was not included in the original models inevitably is encountered, requiring some degree of model update or augmentation. The control system should have a regular maintenance schedule whose frequency is related to drift magnitude or frequency.

The complexity of these systems and the significant development that is necessary for successful implementation is the central theme of this dissertation. The structure of

the control system developed and the derivation of the models associated with the control system will be discussed rigorously in later sections. The dissertation will prove that the automation system developed provides improvements to both manufacturing quality and efficiency in the systems that were investigated.

1.3.5 Gabapentin

Gabapentin (1-(aminomethyl)cyclohexaneacetic acid) is the API that was used in several of the manufacturing control and design space studies of this dissertation. It was chosen by the FDA as the drug formulation to study in a quality by design (QbD) project through the National Institute for Pharmaceutical Technology and Education (NIPTE) titled, "Development of Quality by Design (QbD) Guidance Elements on Design Space Specifications Across Scales with Stability Considerations." It was chosen because it was a marketed drug that had problems due to physical and chemical stability. The FDA believed that manufacturing stress had a direct impact on the stability of gabapentin tablets. This made gabapentin an ideal case study for the development of a manufacturing controls strategy because the operation had to be well understood to ensure final product stability.

Gabapentin is in a class of medications called anticonvulsants or antiepileptic drugs (AEDs), and it is used to control certain types of seizures in patients who have epilepsy.[87,88] It is indicated as an adjunctive therapy of partial seizures and treats seizures by decreasing the abnormal excitement in the brain. Gabapentin is particularly effective against complex-partial seizures as occurring in temporal lobe epilepsy.[89] It is also indicated for the management of pain associated with post-herpetic neuralgia (PHN) by changing the way the body senses pain.[87] Additionally, gabapentin is prescribed for off-

label uses including relieving the pain of diabetic neuropathy and to treat or prevent hot flashes in post menopausal women or women who are being treated for breast cancer.

The drug was derived by adding a cyclohexyl group to the backbone of γ-aminobutyric acid (GABA), so that gabapentin would cross the blood-brain barrier, unlike GABA, but retain the physicochemical properties of GABA.[89] It has a molecular mass of 171.24 g/mole. The structures of gabapentin, GABA, and gabapentin's primary degradant are displayed in Figure 1.3. Gabapentin, however, exhibits no activity at GABA receptors *in vivo*. It does not modify $GABA_A$ or $GABA_B$ radioligand binding and it is not converted metabolically into GABA or a GABA agonist. It does, however, increase the synthesis of GABA in the human brain, enhance GABA release, and potentiate GABAergic inhibition in the portion of the brain thought to be critically involved in seizure propagation. This increases the threshold for seizures and decreases seizure propagation.[89]

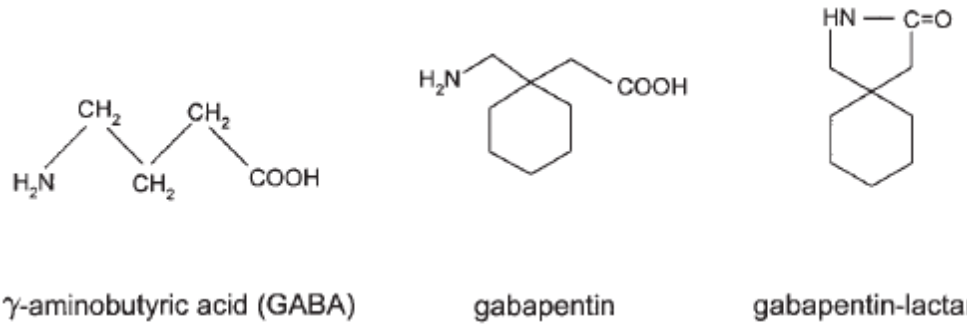

Figure 1.3. Reproduced from Potschka et al.,[89] the chemical structure of GABA, gabapentin, and gabapentin lactam.

Gabapentin has a pK_{a1} of 3.7 and a pK_{a2} of 10.7. It is a BCS class III drug,[90] meaning it is freely soluble in water but has low permeability with a log of the partition coefficient (n-octanol/0.05M phosphate buffer) at pH 7.4 of -1.25.[91] Combined with the fact that it is a low potency drug, gabapentin must be dosed in large amounts to achieve a

pharmacological effect. It also displays delayed pharmacodynamic effects after systemic administration because it does not penetrate the blood-brain barrier via passive diffusion due to its zwitterionic and hydrophilic properties. Therefore, it passes via a saturable active transport process.[89]

It is dosed perorally in capsules, tablets, and oral solutions. Single doses are marketed in hard shell capsules containing 100, 300, or 400 mg, elliptical film coated tablets containing 600 or 800 mg, or oral solutions containing 250 mg/5 mL.[91] Manufacture of 889 mg elliptical tablets containing a 600 mg unit dose of gabapentin is the subject of a portion of this dissertation. The exact formulation will be presented in later sections.

Systemic absorption of gabapentin is not dose proportional, meaning that a lower percentage of the total dose is absorbed as dose increases, which is another reason that high dose delivery systems are required. Food has only a slight effect on the rate of absorption, so it does not have to be administrated in a specific fed state. Less than 3% of the drug is circulated bound to plasma protein, and the approximate fraction of gabapentin in cerebrospinal fluid (CSF) is 20% of the plasma concentration.[91]

Gabapentin is eliminated from systemic circulation via renal excretion, and the drug molecule is unchanged. Hepatic metabolism of gabapentin in humans does not occur. The half-life is 5-7 hours, which is not affected by dose or multiple dosing. The pharmacokinetics is not affected by gender, and there has been no evidence to indicate it is affected by race. Elimination is strongly influenced by a patient's renal function, so plasma clearance is significantly reduced in elderly patients or patients with impaired renal function. Dosage adjustments are required in these situations. Clearance is slightly

increased in pediatric patients under the age of 5, but children over the age of 5 have clearance and plasma concentrations similar to adults. The elimination rate constant is directly proportional to a patient's creatinine clearance, a measure of renal function.[91]

The exact mechanism by which gabapentin exerts its anticonvulsant or analgesic effect is not well understood, but it prevents seizures with a similar effectiveness compared to other marketed anticonvulsants. It has been tested in a wide array of common radioligand binding assays at concentrations up to 100 μM and did not exhibit affinity for any of them. [91] It does not alter cellular uptake of dopamine, noradrenaline, or serotonin. The only potential source of activity was revealed by *in vitro* studies of radiolabeled gabapentin, where a gabapentin binding site in areas of rate brains including the neocortex and hippocampus was shown. Functional correlates of gabapentin binding have yet to be elucidated. Gabapentin as an adjunctive therapy was shown to significantly reduce the frequency of seizures and secondarily generalized tonic-clonic seizures in several clinical trials.[91] It has been shown to reduce seizure generation and seizure propagation, leading to its broad anticonvulsant effect.

For the analgesic effect, gabapentin prevents allodynia and hyperalgesia in animal models. It has not been shown to alter immediate pain related behaviors, but it did prevent pain related responses in animal models of neuropathic pain and decreased pain related responses after peripheral inflammation. The relevance of these animal model results to humans is not known. A clinical study for pain management of PHN showed a significant decrease in the pain experienced by the treatment group.[91]

Like all AEDs, gabapentin increases the risk of suicidal thoughts or behavior in patients using the drug. The FDA suggests that patients treated with any AED for any

indication should be monitored for the emergence or worsening of depression, suicidal thoughts or behavior, or any unusual changes in mood or behavior. In clinical trials, patients in the treatment group had approximately twice the risk of suicidal thinking or behavior as those in the placebo group, an increase in one case for every 530 patients.[91]

Drug reaction with Eosinophilia and Systemic Symptoms (DRESS) or multiorgan hypersensitivity has been reported in AEDs including gabapentin. Gabapentin may cause dizziness, somnolence, and other symptoms related to central nervous system (CNS) depression. Other adverse events occurred in children age 3-12 years old and included emotional lability, hostility, thought disorders, and hyperkinesia. An unexpectedly high incidence of pancreatic acinar adenocarcinomas was identified in male rats that were given gabapentin, so it also has some tumorigenic potential.[91]

Gabapentin, as a drug substance, is a crystalline solid with four known polymorphs. Form I is a monohydrate, while Forms II-IV are anhydrous. Form II is the marketed and most stable form, but polymorphic transformations have been reported following mechanical or thermal stress.[92] Polymorphic transformations have also been demonstrated by the NIPTE research team to depend on the moisture available from the environment and excipient interactions.

Form II has been shown to chemically degrade at a slow rate, while the metastable forms have significantly poorer chemical stability. Therefore, the physical stability is crucial in determining the long term chemical stability because chemical degradation is typically preceded by conversion of Form II to the metastable Form IV.

The only chemical degradant of gabapentin known to date is its lactam analogue (gabapentin lactam) (3,3-pentamethylene-4-butyrolactam) (Figure 1.3). Gabapentin

lactam is dangerous because it has been shown to exhibit a convulsant inducing effect (demonstrated on rats).[89] A recall of a generic gabapentin product occurred in 2007 due to excessive impurities, and it is believed that the quantity of gabapentin lactam exceeded the specification prior to the expiration date.[93]

The FDA believed that the amount of degradation was directly proportional to the mechanical and thermal stress experienced during manufacturing, which made it interesting as a case study for manufacturing controls and design space development. The amount of gabapentin lactam must not exceed 0.4 mole % in the final tablets throughout their shelf life.[94] Completed research by the NIPTE research group as part of this dissertation has proven that manufacturing stress does have an effect on the magnitude and rate of degradation in gabapentin tablets.

Gabapentin easily forms gabapentin lactam via intramolecular cyclization.[95,96] As stated previously, degradation of gabapentin Form II is preceded by a polymorphic transformation. In a study of polymorphic transformations resulting from milling, Lin et al. showed that milling Form II resulted in trace amounts of gabapentin lactam and transformation to form III.[92] The lactamization was attributed to the heating effect induced by milling. Further milling resulted in further transformation to form IV and an additional amount of gabapentin lactam. Metastable forms of gabapentin show higher chemical degradation kinetics over time, so even small amounts of physical transformations can impact long term stability. The polymorphic transformations were both retarded or accelerated in the presence of different excipients.

Hsu and Lin investigated the solid state lactamization kinetics of gabapentin upon heating.[97] There proposed pathway for intramolecular lactamization of gabapentin in the

solid state is displayed in Figure 1.4. Since gabapentin is a zwitterion in the solid state, the lactam formation was proposed to occur by the negatively charged carboxyl group in the zwitterionic state attacking the protonated amino group. This eventually leads to cyclization and the formation of gabapentin lactam and release of a water molecule. There studies again showed that lactamization was preceded by formation of gabapentin Form IV. It appears that this form significantly reduces the activation energy required to initiate lactamization.

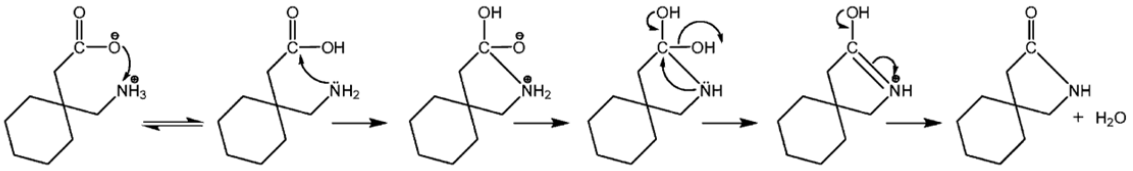

Figure 1.4. The proposed scheme by Hsu and Lin[97] for the intramolecular lactamization of gabapentin in the solid state.

The kinetic mechanism by which the overall physical and chemical degradation occurs following thermal and mechanical stress during processing and storage is hypothesized by the NIPTE research group to be a reversible, autocatalytic branching of crystalline gabapentin to an unstable form of gabapentin, followed by a spontaneous dehydration of the unstable form to gabapentin lactam. This process is displayed in Figure 1.5. The unstable form of gabapentin (G*) was not identified as a separate polymorphic form in NIPTE studies, but as Form II with significant crystal damage, disorder, and higher energy. This high energy form and subsequent dehydration agree with the formerly proposed mechanisms.

Figure 1.5 illustrates that the amount of gabapentin lactam formed is dependent on the ratio of the k_1 and k_2 rate constants to the k_3 rate constant. Manufacturing stress

(shear and thermal) is believed to cause a small amount of gabapentin lactam formation directly from crystalline gabapentin, but the bulk of the degradation is from the disordered crystalline state. The stress applied creates the disordered gabapentin, and the amount formed is dependent on the magnitude of the stress applied and the amount of disordered gabapentin from previous stress. To prevent degradation, k_1 must be decreased by limiting the amount of stress applied. Once disordered gabapentin is formed, the rate constant k_2 is then significantly higher than the rate constant for direct degradation of Form II, and the only method for reducing the rate of gabapentin lactam formation is to recover or heal the stable crystalline form. Therefore, the larger k_3 is in relation to k_2, the less disordered gabapentin is available for degradation per unit time.

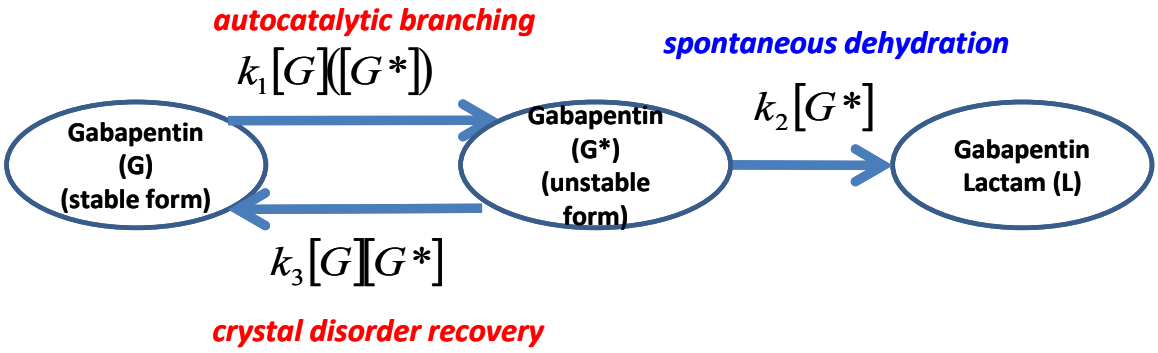

Figure 1.5. The proposed degradation mechanism from gabapentin to gabapentin lactam during processing.

The presence of moisture increases the molecular mobility of the gabapentin crystals, so while polymorphic transformations are more probable with added moisture, recovery/recrystallization of the stable crystalline form from the disordered state occurs at a much higher rate. The probability of polymorphic transformation of gabapentin at moisture contents encountered during processing or storage is very small, so the main effect of moisture is to increase k_3. Therefore, moisture remaining in the finished product or storage at an elevated humidity actually facilitates crystal recovery of Form II and decreases the rate of lactamization during storage.

The susceptibility of gabapentin to thermal and mechanical stress, the potential interactions with excipients, the dangerous effects of the lactam degradant, and the unique effect of moisture with respect to stability make the optimization of manufacturing controls critical. This supports the choice of gabapentin as a good case study for manufacturing design space development. This dissertation will develop an automated control system for the fluid bed drying of a model gabapentin formulation and determine a design space that assures product stability over the required shelf life.

Chapter 2: Hybrid Controls Combining First Principle Calculations with Empirical Modeling for Fully Automated Fluid Bed Processing

2.1 Introduction

The pharmaceutical industry has invested a substantial amount of resources in recent years to develop manufacturing systems that offer improved product quality while limiting costs. The United States Food and Drug Administration (FDA) has encouraged the use of the guidelines put forth by the International Conference on Harmonization (ICH-Q8)[2] that allow for operational flexibility within a design space to allow fully automated systems that incorporate real-time data management to be possible. These systems offer the opportunity for continuous improvement of the process and resulting drug product by allowing information gained during manufacturing through online process measurements to inform the process to ensure constant product quality.[3]

Fluid bed processing of pharmaceutical powders is an excellent case study for the development of a fully automated control system because of its complexity and the multiple phases that are encountered during a given fluid bed process.[4,5] A single fluid bed unit operation can take raw powders through blending, wet granulation, drying, and cooling. A fully automated control system must be able to define the state of the process, define meaningful end points of each phase before moving into the next phase, and incorporate information from process measurements back into the process so that the manufacturing parameters can be adjusted to control the process. This requires a well developed communication system that can synchronize multiple process measurements

and organize data for analytical and process models. The models require comprehensive experimental designs to be performed so that prediction results are assured to be accurate and robust. Development of these systems requires a substantial initial investment, but leads to a rapid return on investment through improvements in product quality and efficiency, reduced batch failures, reduced inventory storage, and the potential for real-time release.

Two separate approaches have traditionally been used to model and control the fluid bed unit operation. The first approach uses first principle calculations based on thermodynamic heat and mass balance equations to define and control the environment inside the fluid bed chamber. The second approach is empirical and uses online process measurements, spectroscopy, design of experiments (DOE), and process modeling to control the unit operation. Each method has benefits and disadvantages, often complimentary, but they have not been used together to their full extent in a single system. This chapter demonstrates the development and implementation of a hybrid control system that uses both first principle calculations and empirical data management for the manufacture of pharmaceutical granules to tight specifications.

First principle controls have been used for several decades to model drying, aqueous film coating, and fluid bed processes. The controls include the temperature difference method,[26-28] thermodynamic environment controls,[29-31] fluidization regimes,[4] computational fluid dynamics,[32-36] and transport phenomena.[37, 38] All of these methods use material properties and measurements of mass, humidity, and heat at different points of the process to define the thermodynamic state of the bulk powder or surrounding environment.

The thermodynamic calculations used for this dissertation were Ebey's environmental equivalency factor (EFF),[29] which was established in 1987 for aqueous film coating. The same evaporative drying mechanisms control spray granulation and drying in aqueous fluid bed processing.

The first principle controls offer several advantages that are essential for robust and efficient processes. By definition the calculations are based on material and environmental properties, so the calculations are universal for all systems. Separate calibrations for new or adjusted formulations are unnecessary. The equations are also independent of scale or specific equipment, meaning all controls based in first principles are directly scalable and transferable. Scaling up processes from lab scales to full manufacturing scales is a major hurdle for pharmaceutical processes,[24,25] therefore eliminating any variables that need to be adjusted between scales is a major advantage.

The internal fluid bed environment, which is defined using the EEF calculations, controls the evaporative drying mechanism and resulting drying rate to allow the final granule properties to be controlled more precisely. The rate at which water is removed from granules is often a significant factor in determining final granule material attributes. Even if all process parameters remain constant, small fluctuations in the external environment will affect the incoming air stream, thus altering the drying mechanism without additional controls. To maintain a constant drying rate without a control system, input air must be preconditioned to have constant properties. These preconditioning HVAC systems are expensive, and thermodynamic controls, which continuously modify the air temperature to account for moisture variation, make preconditioning systems unnecessary.

The final advantage offered by first principle controls is variable reduction. This is the most significant advantage in terms of reducing experimentation and cost. As an example, the EEF calculation takes nine measurements – inlet air temperature, inlet air humidity, heated air temperature, product temperature, outlet air temperature, exhaust air temperature, exhaust air humidity, airflow velocity, and spray rate – and produces a single value (EEF). Four of the nine measurements, inlet air humidity, heated air temperature, airflow velocity, and spray rate, are factors that would be typically altered independently in a purely empirical approach. By reducing the number of input factors to be explored in a DOE by three, the cost of development can be significantly reduced.

There are several disadvantages to first principle controls, however. The calculations do not account for effects of atomizing air, changes in the droplet size of the spray, changes in the kinetic energy of process air and water vapor, and loss of heat from the drying bowl. Typically, these are minor factors, but can have more serious effects in sensitive processes. These factors can be used to control the final particle distribution to narrow specifications with additional optimization. The measurements associated with the first principle calculations do not give actual moisture or chemical concentrations in the product, nor do they provide estimates of particle size. Therefore, the definition of phase end points are difficult to determine. There is also no access to additional information such as material phase changes or chemical decomposition. Finally, measurements including temperature, which are critical to the first principle controls, often have slow response times, so the full extent of excursions from the process trajectory are often detected minutes after they occur. This can have deleterious consequences for a particular batch.

Full empirical controls for fluid bed processors have become feasible with the success of online spectroscopy, multivariate modeling, and complex communication and data management systems. These systems began with traditional DOE studies of the fluid bed process factors,[42] expanded to include online measurements of critical material attributes (CMA) using spectroscopy,[46-49] imaging systems,[50,51] and other probes,[52, 53] to finally creating fully automated processes[54, 55] of limited complexity.

The advantages of empirical controls complement those of the first principle controls. Online sensors provide direct moisture and particle size measurements of the product in real time for immediate CMA information and the simple and intuitive definition of phase end points. The information contained in near infrared (NIR) or Raman spectra, common online techniques, also includes chemical and physical phase information and gives insight into the water-solid interactions for improved process understanding.[70-72] For example, an API's crystalline phase or percent purity can be followed in real time. Finally, the online sensors reflect changes in the process immediately. Any excursion from a desired process trajectory can be identified and corrected before the batch is lost.

Disadvantages of empirical controls include calibration building and large experimental designs. Spectroscopic calibrations are formulation-, equipment-, and scale-specific, so a new calibration must be created for each system, or a rigorous transfer technique must be applied. The process DOE for these systems are large, especially when considering external environment factors. Including any variable that could potentially affect the process creates unreasonably large designs. Adding to this problem, empirical process models are not directly scalable. Therefore, the DOE must be

replicated for new equipment, scale-up, or formulation adjustments. These factors lead to substantial costs in development and maintenance.

Two final disadvantages of the empirical approach address sampling of the process. Online measurements of full scale fluid bed processes require several probes for each measurement to ensure that the measurements represent the bulk material. This requires complex data management systems and calibration transfer techniques. The windows through which the sensors collect data can also become clogged, rendering the measurement irrelevant, with possible product quality consequences.

This chapter was part of a project through the National Institute for Pharmaceutical Technology and Education (NIPTE) titled, "Development of Quality by Design (QbD) Guidance Elements on Design Space Specifications Across Scales with Stability Considerations." The research was originally published in the Journal of Pharmaceutical Innovation.[129] This chapter introduces a hybrid fluid bed drying control system that combines first principle calculations with empirical modeling. The EEF calculations allow the internal fluid bed environment to be defined despite external environment fluctuations for tight product specifications. The reduction of fluid bed processing parameters allows the empirical models to be created efficiently. These models track granule CMAs in real time to provide immediate process feedback and intuitive phase end points. The system is designed to negate the drawbacks of the traditional approaches, while allowing the system to be developed efficiently. Although the controls are designed to take a product through all four fluid bed process phases, this chapter will focus on developing drying controls only. Expansion of the controls to blending and spray granulation will be addressed in chapter 5.

2.2 Theory

Data matrices will be represented by bold, capital letters (**X**), vectors will be bold, lowercase letters (**x**), and scalars will be italics, lowercase letters (*x*). A summary of variables can be found in Table 2.1. The nomenclature used in Ebey's original manuscript[29] is used for the description of the EEF calculations in this chapter.

Table 2.1. Nomenclature used in this chapter.

A_H	Heat-transfer surface area
A_H	Mass-transfer surface area
C_p	Specific heat capacity of air
h_H	Average heat-transfer coefficient
h_M	Average mass-transfer coefficient
h_{tg}	Enthalpy of vaporization
Le	Lewis Number
M	Molecular weight of water
p_∞	Partial pressure of water vapor at heated air stream
p_w	Partial pressure of water vapor at mass-transfer conditions
R	Ideal gas constant
T_∞	Temperature of the heated air stream
T_B	Heat-transfer surface temperature
T_w	Mass-transfer surface temperature
ρ	Density of air stream
$\dot{m}$	Mass rate of water evaporation

2.2.1. First Principle Calculations: The Environmental Equivalency Factor (EEF)

The EEF calculations are based on conservation of mass and the first law of thermodynamics, namely the conservation of internal energy. It is assumed that the system is adiabatic and that any deviation from this condition can be modeled linearly. Therefore, the temperature, flow rate, and humidity of the inlet airstream and delivery

rate of the solution are compared to the temperature and humidity of the exhaust air, and the difference is the work performed by the system. By this description, fluid bed granulation and drying are adiabatic evaporative cooling processes, with the evaporation rate controlling the quality of the granules.

The evaporation of water from the surface of granules results from two competing mechanisms, heat and mass transfer. The heat transfer mechanism is driven by the difference in temperature between the heated airstream and the surface of the granules.[29]

$$h_H A_H (T_\infty - T_B) = \dot{m} h_{tg} \tag{2.1}$$

The mass transfer mechanism is driven by the vapor pressure differential between the heated airstream and the surface of the granules.[29]

$$h_M A_M \left[\frac{Mp_w}{RT_w} - \frac{Mp_\infty}{RT_\infty} \right] = \dot{m} \tag{2.2}$$

These equations assume ideal behavior in the system.

Equations 2.1 and 2.2 can be equated using the mass of water evaporation rate ($\dot{m}$) and rearranged to relate the effective area in which the heat transfer mechanism acts on the granules to the effective area in which the mass transfer mechanism acts on the granules.[29]

$$\frac{A_H}{A_M} = \frac{\left[\frac{Mp_w}{RT_w} - \frac{Mp_\infty}{RT_\infty} \right] h_M h_{tg}}{h_H (T_\infty - T_B)} \tag{2.3}$$

This ratio describes the contribution that each mechanism provides to the drying rate and is defined as the EEF.

The ratio of the heat and mass transfer coefficients can be written[29]

$$\frac{h_H}{h_M} = \rho C_p (Le^{2/3}) \tag{2.4}$$

with the Lewis number (*Le*) approximately equal to 1. Substituting equation 2.4 into equation 2.3 results in the EEF calculation that is used to control the fluid bed drying rate.

$$EEF = \frac{\left[\frac{Mp_w}{RT_w} - \frac{Mp_\infty}{RT_\infty}\right] h_{tg}}{\rho C_p (T_\infty - T_B)} \tag{2.5}$$

The EEF calculations were derived for an equilibrium drying system or a steady state operation. Spray granulation and drying are not steady state operations due to the substantial change in mass with additional and removal of water. As a result, the EEF calculation is more accurate in determining the overall drying rate during the constant rate drying period when heat transfer is the rate limiting mechanism for evaporation of water and an equilibrium condition is maintained. During the falling rate drying period, diffusion of water from granule cores to the surface of particles is the rate limiting step, and the EEF calculation is less accurate at calculating the drying rate. The calculations still provide information to the control system needed to approach the target drying rate, however, and the variability in the drying rate is reduced compared to a constant temperature system. The major value of the EEF calculations is reducing the batch to batch variability with respect to the drying rate caused by fluctuations in the inlet air humidity over time.

Empirical testing is necessary to define the optimum EEF value for a given system, which is defined by the best final product CQAs or minimum patient risk. Once determined, any of the fluid bed parameters can be adjusted as long as the EEF value remains unchanged, the granule properties that are affected by the drying rate will remain

unchanged. Variable EEF programs can be established, as long as the EEF profile for a given experiment is the same as the validated process. The fluid bed system can be run at different temperatures and airflow velocities using trial batches to estimate the heat exchange with the environment over a range of EEF values. This knowledge can be used to correct the above calculations for errors associated with the adiabatic assumption.

2.3 Materials and Methods

2.3.1 Granule Formulation

The granule formulation for this project consisted of 93.75% gabapentin (Hangzhou Starshine Pharmaceutical Co., LTD, Hangzhou, China, Batch 0803023) as the API and 6.25% hydroxypropyl cellulose (HPC) (Klucel EF, Ashland Aqualon Functional Ingredients, Wilmington, DE, USA) as the binder. Gabapentin was selected as the API because it has processing induced stability concerns, so the control systems were very important.

Gabapentin and HPC were granulated using a Collette MicroGral (GEA Pharma Systems, Columbia, MD, USA), a top driven high shear granulator with a 4L glass bowl. The two powders were dry mixed in the granulator by the impeller at 500 rpm for five minutes. Water was sprayed onto the dry mixture using a six-inch atomization nozzle (Spraying Systems Co., Wheaton, IL, USA) with a stainless steel, flat, fan spray pattern and peristaltic pump (323U/D, Watson-Marlow, Wilmington, MA, US). The water addition rate was 16 mL/min with 15 psi atomization air pressure, and the total water amount was 5% by weight. The impeller speed and chopper speed during granulation

was 500 and 1000 rpm, respectively. The impeller and chopper continued mixing after spray granulation was complete for 30 seconds (wet massing period).

2.3.2 Fluid Bed Processor (FBP)

Fluid bed drying was performed using a Diosna Minilab (Dierks & Sohne GmbH, Osnabruck, Germany) fitted with an 11 L insert. The inlet airflow velocity was optimized to maintain a constant bed height, and is constant for a given batch size after an initial burst to ensure fluidization. The 450 gram batch sizes required 5 m^3/hr, while the 650 gram batches required 10 m^3/hr. The filter bags were cleared using a back pressure pulse every 60 seconds at 30 psi for all experiments.

The FBP contained an internal EGE-Electronik series LN/LG air flow sensor (Spezial-Sensoren GmbH, Gettorf, Germany) to measure volumetric airflow velocity in the inlet air pipe. Three internal thermocouples measured temperature of the heated air, product temperature, and outlet air. Two series RHL temperature/humidity transmitters (Dwyer Instruments, Inc., Michigan City, IN, USA) were added to the system to measure the temperature and humidity of the inlet and exhaust air, respectively. A series 616 differential pressure transmitter (Dwyer Instruments, Inc, Michigan City, IN, USA) was added to the system to measure the pressure drop across the fluid bed. Near infrared spectra were collected through the front viewing window of the FBP using a model NIR256L-2.2T2 spectrometer (Control Development Inc., South Bend, IN, USA). It is a 256 element photodiode array spectrometer with an extended InGaAs detector (1085-2229 nm). An external halogen light source (Control Development Inc., HL-2000) was used with a fiber optic probe (Control Development Inc., South Bend, IN, USA, 6 around 1 reflectance probe). A schematic of the FBP and its sensors is presented in Figure 2.1.

The EEF value (which adjusts and controls the heated air temperature to maintain a constant drying rate), heated drying end point (NIR predicted moisture content), cooling amount (product temperature at discharge), and batch size were factors varied in a 2^4 full factorial design to study the drying factors that were identified during risk analysis as potentially influencing granule properties. The drying DOE and measured results are listed in Table 2.2.

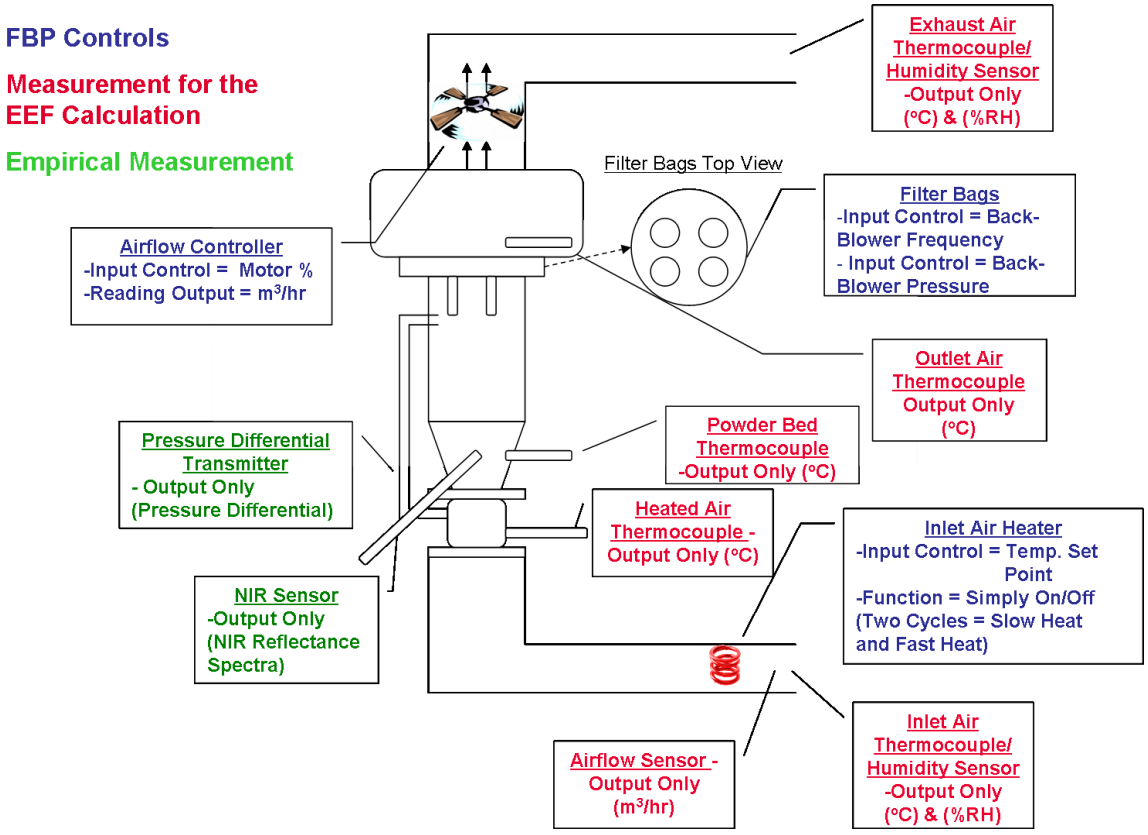

Figure 2.1. The FBP schematic of the available input controls, measurements for the EEF calculation, and empirical measurements.

Table 2.2. The FBP DOE factor levels and response results. (Yellow = experiments pooled for error estimates.)

Two-level 4-Factor Full-Factorial Design							
Combination	**Run Order**	**Factors**				**Responses**	
		EEF (a)	Target Mois. End pt. (%) (b)	Batch Size (grams) (c)	Prod. Temp at Completion (^{o}C) (d)	Median PS (μm)	Lactam Concentration (Mole %)
-	8	0.450	0.5	450	25	289	
a	7	0.175	0.5	450	25	296	
b	13	0.450	1.0	450	25	328	0.019
ab	14	0.175	1.0	450	25	298	
c	16	0.450	0.5	650	25	334	
ac	2	0.175	0.5	650	25	310	0.028
bc	1	0.450	1.0	650	25	330	
abc	3	0.175	1.0	650	25	353	0.016
d	11	0.450	0.5	450	30	274	0.016
ad	12	0.175	0.5	450	30	290	
bd	4	0.450	1.0	450	30	284	0.021
abd	5	0.175	1.0	450	30	332	
cd	10	0.450	0.5	650	30	338	0.022
acd	6	0.175	0.5	650	30	316	0.026
bcd	9	0.450	1.0	650	30	329	0.016
abcd	15	0.175	1.0	650	30	351	
Repeat	17	0.450	0.5	650	25		0.018
Repeat	18	0.450	0.5	650	25		0.016
Repeat	19	0.450	0.5	650	25		0.017
Repeat	20	0.450	0.5	650	25		0.019

2.3.3 Control System

A schematic of the control system is presented in Figure 2.2. The system was set to sample data and send commands at a set frequency of 5 seconds. The FBP internal measurements, which included airflow velocity, heated air temperature, product temperature, and outlet temperature, were collected by an onboard programmable logic controller (PLC) (Allen-Bradley, Rockwell Automation, Milwaukee, WI, USA). The PLC also communicated the process set points to the FBP and contained the necessary ladder logic to run the heater and airflow motor. The PLC sent the FBP process measurements and the previous set points to a DeltaV digital automation system (Emerson Process Management, Equipment & Controls, Inc., Lawrence, PA, USA) via open process control (OPC).

DeltaV received the process measurements from the PLC and the 4-20 mA analogue inputs from the temperature/humidity sensors and differential pressure transmitter and transformed the inputs into digital readings. The DeltaV software contained internal logic for safety switches, alarms, and unit conversions, as well as PID controllers for the fluid bed set points. It also tagged readings from the FBP and input controls from the control software to organize the communication between these two systems.

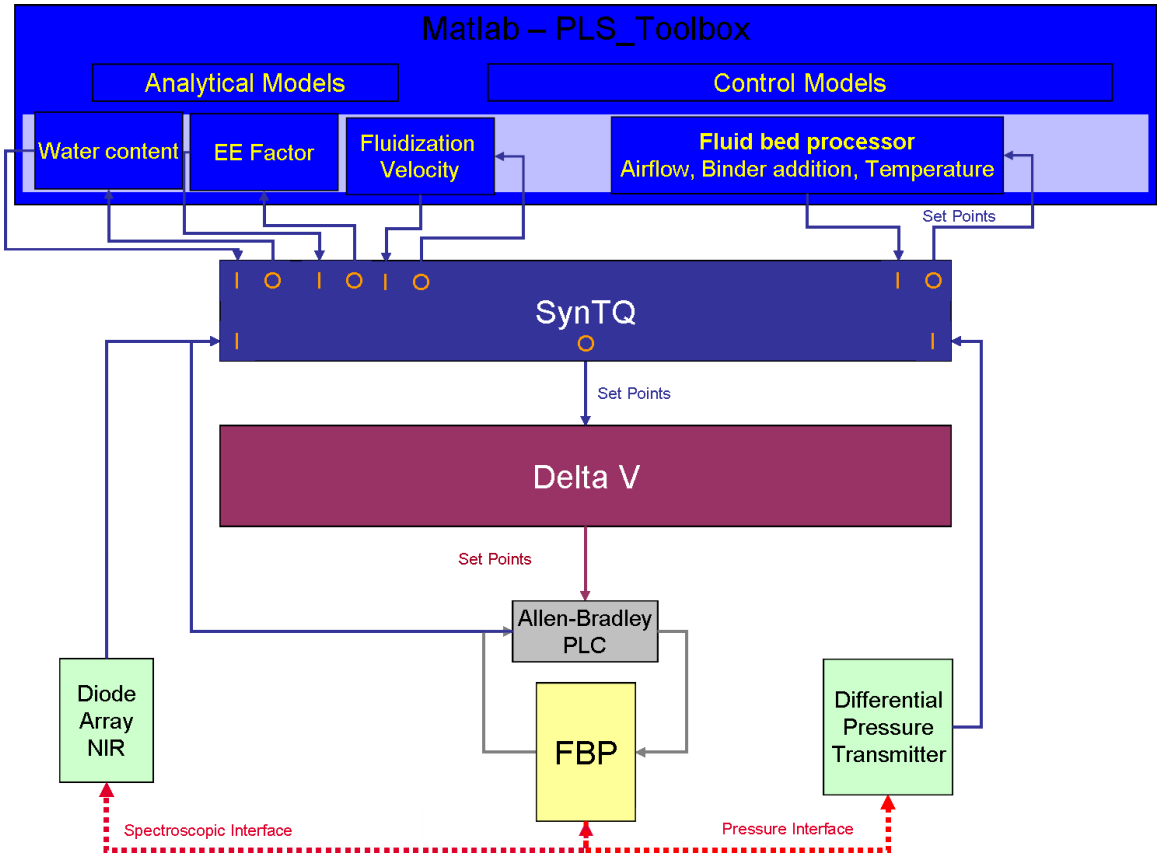

Figure 2.2. A schematic presenting the control systems' communication network.

The control software for the system was synTQ version 3.5 (Optimal, Bristol, UK). This software synchronized all measurements on the FBP at a fixed cycle, so that each measurement could be compared for a specific moment. SynTQ received all process measurements from DeltaV via OPC and received NIR spectra directly from the spectrometer. SynTQ organized the raw data and sent the information to the necessary analytical models. All of the analytical and process models were compiled and input directly into the synTQ software. The analytical models output product or process property predictions, which were then passed within synTQ to the process models. The process models took the property predictions and predicted the process parameters (airflow velocity and heated air temperature) necessary to continue the process along the

trajectory for the next cycle. These parameter predictions were then passed via OPC from synTQ to DeltaV, which translated the parameters for communication to the PLC, and the PLC finally adjusted the process parameters as directed.

Also included within the synTQ software was all of the necessary logic to define phase boundaries within a batch. A given batch's logic chart is called an orchestration. A flow chart depicting the orchestration for all four phases of a fluid bed process is shown in Figure 2.3. In the current chapter, the process began at phase 3 (drying) and continued through phase 4 (cooling) before ending. The orchestration collected all of the data inputs and sent them to their proper analytical models to predict product and process properties (e.g. granule moisture content, EEF, etc.). A decision directed the orchestration to the proper FBP phase, where the logic conditions for the phase were contained. A logic decision determined how far into a given phase the process was at the moment of data collection. The analytical predictions were then sent to their proper process models to predict the process parameters that needed to be sent to the FBP.

For a full, four phase FBP process, the dry blending phase was set to a constant airflow velocity, ambient heat, and no spray for a set amount of time. It is possible to train a NIR chemical concentration model to predict end point homogeneity, and moderate heat can be applied to preheat the system. When the allotted time for blending is complete, synTQ moves the system to phase 2, to begin spray granulation.

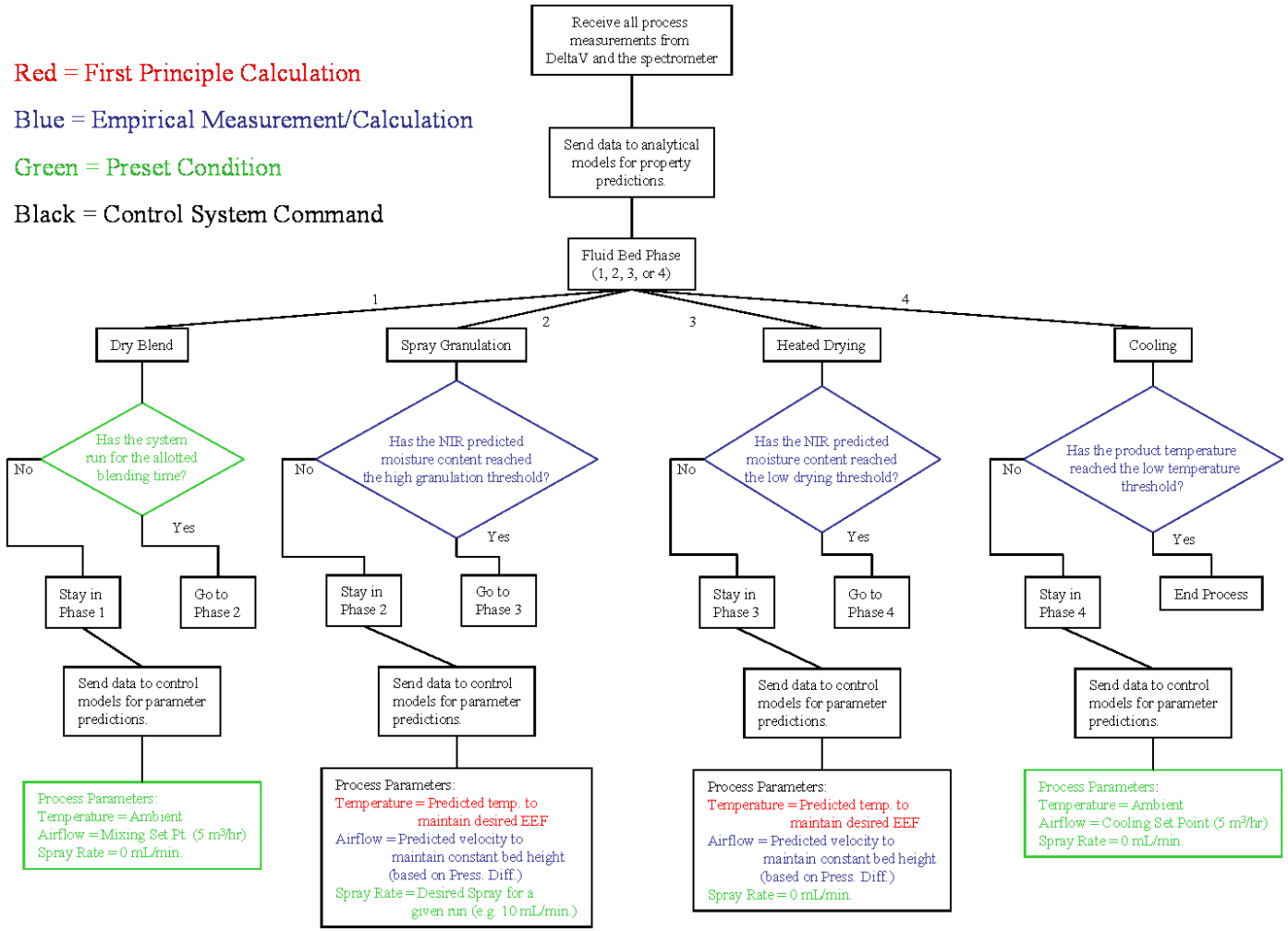

Figure 2.3. FBP synTQ orchestration flow chart.

For the spray granulation phase, a constant spray rate is used and the airflow velocity is adjusted to maintain a constant bed height using the differential pressure measurement. The inlet air temperature is adjusted to maintain a constant EEF after accounting for all other factors. Spray granulation continues until the NIR predicted moisture content reaches a predetermined threshold over a set number of consecutive cycles. The parameters over a typical drying batch are displayed in Figure 2.4. When the threshold is reached, synTQ moves the system to phase 3, the drying phase.

During drying, the liquid addition was ceased, but the airflow velocity continued to be adjusted by the differential pressure measurement, while the inlet air temperature was altered to maintain a constant EEF. The phase continued until the NIR predicted moisture content reached a minimum threshold and a window containing the previous one minute of moisture predictions reached a minimum standard deviation threshold.

In the current chapter, wet granulate from the high shear granulator was charged into the FBP and the orchestration began at phase 3. An initial burst of maximum airflow (100 m^3/hr) was necessary to fluidize the wet powder, but once fluidized, the granules dried rapidly enough that a constant airflow that was dependent on the batch size could maintain a constant bed height. The moisture threshold was adjusted as part of the drying DOE with the low moisture level being 0.05% because the dry powder moisture content was approximately the same. The standard deviation threshold was 0.005% moisture content. This assured that the bulk of the granules had reached the threshold. Once the threshold was reached, synTQ moved the system to phase 4, the cooling phase.

When cooling began, the heater was turned off and the airflow motor was set to remain at a constant velocity. This continued until the product temperature reached a

minimum threshold. The static airflow velocity was dependent on the batch size for the current system, and the minimum product temperature threshold was adjusted as part of the drying DOE.

2.3.4 Data Analysis

The analytical and process models that were included in the control system were created using MATLAB v. 7.1 R14 (The Mathworks, Natick, MA, USA) equipped with the PLS_Toolbox v. 3.0.4 (Eigenvector Research Inc., Wenatchee, WA, USA) and programs written in house. MATLAB code was compiled using MATLAB Compiler (The Mathworks, Natick, MA, USA) for use by the synTQ software. The DOE results were analyzed using the statistical software, jmp 8 (SAS, Cary, NC, USA). All possible main effects and second order interactions were investigated, and variables were screened for significance using the p-value statistic at the α-level 0.10.

The NIR calibration for moisture content was created by sampling granules from several trial drying batches. The moisture content was measured using loss on drying (LOD) on a Computrac Max-2000 moisture analyzer (Arizona Instruments, Chandler, AZ, USA). The model was created using partial least-squares (PLS) regression on standard normal variate (SNV) corrected spectra. The model required one PLS latent variable.

The heated air temperature needed to maintain a constant EEF value was determined by solving the EEF equation (2.5) for the T_∞ variable. This required solving a quadratic equation, with the negative solution (-*b*) being the solution that resulted in the meaningful temperature estimate. Figure 2.4 displays the calculations that are required

for controlling the three major process set points - heated air temperature, fluid bed phase, and airflow velocity – for a batch in the drying DOE.

For systems requiring the spray granulation phase, a simple univariate regression with differential pressure being the independent variable and volumetric airflow velocity being the dependent variable was necessary to predict the airflow velocity to maintain a constant bed height. The model was trained by running several trial granulations while adjusting the airflow velocity to maintain a constant bed height via visual observation. In this chapter, the process began at drying with a maximum moisture content of only 5%, so after the initial airflow burst, a static velocity set point was used to maintain a constant bed height.

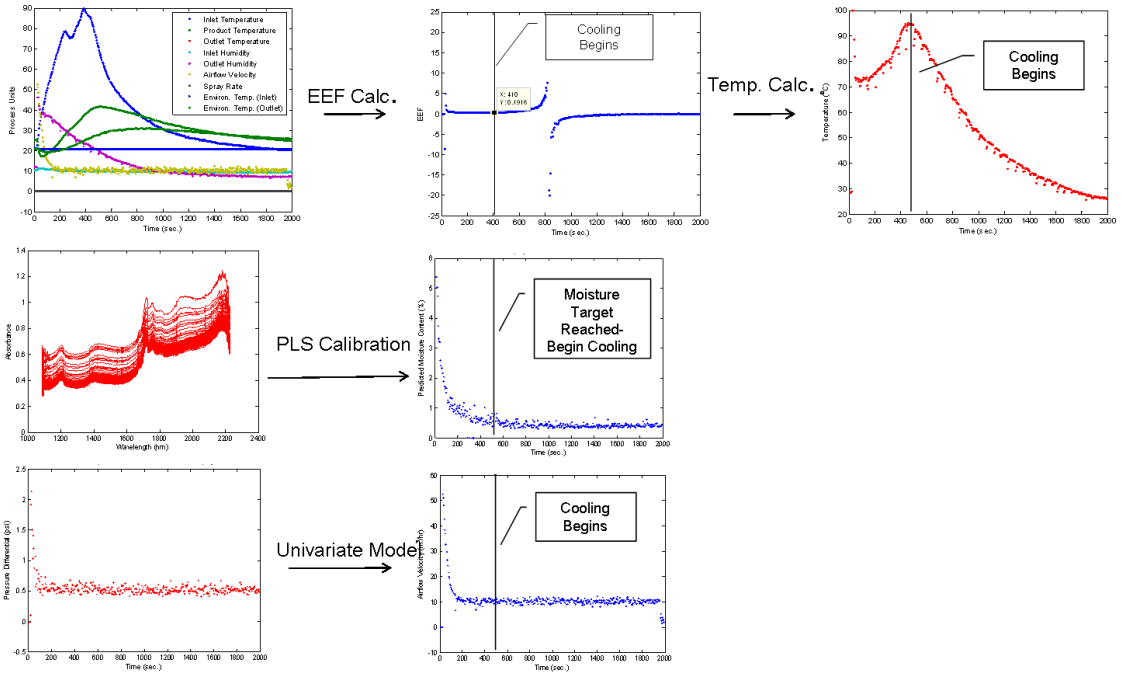

Figure 2.4. The calculations required for the three main controls of a fluid bed drying operation. The top row displays the calculations necessary to define the heated air temperature. Nine measurements are used to calculate the EEF value, which is then used to calculate the heated air temperature necessary to maintain the EEF at it set point. The second row displays the online moisture monitoring. NIR spectra are collected and generate moisture predictions via a PLS calibration. When the moisture threshold is reached, the process begins cooling. The third row displays the airflow calculations. A measurement of the pressure differential informs a univariate model to adjust the airflow velocity to maintain a constant bed height.

A 2^4 full factorial design was created to study the 4 drying factors (Table 2.2). It was assumed prior to experimentation that the third and fourth order interactions would not be significant variables, so the experiments to discover these effects were pooled for error estimates. Upon completion of the design, the experiment that resulted in the best granule properties (run order 16 in Table 2.2) was repeated with four additional experiments to increase the power of the models and estimate experimental precision.

Many granule, blend, and tablet response variables were measured as part of the NIPTE study to determine the effects of each unit operation. Reporting the significant process models that create the final design space will be addressed in chapter 3, so granule median particle size and a stability indicator were chosen as examples of product properties than can be controlled using the control system designed in this chapter.

The median particle size was determined by sieve analysis of 100 gram granule samples using U.S. standard test sieves (Fisher Scientific, Pittsburgh, PA, USA & VWR, West Chester, PA, USA). The samples were shaken using a sieve shaker (CSC Scientific, Fairfax, VA, USA) for five minutes at level five. Ten sieve cuts were collected for each sample (U.S. standard mesh #s: 18, 25, 35, 45, 60, 80, 120, 170, 230, and pan). A cumulative mass distribution was determined for each sample and the linear portion of the distribution was fit by linear least-squares to solve for the median (d_{m50}) value. The four replicate experiments were not sampled for particle size to conserve material for further studies. Therefore, the models to predict median particle size contain 16 samples (Table 2.2).

The chemical degradent for gabapentin is gabapentin lactam, so the gabapentin lactam concentration (mole %) in the final blends of these dried granule experiments was

measured as a response (stability). The lactam concentration was measured via high pressure liquid chromatography (HPLC) with a SpectraSystem P4000 quaternary gradient pump, AS3000 variable-volume autosampler, and UV 6000 LP photodiode array detection system (Thermo Fisher Scientific Inc., Waltham, MA, USA) by collaborators at the University of Iowa using a μBondpak CN-RP 3.9x300 mm column (Waters, Milford, MA, USA). The HPLC method used 5% acetonitrile in phosphate buffer as the mobile phase and a flow rate of 1.0 mL/mL and collected UV data at 210 nm. All of the drying experiments were not taken through the blending and compression unit operations for the NIPTE study because of material constraints, so the optimum point based on the granule particle size distribution, extreme points of the DOE, and all replicates were selected for further study. Therefore, the stability models contained 12 samples (Table 2.2).

2.4 Results and Discussion

The two response factors chosen for investigation in this study were selected to demonstrate the control systems' ability to create process models using efficient designs to predict two of the major properties that are affected during drying: granule physical properties and stability. The process model statistics for the response variables are presented in Table 2.3. Measured versus predicted plots and surface plots depicting the modeled experimental space for the response factors are presented in Figure 2.5.

The results for the prediction of median particle size were consistent with sieve analysis. This technique is associated with variability (note the variability within the four groups in Figure 2.5a) because a range of particle sizes are present within each sieve fraction. Despite the inherent reference variability, the control system was able to identify significant process factors that affected particles size. The two factors from the

drying DOE that were predictors of particles size were batch size and the end moisture target (EMT). The EMT variable was an expected factor when considering particle size because residual moisture in the granulation reduced the total drying time, reduced the amount of attrition among particles, and led to a higher probability of larger granules staying together.

Table 2.3. Model statistics for two of the response variables investigated during the drying DOE. (*Root mean squared error)

Model Statistics		
	Median PS (μm)	**Lactam Mole %**
Samples	16	12
Number of Model Parameters	2	3
R^2	0.67	0.78
RMSE*	15.12 μm	0.0023 Mole %
P-Value	0.0007	0.0057

The batch size (BS) variable's relationship with particle size was unexpected. For the drying operation, a larger mass may have created enough force at the bottom of the bowl during powder transfer to create stronger interactions, but the major influence more likely resulted from the high shear granulation unit operation. A change in batch size also changed the ratio of the powder fill height to bowl diameter, which changed the mixing characteristics in the granulator. The 200 gram difference in batch size in the DOE experiments was a significant difference in a four liter granulator bowl, so the mixing characteristics were substantially altered. This change had the greatest potential for affecting particle size from different batch sizes.

The models to predict granule stability (lactam mole %) were important for this study because the gabapentin lactam degradant is harmful to patients and must be limited to less than 0.4 mole %. All of the samples had significantly less than the required limit

(Figure 2.5b), however the time allotted for the study was inadequate to characterize long term stability. Therefore, it was important to understand the drying factors that caused changes in stability, so that the amount of lactam or the propensity to form the lactam over time as a result of manufacturing could be minimized.

Considering the complexity of the fluid bed drying unit operation, the reduced sample set, and the lack of a large number of replicate experiments, the model statistics for predicting stability were satisfactory (Table 2.3). The three factors that significantly affected granule stability include EEF, EMT, and their interaction term. The effect of the EEF variable was expected because it controlled the amount of thermal stress applied during fluid bed drying. Low EEF values, which correspond to higher heated air temperature (EEF = 0.175; high drying rate) increased the degradation kinetics and created a larger amount of gabapentin lactam in the final blends. The EEF variable was the second most influential drying factor, however, because NIR moisture predictions in the drying controls stop the drying process immediately when the granules reach their desired moisture threshold. Therefore, the granule temperatures were kept significantly lower than the heated air temperature due to the cooling imparted by evaporation (data not shown). Without the strict, automated controls and online spectroscopy, continued heating of dried granules could have resulted in elevated granule temperatures, which would have had a severe stability consequence.

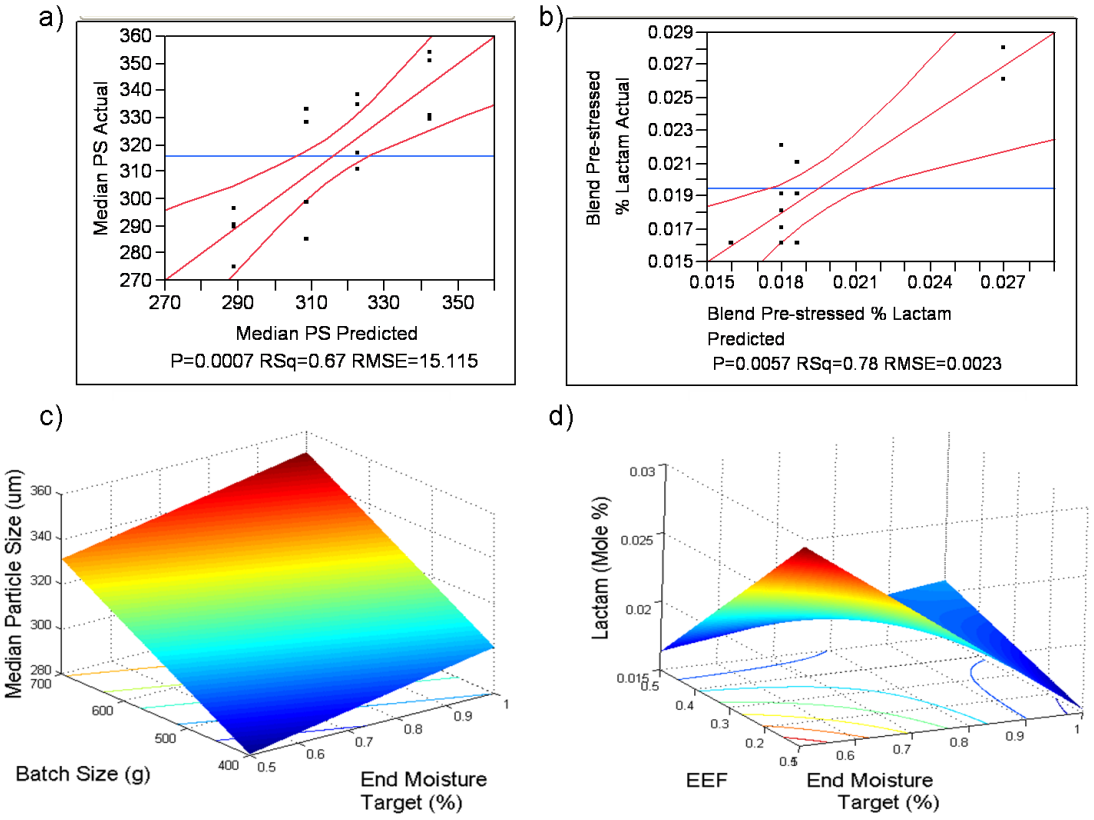

Figure 2.5. Measured versus predicted plots for **a)** Median Particle Size and **b)** Blend Pre-Stressed Gabapentin Lactam Concentration; and surface plots depicting the modeled drying space for the **c)** Median Particle Size and **d)** Blend Pre-Stressed Lactam Concentration. The red lines in **a)** and **c)** represent the 95% confidence interval for the best fit line. The blue line represents the mean response of the samples.

The EMT variable was the strongest predictor of gabapentin lactam mole % in the blend samples. Moisture in a pharmaceutical product often effects stability, but for this gabapentin formulation higher residual moisture resulted in more stable granules. This result was confirmed repeatedly throughout the NIPTE study and with several stability stress tests. Part of this effect in the drying operation was the result of suppressing the temperature of the granules with increased moisture, but increased stability was also observed with higher moisture content samples in stability tests where temperature was not a factor. In a separate stability study (data not shown) residual moisture was shown

to facilitate crystal recovery of damaged gabapentin crystals back to the stable crystalline form.[102] This prevented higher rates of chemical decomposition.

The significance of the interaction term resulted from experiments that were dried at higher temperatures (EEF = 0.175) and low residual moisture (EMT = 0.5%) whose samples had higher concentrations of lactam than would have been predicted by the main effects themselves. These factors must be controlled together to fully minimize the formation of the gabapentin lactam degradant.

To summarize the results of the process models, samples dried at higher temperatures resulted in similar drying times because of extended cooling (data not shown,) and resulted in increased lactam formation, so the data showed that drying at lower temperatures (EEF = 0.45; low drying rate) was beneficial. With low drying temperatures, the EPTT variable was irrelevant because the product temperature never increased beyond the 25°C threshold, so cooling was unnecessary. The batch size variable was more significant in the granulation unit operation than the drying unit operation. Residual moisture in the granules (high EMT) resulted in increased stability, but had poorer downstream product properties. High levels of residual moisture cause granules to exhibit poor flow behavior, resulting in poor mixing during blending and difficulty in filling dies of the rotary tablet press. Therefore, the drying DOE showed that it was important to control the EEF and EMT variables for optimum product properties, with lower drying temperatures and a moderate EMT threshold as the optimum drying condition.

The automated drying controls with the hybrid control strategy facilitated the creation of the drying DOE, the collection of data, and the analysis of the results. The

system allowed for all data measurements and calculations to be collected simultaneously at five second increments for all of the experiments, while providing a wealth of available data. The EEF calculations reduced three process factors – inlet air temperature, inlet air humidity, and heated air temperature – to a single factor, which reduced the DOE from 64 experiments to 16 experiments. In a real setting, a full factorial design with 6 factors would not be performed due to economic concerns, so the 64 experiments is an overestimate. Reducing the number of drying factors to 4 allowed a full factorial design to be performed, however, which significantly increases the information available to the analyst. All main effects and first order interactions could be investigated in an economically feasible design. This was important for the gabapentin study because there was a strong interaction between the EEF and EMT drying factors. This interaction may not have been indentified with a simple, less rigorous design, which would have limited the effectiveness of the control system.

The EEF calculations also eliminated the need to have laboratory controls of room temperature and humidity or a preconditioned air system. When the moisture content of the inlet air fluctuated, the heated air temperature was modified accordingly so that the capacity to absorb moisture within the dryer remained the same, thus controlling the drying rate. The controls made expensive building or equipment designs unnecessary.

Examining the heated air temperature profiles in Figure 2.6a for all 16 experiments demonstrates the importance of the EEF calculations for maintaining a constant drying mechanism across several days and environmental conditions. The experiments were randomized over only nine days, and the heated air temperature needed to maintain the two EEF levels was quite variable. Much of the offsets among the

temperature profiles within each EEF group in Figure 2.6a were the result of day to day fluctuations in laboratory humidity. The sinusoidal fluctuations resulted from the heater controls inability to maintain a constant temperature, while others are due to variable drying end points as part of the drying DOE. If the runs were extended over several climate seasons or years, these fluctuations become more severe and increase the importance of utilizing an EEF-based control system.

The high temperature (high drying rate, low EEF) EEF experiments had temperature differences between runs as large as 30^{o}C to maintain a constant drying rate, while the lower temperature (low drying rate, high EEF) EEF experiments had temperature differences as large as 20^{o}C between runs. Without the EEF controls, experiments would have been dried at a constant temperature and the drying rate would have fluctuated substantially between runs, resulting in product variability. Figure 2.6b illustrates the results of simulating the EEF and thus the drying rate of each of the batches if a constant temperature was used for all batches within each group.

The temperature profiles also display the importance of varying the temperature during a batch as moisture was removed from the powder bed. Batch processes are not steady state experiments, so the environment inside the FBP changed as more moisture was removed. The temperature had to be adjusted accordingly to maintain a constant drying rate. The NIR prediction of moisture content assured that the process ended precisely when it should. This limited the time that granules were exposed to heat energy with low moisture contents, and thus reduced the maximum temperature experienced by the granules resulting in stability improvements. All of these benefits are impossible

without the fully automated control system that combines first principle calculations with empirical modeling and rigorous designs of experiments.

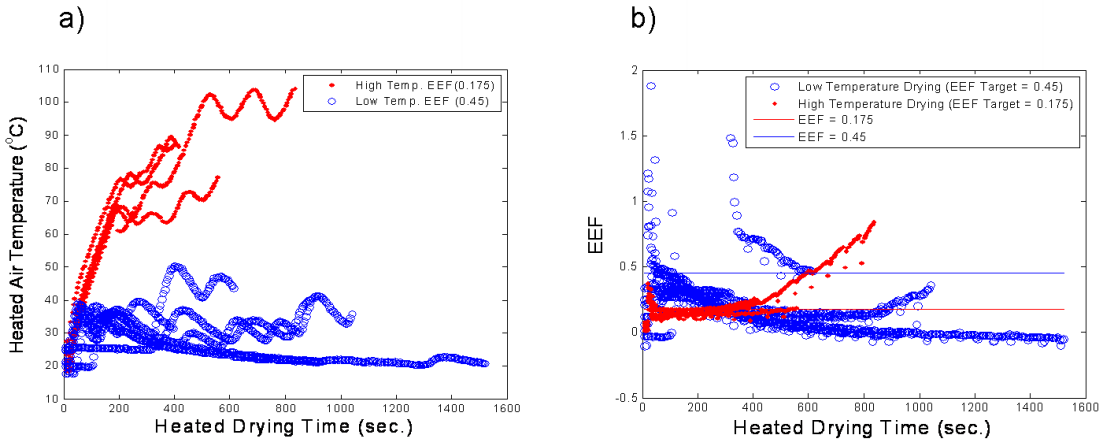

Figure 2.6. **a)** Heated air temperature profiles for the drying DOE separated by the EEF variable. **b)** Simulated EEF (and thus drying rate) of the 16 batches if a constant temperature was used for each of the two groups.

The hybrid control strategy also controlled the major factors and mechanisms that affect the granule properties – evaporation rate/drying mechanism, final granule moisture content, and the temperature of the product at discharge – instead of controlling process factors through empirical models that affect these important mechanisms. This allowed for greater control of product properties and reduced variability between similar runs, which facilitated data analysis and allowed for the extraction of significant drying factors with fewer experiments and increased statistical power.

2.5 Conclusion

This study demonstrated the creation of a hybrid control system for fluid bed processing that combines first principle calculations with online data collection and empirical modeling. The control system was fully automated and enabled tight control of granule properties affected by drying and potentially for all four fluid bed phases. The

system reduced the number of experiments necessary in the DOE by describing the drying environment with a single value, eliminated the need to install expensive preconditioned air systems, and provided a wealth of information about the process and the granule properties via online spectroscopy. The controls facilitated the identification of significant FBP factors for the definition of optimum process conditions, and reduced the risk of batch failures due to stability concerns.

The study demonstrated the control system's ability to control two significant responses from the drying unit operation – particle size and stability – on a formulation that required strict controls to minimize process induced instability. The results of the drying DOE showed low variability in granule properties among similar runs, which allowed significant process models to be developed with the reduced data set. The FBP controls and sensors facilitated the collection of precise data in an efficient manner, which would, ideally, be implemented for the creation of design spaces for the FBP unit operation.

Chapter 3: Development of a Statistical Tolerance Based Fluid Bed Drying Design Space

3.1 Introduction

Fully automated control systems are feasible and desirable in the pharmaceutical industry since the FDA encouraged the use of the guidelines put forth by the International Conference on Harmonisation (ICH-Q8)[2] that allow for operational flexibility within a validated design space. These systems offer opportunities for continuous improvement of the process and resulting quality improvement through drug product information gained during manufacturing via online process measurements to inform process adjustments to ensure constant product quality.[3] They have also been established to provide an economic incentive for pharmaceutical manufacturers.[1, 78-80]

The process set points within the automated control system are optimized using empirical design of experiments to establish the relationship to final product quality metrics called critical quality attributes (CQAs). The process parameters that are significant predictors of final product CQAs are identified as critical process parameters (CPPs), and they can be adjusted in real time to consistently meet product specifications despite external environmental fluctuations, raw material variability, equipment aging, and sensor drift. The entire modeled space is defined as the knowledge space. Specification limits are placed on the predicted CQAs, and the combinations of CPPs that manufacture product within the CQA specifications constitute the design space.

Appropriately developed designs of experiments (DOE) are typically necessary to elucidate the relationship between CPPs and CQAs in an economically efficient manner. An adequate number of experiments is necessary to investigate all possible main effects and first order interactions of the material and process variables that are identified during the initial risk analysis. Information regarding statistical power and the necessary confidence in the process model predictions is used to inform the DOE, so that optimized models can be created that fulfill user or process needs. A stochastic DOE approach is popular, where a large number of possible factors are screened efficiently, a secondary DOE more rigorously investigates the significant factors to create the knowledge space, and a third level of experiments are augmented to local regions of the knowledge space to increase statistical power in the future operating or design space. High order process interactions are rarely found to be statistically significant, so experiments to investigate these effects are typically eliminated to reduce development costs.

First principle equations that quantitatively describe the mechanisms that affect the product properties in a manufacturing process are desirable because they reduce the dimensionality of the final DOE. These equations describe the multidimensional effect of traditional input variables that would have to be investigated independently in a purely empirical design.

The current chapter will use a fully automated, hybrid control system to incorporate first principle controls for variable reduction and mechanistic control, while also using empirical models and online sensors to provide immediate feedback of product properties during the process. This control system was discussed extensively in chapter 2. The environmental equivalency factor (EEF)[29] was used to quantitatively describe the

thermodynamic environment within the fluid bed chamber that was the driving force for the removal of water, the major mechanism through which the fluid bed drying unit operation impacts product quality. It combined three variables that affected the water removal rate (heated air temperature, inlet air humidity, and airflow velocity) into a single value. This substantially reduced the number of experiments necessary for establishing a design space. In addition, the EEF allowed for direct scale-up because it is based in first principles, and eliminated the need for a preconditioned air system. Environmental fluctuations that impacted the air properties and affected the drying rate were measured, and process variables (airflow velocity and heated air temperature) were adjusted to maintain a constant drying rate. All of these qualities of the automated control system allowed for substantial reductions in developmental and equipment costs.

The addition of online sensors to the automated control system allowed for product properties to be monitored in real time, so that each phase of the unit operation could be ended reproducibly with respect to product CQAs. The current study used an online near infrared (NIR) sensor to monitor the water content of the pharmaceutical granules so that the drying operation was ended consistently from batch to batch. Additionally, a differential pressure transmitter was used to measure the pressure drop across the fluid bed, which was used to predict the airflow velocity that is necessary to maintain a constant bed height despite the substantial change in total mass and granule density within the dryer as water was removed. The automated control system reduced developmental costs, facilitated data collection and process understanding, enabled feedback control for continuous process improvement, and reduced the variability between batches. These advantages allowed for the identification of significant CPPs

with fewer repeat experiments during development and assured product quality in future production.

In addition to good development practices and process/product understanding, rigorous statistical analysis was necessary for robust modeling and design space identification. A design space is a global model that incorporates multiple process models that are limited by a series of specifications. As such, it must be developed rigorously and maintained over time.[98] Each prediction within the process models is associated with a finite amount of uncertainty, which increases as the predictions move away from the center of the model. Therefore, the knowledge space can be created to reflect either the confidence or risk associated with each point in the modeled space. The design space can then be defined by the area of the knowledge space that maximizes user confidence with regards to producing CQAs within specifications during future production. This chapter aims to provide a case study for this development.

This study was part of a project through the National Institute for Pharmaceutical Technology and Education (NIPTE) titled, "Development of Quality by Design (QbD) Guidance Elements on Design Space Specifications Across Scales with Stability Considerations." The research was originally published in the Journal of Pharmaceutical Innovation.[130] As part of the requirements of the project, the formulation was fixed, so the specifications on the CQAs had to be met through optimization of the CPPs of the manufacturing unit operations. The active pharmaceutical ingredient (API) for the formulation, gabapentin, was chosen due to its stability considerations,[89] so the CQAs for the product include stability indicators, final tablet release indicators, and manufacturing variables that include particle flow and tablet strength properties.

3.2 Materials and Methods

3.2.1 Granule Formulation

The granule formulation for this project consisted of 93.75% gabapentin (Hangzhou Starshine Pharmaceutical Co., LTD, Hangzhou, China, Batch 0803023) as the API and 6.25% hydroxypropyl cellulose (HPC) (Klucel EF, Ashland Aqualon Functional Ingredients, Wilmington, DE, USA) as the binder.

Gabapentin and HPC were granulated using a Collette MicroGral (GEA Pharma Systems, Columbia, MD, USA), a top driven high shear granulator with a 4L glass bowl. The two powders were dry mixed in the granulator by the impeller at 500 rpm for five minutes. Water was sprayed onto the dry mixture using a six inch atomization nozzle (Spraying Systems Co., Wheaton, IL, USA) with a stainless steel, flat, fan spray pattern and peristaltic pump (323U/D, Watson-Marlow, Wilmington, MA, USA). The water addition rate was 16 mL/min with 15 psi atomization air pressure, and the total water amount was 5% by weight. The impeller speed and chopper speed during granulation was 500 and 1000 rpm, respectively. The impeller and chopper continued mixing after spray granulation completed for a 30 second wet massing period.

3.2.2 Fluid Bed Processor (FBP)

Fluid bed drying was performed using a Diosna Minilab (Dierks & Sohne GmbH, Osnabruck, Germany) fitted with an 11 L insert. The FBP contained an internal EGE-Electronik series LN/LG air flow sensor (Spezial-Sensoren GmbH, Gettorf, Germany) to measure volumetric airflow velocity in the inlet air pipe. Three internal thermocouples measured temperature of the heated air, product temperature, and outlet air. Two series

RHL temperature/humidity transmitters (Dwyer Instruments, Inc., Michigan City, IN, USA) were added to the system to measure the temperature and humidity of the inlet and exhaust air, respectively. A series 616 differential pressure transmitter (Dwyer Instruments, Inc, Michigan City, IN, USA) was added to the system to measure the pressure drop across the fluid bed. Near infrared spectra were collected through the front viewing window of the FBP using a model NIR256L-2.2T2 spectrometer (Control Development Inc., South Bend, IN, USA). It is a 256 element photodiode array spectrometer with an extended InGaAs detector (1085-2229 nm). An external halogen light source (Control Development Inc., South Bend, IN, USA; HL-2000) was used with a fiber optic probe (Control Development Inc., South Bend, IN, USA; 6 around 1 reflectance probe).

The EEF value, drying end point (End Moisture Target (EMT) (%w/w), end product temperature target (EPTT) (^{o}C), and batch size (g) were factors varied in a 2^4 full factorial design to study the drying factors identified during risk analysis. The drying DOE and major results are listed in Table 3.1. The inlet airflow velocity was optimized to maintain a constant bed height, and is constant for a given batch size after the initial constant rate drying period. The 450 gram batch size required 5 m^3/hr, while the 650 gram batches required 10 m^3/hr. The filter bags were cleared using a backpressure pulse every 60 seconds at 30 psi for all experiments.

Table 3.1. The FBP DOE factor levels and response results. (Yellow = Experiments pooled for error estimates).

Two-level 4-Factor Full-Factorial Design										
Combination	**Run Order**	**Factors**				**Responses**				
		EEF (a)	End Moisture Target (%w/w) (b)	Batch Size (grams) (c)	End Prod. Temp Target (°C) (d)	Median PS (µm)	Blend Lactam (mole %)	Cohesion (kPa)	Tablet Crushing Force (kP)	
									Compaction Force (lbs F)	
-	8	0.450	0.5	450	25	289				
a	7	0.175	0.5	450	25	296				
b	13	0.450	1.0	450	25	328	0.019	0.377		
ab	14	0.175	1.0	450	25	298				
c	16	0.450	0.5	650	25	334				
ac	2	0.175	0.5	650	25	310	0.028	0.439	2815	5.52
									2195	4.52
									1435	3.42
bc	1	0.450	1.0	650	25	330				
abc	3	0.175	1.0	650	25	353	0.016	0.352	3045	3.84
									2230	5.48
									1700	4.34
d	11	0.450	0.5	450	30	274	0.016	0.273	2675	5.06
									1930	4.14
ad	12	0.175	0.5	450	30	290				
bd	4	0.450	1.0	450	30	284	0.021	0.4	2955	5.48
									2230	4.42
abd	5	0.175	1.0	450	30	332				
cd	10	0.450	0.5	650	30	338	0.022	0.289	3030	5.56
									2425	4.9
									1560	3.56
acd	6	0.175	0.5	650	30	316	0.026	0.725		
bcd	9	0.450	1.0	650	30	329	0.016	0.373		
abcd	15	0.175	1.0	650	30	351				

Two-level 4-Factor Full-Factorial Design (Continued)										
Combination	**Run Order**	**Factors**				**Responses**				
		EEF	End Moisture Target (%w/w)	Batch Size (grams)	End Prod. Temp Target (^{o}C)	Median PS (µm)	Blend Lactam (mole %)	Cohesion (kPa)	Tablet Crushing Force (kP)	
									Compaction Force (lbs F)	
Repeat	17	0.450	0.5	650	25		0.018	0.591	2655	4.4
									1840	3.9
									1540	3.3
Repeat	18	0.450	0.5	650	25		0.016	0.506	2870	5.6
									2160	4.4
									1540	3.4
Repeat	19	0.450	0.5	650	25		0.017	0.407		
Repeat	20	0.450	0.5	650	25		0.019	0.407		

3.2.3 Fluid Bed Processor Control System

The control system was set to sample data and send commands at a set frequency of 0.2 Hz. The FBP internal measurements, which included airflow velocity, heated air temperature, product temperature, and outlet temperature, were collected by an onboard programmable logic controller (PLC) (Allen-Bradley, Rockwell Automation, Milwaukee, WI, USA). The PLC also communicated the process set points to the FBP and contained the necessary ladder logic to run the heater and airflow motor. The PLC sent the FBP process measurements and the previous set points to the DeltaV Ver.9 digital automation system (Emerson Process Management, Equipment & Controls, Inc., Lawrence, PA, USA) via open process control (OPC).

DeltaV received the process measurements from the PLC and the 4-20 mA analogue outputs from the temperature/humidity sensors and differential pressure transmitter and transformed the inputs into digital readings. The DeltaV software contained internal logic for safety switches, alarms, and unit conversions, as well as PID controllers. It also tagged readings from the FBP and input controls from the control software to organize the communication between these two systems.

The control software for the system was SynTQ version 3.5 (Optimal, Bristol, UK). This software synchronized all measurements on the FBP at a fixed cycle, so that all measurements within a cycle could be compared for a specific moment. SynTQ received all process measurements from DeltaV via OPC and received NIR spectra directly from the spectrometer. SynTQ organized the raw data and sent the information to the necessary analytical models. All of the analytical and process models were compiled and input directly into the SynTQ software. The analytical models output

product or process property predictions, which were then used as inputs for the control models. The control models took the property predictions and predicted the process parameters necessary to continue the process along the desired trajectory for the next cycle. These parameter predictions were then passed via OPC from SynTQ to DeltaV, which translated the parameters for communication to the PLC, and the PLC finally adjusted the process parameters as directed. The automated, hybrid control system was described in detail in chapter 2.

3.2.4 Blending

A 3.5 quart, stainless steel, custom made V-blender was used to mix the dried granules with the extragranular excipients: 11.25% microcrystalline cellulose (MCC) (Comprecel M102D+, Mingtai Chemical Company Ltd., Taoyuan Hsien, Taiwan), 6.75% starch (Lycatab C, Roquette America Inc., Geneva, IL, USA), 4.50% HPC, 2.47% crospovidone (Polyplasdone XL, ISP Chemicals, Wayne, NJ, USA), 1.23% Poloxamer 407 (WLS Enterprises, Indianapolis, IN, USA), 1.01% talc (IMI FABI LLC/Mutcher Inc., Benwood, WV, USA), 0.79% magnesium stearate (Mg. St., Mallinckrodt, Hazelwood, MO, USA) for powder blending. The final concentration of Gabapentin in the blend was 67.49% and the final concentration of HPC (intra- and extra-granular) was 9.00%.

The blender was charged in the same order for each experiment, from the bottom of the vessel. Two SpectralProbe Process NIR spectrometers (Thermo Fisher Scientific, Wilmington, MA, USA; Serial numbers 1277 and 1502) were used to monitor the two arms of the v-blender in real time. The instruments collected 100 absorption values between 1,600 and 2,400 nm in reflection mode (interpolation from 8.71 to 7.31 nm) and

were triggered by a light intensity sensor (intensity rises when powder falls against the sampling window, enabling collection). Measurements were made through a sapphire window in the top of either arm of the blender. Spectra were sent wirelessly to a computer and imported into a custom-made acquisition and analysis system. The system had a response time of less than two seconds to allow real-time, online monitoring of the blend homogeneity.

The Root Mean Squared Error from the Nominal Value (RMSNV) algorithm was used to monitor blending.[99] The RMSNV statistic is a weighted, cumulative, pooled standard distance metric that takes into account the deviation of the predicted concentration of the major components (gabapentin, starch, MCC, and HPC) of a mixture from their target concentration, over a given number of rotations (1 minute of blending). The blend end point was determined by the trend of the pooled RMSNV of the two sensors and defined as the time at which the pooled RMSNV remained constant for a minimum of two minutes.

Models for predicting constituent concentration were developed using an efficient calibration approached, which is described in detail in chapter 6. The CLS/PLS algorithm for multivariate modeling was used to calculate the regression vector for each component.[100] All components except magnesium stearate were blended until the homogeneity criterion was reached. Finally, magnesium stearate was added and blended for five minutes in an additional lubrication blend that was not monitored by NIRS.

3.2.5 Tablet Compression

The final blends were compressed on a 16-station, instrumented tablet press (B2 Stokes, Key Industries, Farmingdale, NJ, USA), fitted with load cells to measure the

tablet compression forces. Only one set of 12.7 mm (0.5") flat faced, beveled edge, round punches and a cylindrical die was used. The press speed was kept constant at 27 rpm. Each batch was compressed at 3 compression forces (3000, 2000, and 1500 lbs.). Each compression force was allowed to stabilize and then tablets were collected during the steady state into one minute time bins for each of the six minutes of compression. Tablets were randomly sampled from each time bin for the crushing strength measurements.

3.2.6 Data Analysis

The analytical and process models that were included in the control system were created using MATLAB v. 7.1 R14 (The Mathworks, Natick, MA, USA) equipped with the PLS_Toolbox v. 3.0.4 (Eigenvector Research Inc., Wenatchee, WA, USA) and programs written in house. MATLAB code was compiled using MATLAB Compiler (The Mathworks, Natick, MA, USA) for use by the SynTQ software. The DOE results were analyzed using the statistical software, jmp 8 (SAS, Cary, NC, USA). All possible main effects and first order interactions were investigated, and variables were screened for significance using the p-value statistic at the α-level 0.10.

The NIR calibration for moisture content was created by sampling granules from several trial drying batches. The reference moisture content was measured using loss on drying (LOD) on a Computrac Max-2000 moisture analyzer (Arizona Instruments, Chandler, AZ, USA). The predictive model was created using partial least-squares (PLS) regression on standard normal variate (SNV) corrected NIR spectra. The model required one PLS latent variable.

A 2^4 full factorial design was created to study the 4 drying factors (Table 3.1). It was assumed prior to experimentation that all interactions above first order would not be significant, so the experiments to discover these effects were pooled for error estimates. Upon completion of the design, the experiment that resulted in the best granule properties (run order 16 in Table 3.1) was repeated with four additional experiments to increase the power of the models and estimate experimental precision.

Four response factors of each batch were selected during the initial risk analysis to represent the product CQAs. These properties included the median particle size of the finished granules, the amount of gabapentin lactam in the final blend (stability indicator), the cohesion of the final blend (flow indicator), and the mean tablet crushing strength for each compression force within each batch. The median particle size was determined by sieve analysis of 100 gram granule samples using U.S. standard test sieves (Fisher Scientific, Pittsburgh, PA, USA & VWR, West Chester, PA, USA). The samples were shaken using a sieve shaker (CSC Scientific, Fairfax, VA, USA) for five minutes at level five. Ten sieve cuts were collected for each sample (U.S. standard mesh #s: 18, 25, 35, 45, 60, 80, 120, 170, 230, and pan). A cumulative mass distribution was determined for each sample and the linear portion of the distribution was fit by linear least-squares to solve for the mass median (dm_{50}) value. The four replicate experiments were not sampled for particle size to conserve material for further studies. Therefore, the models to predict median particle size contained 16 samples (Table 3.1).

The chemical degradent for gabapentin is gabapentin lactam, so the gabapentin lactam concentration (mole %) in the final blends of these dried granule experiments was measured as the stability response. The lactam concentration was measured via reverse

phase high pressure liquid chromatography (HPLC) with a SpectraSystem P4000 quaternary gradient pump, AS3000 variable-volume autosampler, and UV 6000 LP photodiode array detection system (Thermo Fisher Scientific Inc., Waltham, MA, USA) at the University of Iowa using a μBondpak CN-RP 3.9x300 mm column (Waters, Milford, MA, USA). The HPLC method used 5% acetonitrile in phosphate buffer as the mobile phase and a flow rate of 1.0 mL/mL and collected UV data at 210 nm. All drying experiments were not taken through the blending and compression unit operations for the NIPTE study because of material constraints, so the optimum point based on the granule particle size distribution, extreme points of the DOE, and all replicates were selected for further study. Therefore, the stability models contained 12 samples (Table 3.1).

The flow measurements were performed at Rutgers University. Cohesion, which is inversely proportional to flowability, was measured using the shear cell module of an FT4 powder rheometer (Freeman Technology, Malvern, UK) on 85 cm^3 samples. Cohesion is the shear strength at zero consolidation stress of a bulk powder. It was measured using samples from the same dried granule experiments that were taken all the way through blending and compression, so their models also contained 12 samples (Table 3.1).

Tablet compression and subsequent crushing strength measurements were performed at the University of Maryland, Baltimore. The crushing strength was determined using a diametric compression tester (Model HT-300, Key International, Inc., Englishtown, NJ, USA). During the test, the compressive force is applied at a constant rate. Fifteen tablets were randomly sampled across all time bins within each compression force for each batch and tested to determine the mean crushing strength.

3.3 Results and Discussion

In the QbD paradigm of the pharmaceutical industry, the CQAs should reflect properties of the final product that have an impact on the effectiveness or safety of the product.[101] These include drug release properties, drug stability, batch uniformity, product physical properties that are conducive to handling, packaging, shipping, etc., and properties that ease the manufacturability of the dosage form (flow properties, etc.). It is unnecessary to optimize upstream product properties (e.g. granule particle size) that are not demonstrated to impact downstream manufacturing or final tablet properties. Upstream CPPs, such as fluid bed drying parameters, must be related to final product characteristics or downstream product properties that have a clear correlation to final product properties. For this reason, it is ideal to adjust drying CPPs in a DOE and take each batch all the way through tablet compression and release testing.

A 2^4 full factorial design (Table 3.1) was developed to investigate the four major drying factors that were identified as potential CPPs during risk analysis. These factors included the EEF set point (EEF), the end moisture target (EMT), the end product temperature target (EPTT), and the batch size (BS). The EEF set point controlled the drying rate, and the automated controls used the EEF set point to calculate the heated air temperature necessary to provide the drying rate, given the airflow velocity and inlet air humidity. The EMT was the NIR predicted moisture content (%w/w) of the granules that ended the heating cycle and sent the process into the cooling phase. The EPTT was the product temperature (^oC) that ended the drying unit operation. It controlled the length of the cooling phase. Finally, the batch size (g) was investigated over a small range based on the usable capacity of the FBP.

High order interaction terms (2nd order and above) were not anticipated to be significant, so experiments to investigate these effects were pooled as repeat experiments for error calculations. This provided an efficiency benefit using *a priori* information. Additionally, four true repeat batches were manufactured to determine experimental repeatability, which created a total of 20 experimental batches (Table 3.1).

Ideally, all batches would have been blended and compressed, but due to material and time constraints put on the NIPTE research project, only 12 of the 20 batches were blended and compressed. The midpoint experiments and all extremes of the DOE were chosen for full tablet manufacturing, and all batches to investigate the interaction of the EEF and EMT variables, because these were identified as the most likely CPPs during risk assessment.

The CQAs were identified during the initial risk assessment and were refined after initial trial experimentation. Gabapentin stability, reflected by limiting the amount of the gabapentin lactam degradant in the product, was identified as the most important CQA. Tablet and shelf life stability results were not available for this portion of the project, so the furthest downstream stability data was the amount of gabapentin lactam (mole %) in the final blends. As mentioned previously, 12 of the 20 batches were blended.

Table 3.2. Model statistics for the CQA response variables investigated during the drying DOE. (*Root mean squared error)

Model Statistics				
	Median PS (µm)	**Lactam (Mole %)**	**Cohesion (kPa)**	**Tablet Crushing Forces (kP)**
Samples	16	12	12	19
Number of Model Parameters	2	3	3	4
R^2	0.67	0.78	0.73	0.95
RMSE*	15 µm	0.0023 Mole %	0.077	0.23
P-Value	0.0007	0.0057	0.0109	<0.0001

The process model to predict gabapentin lactam concentration in the final blends based on drying CPPs, as with all process models, were calculated using mixed (forward and backward) stepwise regression in jmp 8. Statistical results for all optimized process models are presented in Table 3.2, while the prediction results are presented in Figure 3.1.

The drying CPPs with regards to the stability CQA were the EEF and EMT variables. The EEF variable controlled the amount of heat energy used during drying (drying rate), so increased heat energy (low EEF) resulted in increased gabapentin lactam formation. The amount of moisture allowed to remain in the granules was inversely proportional to the amount of gabapentin lactam formed. Increased moisture reduced the temperature experienced by the granules during drying, reduced the drying time and thus particle collisions, and allowed for crystal healing of the gabapentin molecules that had been damaged during high shear granulation, which reduced the rate that the degradation pathway progressed.[102] There was also a strong interaction between the EEF and EMT variables, causing curvature in the process model (Figure 3.1a). Therefore, the lowest amount of gabapentin lactam was formed at high EEF (low temperature) and larger amounts of residual moisture over the studied range.

The second highest priority among the CQAs was tablet crushing strength. The formulation had a high dose of gabapentin, which limited the mechanical strength of the finished tablets. Additionally, gabapentin is a BCS class III drug (high solubility, low permeability), so tablet disintegration and dissolution were not an issue with any of the investigated batches. The drying CPPs for the prediction of tablet crushing strength were the same as the stability process model (EEF, EMT, and interaction term) (Figure 3.1b).

As expected, increased residual moisture resulted in stronger tablets. Higher drying rates (low EEF, higher temperatures) also resulted in stronger tablets, which may have resulted from a decrease in drying time and less work hardening of the granules during drying. Therefore, high EMT and low EEF are ideal in terms of the tablet crushing strength CQA because it was necessary to maximize the possible tablet strength.

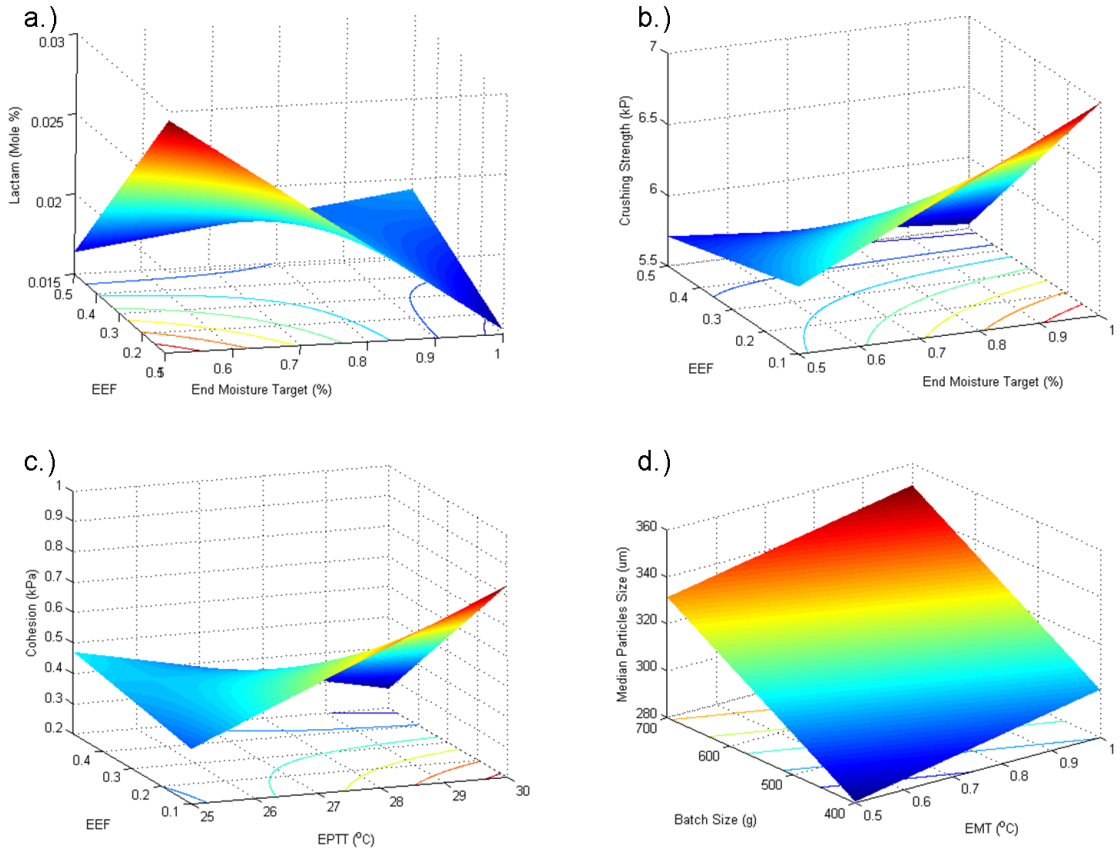

Figure 3.1. The process models (knowledge space) for each of the 4 CQA response factors: **a.)** Gabapentin Lactam Concentration **b.)** Tablet Crushing Force **c.)** Blend Cohesion **d.)** Granule Median Particle Size.

The third highest priority among the CQAs was final blend flow properties, because these impacted tablet manufacturability and the ability to fill compression dies efficiently. Powder cohesion, which is inversely proportional to powder flow, was used as the CQA for final blend flow properties. The EEF, EPTT, and their interaction term

were the significant drying CPPs that predicted blend cohesion (Figure 3.1c). Drying batches that were not allowed to cool to ambient conditions (high EPTT) had poor flow compared to batches that were cooled. The upper right corner of the process model in Figure 3.1c shows good flow at high EPTT, but this area reflected the results of drying at low temperatures. These batches were dried at close to ambient temperatures, so the product temperature never increased to require cooling, despite having the same ending target. Therefore, the ideal combination of drying factors with regards to the flow CQA is low EPTT at all EEF levels except for the absolute highest (slowest drying).

The final CQA for the drying unit operation was the median particle size of the dried granules. Increased drying times or batches with increased energy input can cause elutriation of the granules, which results in an increase in the fraction of fines. Some granule attrition is desirable, however. The force of a granule collision is proportional to the mass of particles, so the largest particles have a higher probability of breaking. This allows large clumps to break and return to the middle of the particle size distribution. A finite number of fine particles were also necessary to assure efficient packing inside tablet dies during the compression operation leading to low tablet weight variability.

The batch size and EMT variables were identified as drying CPPs to predict the median particle size of the dried granules (Figure 3.1d). The effect of residual moisture was expected. Increased moisture provided more interactions between particles and shortened drying times, which resulted in reduced granule attrition and elutriation. It was determined during data analysis that the batch size effect was a function of the wet granulation unit operation, not fluid bed drying. A change in batch size inherently changed the high shear granulator bowl fill height to diameter ratio, which changed the

mixing dynamics and effected moisture distribution. Therefore, the batch size variable was not considered significant for the drying unit operation.

Figure 3.1 constitutes the total knowledge space of the CQAs obtained through investigation of the DOE. The predicted value of all four CQAs can be determined within the given knowledge space at any combination of the fluid bed drying CPPs. The single point prediction drying design space can now be identified by using the specifications of all four CQAs to limit the process models to determine the combination of CPPs that are predicted to result in CQAs that pass specifications.

The USP specification for the amount of gabapentin lactam in the final product is less than 0.4 mole % over the course of a 2 year shelf life. Using projections from the initial lactam formation kinetic studies for this formulation (data not shown), the specification for gabapentin lactam in the final blend was less than or equal to 0.02 mole %. The tablet crushing strength specification was an industry standard that requires tablets to have a crushing strength of at least 6 kiloponds to be feasible for future handling, packaging, or film coating. The specifications for cohesion and median particle size were determined from trial batches that were compressed on a rotary tablet press. Blend cohesion was required to be less than 0.45 kPa, while granule median particle size was required to be between 250 and 500 μm. With these specifications, the single CQA design spaces for the fluid bed drying unit operation are presented in Figure 3.2.

From Figure 3.2 and from the rankings of the CQAs, it can be seen that drying at low temperatures (high EEF) with higher EMT values was necessary to prevent gabapentin lactam formation. This decision to dry at low temperatures and allow residual moisture rendered the EPTT variable insignificant because granules dried at low

temperatures never reached the high temperature threshold (30^{o}C). The batch size variable had already been eliminated as a CPP, so the final drying CPPs were the EEF and EMT variables. The tablet crushing strength specification was also satisfied at high EMT values, while needing medium EEF values. All batches met the granule median particle size specification. For the cohesion specification, only the low EPTT section was relevant, so all EEF values except for the very highest (lowest drying rate, upper-left-hand corner of Figure 3.2c) satisfied the flow CQA. The final single point prediction fluid bed drying design space where the combination of the two fluid bed drying CPPs are predicted to produce all CQAs within specifications is displayed in Figure 3.3.

It is important to note, however, that the knowledge/design space is a combination of process models, which by definition, contain uncertainty. This uncertainty should be reflected in the final design space. The range over which an experimental result may reside around the prediction can be defined be either the confidence interval or the tolerance interval, and the magnitude of either range depends on the level of confidence the user requires, the error associated with the model, the pure process/experimental variability, the number of samples in the calibration set, the structure of the calibration set, and the distance from the center of the model in the experimental space. Uncertainty can be reduced in certain areas of the modeled space by including a large number of data points to reduce model error in this region, but there is a diminishing return. A model cannot produce lower error than reference error or pure process variability. A completed DOE can be augmented with additional samples within desired regions of the modeled space to reduce uncertainty in important regions.

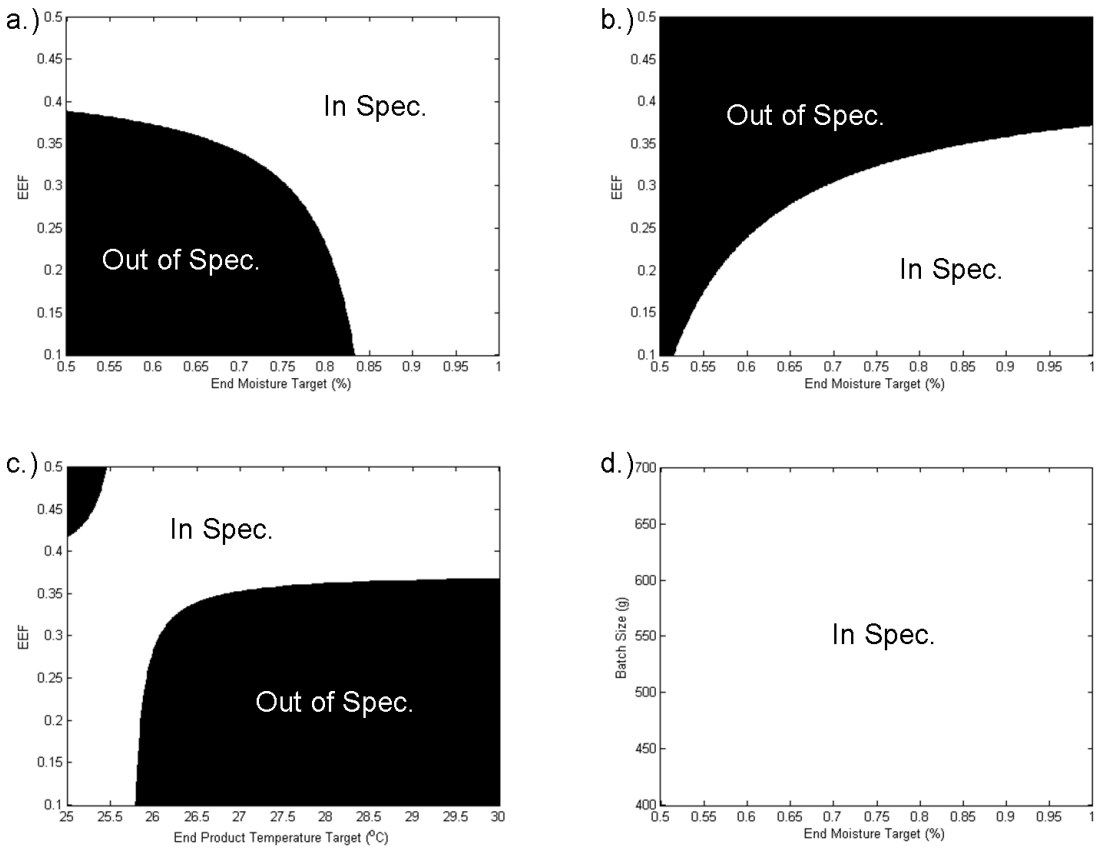

Figure 3.2. The single point prediction design space for each of the 4 CQA response factors: **a.)** Gabapentin Lactam Concentration **b.)** Tablet Crushing Force **c.)** Blend Cohesion **d.)** Granule Median Particle Size

In linear modeling, the user often assumes a normal distribution of error (pure random error) around the predictions, so the width of the confidence or tolerance interval is defined by the percent likelihood that the interval will contain the actual experimental result. A typical confidence/tolerance level is 95% ($\alpha = 0.05$), but the level of confidence/tolerance should be defined by the user to fulfill the needs of a given application. As the level of confidence/tolerance required increases, a wider interval is used. The intervals around predictions are not constant either. As experiments move away from the center of the model, the resulting intervals become wider. Linear models define step changes of the response variable away from the mean that result from step

changes in the independent variables. Therefore, larger distances from the mean are associated with larger uncertainty.

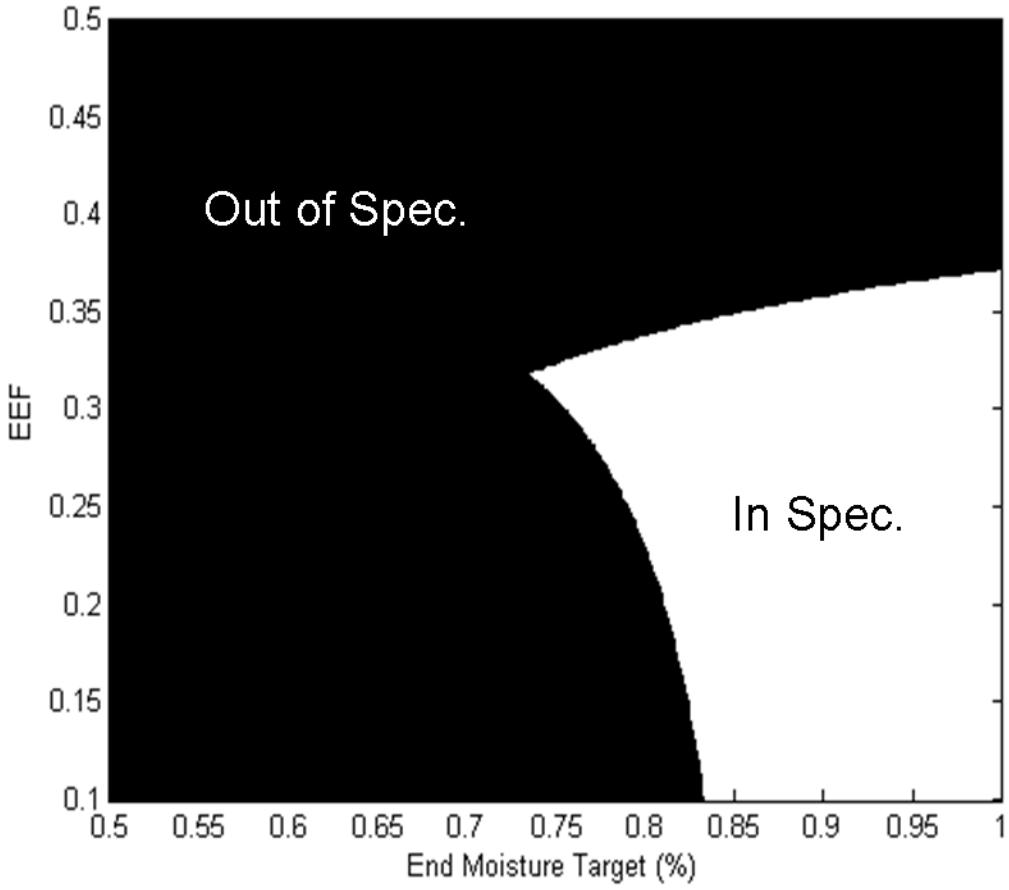

Figure 3.3. The single point prediction design space where the predictions of all 4 CQAs meet specifications for the combination of the 2 fluid bed drying CPPs (EEF & EMT).

A confidence interval reflects the probability that the mean of all future batches will reside within the given range.[103]

$$\hat{y} \pm t_{n-1,1-\alpha} S.E. \tag{3.1}$$

In equation 3.1, $\hat{y}$ is the point estimate or prediction, t is the critical value of Student's t distribution that satisfies α, which is the accepted risk of committing a Type I error, n is the number of samples, and $S.E.$ is the estimated standard error of the predictions. For

manufacturing processes, the confidence interval does not adequately mitigate process risk. While the user may have a high degree of confidence that the mean of all future responses meets specifications; the risk of a single batch failing specifications may not have been mitigated. Therefore, tolerance intervals, which are wider than confidence intervals, provide the more appropriate risk evaluation tool to assure batch quality during future production.

$$\hat{y} \pm k \cdot s \tag{3.2}$$

In equation 3.2, $\hat{y}$ is the point estimate or prediction, s is the standard deviation of the predictions, and k defines the width of the tolerance interval and is calculated by

$$k = \sqrt{\frac{(n-1)\left(1+\frac{1}{n}\right)z^2_{(1-p)/2}}{\chi^2_{\gamma,n-1}}} \tag{3.3}$$

where n is the number of samples, z is the critical value of the standard normal distribution that includes p, the desired proportion of the population, χ^2 is the critical value of the chi-square distribution that is exceeded by probability γ, which is the necessary percent confidence. Tolerance intervals reflect the probability that a certain portion (defined by the user) of the future population of batches will meet specifications.[67]

Due to model uncertainty, it is not rigorously correct to define a design space by the portion of the knowledge space where the predictions alone satisfy the CQA specifications (Figure 3.3). A tolerance interval must be defined for each prediction, and the probability that a portion of future experimental results falls outside of the CQA specifications should be considered. For example, it is possible to define 95% tolerance intervals around all of the predictions within the gabapentin lactam knowledge space

(Figure 3.4). This tolerance interval reflects the range around each prediction where there exists a 95% probability that 95% of the future batch population will meet the required CQA specifications. The specification on the gabapentin lactam is a one sided criterion (<0.02 mole %), so the upper tolerance limit is the only side that is important. For any combination of CPPs within the knowledge space, there is a 95% chance that the amount of gabapentin lactam produced in 95% of the future batches is below the upper confidence surface in Figure 3.4. This surface should be used to define the one factor, tolerance design space, not the actual predictions.

A continuous "tolerance design space" that reflects the probability that a given combination of CPPs will produce CQAs within specifications was produced by creating tolerance surface plots for each process model (Figure 3.5), and then combining the results for the final tolerance design space (Figure 3.6) that reflects the overall probability of 95% of future batches meeting all 4 CQA specifications. The probability results in Figure 3.5 were a function of model uncertainty for each point in the model and also the predicted distance from the specification threshold. If a combination of CPPs resulted in less than 50% probability of success, the resulting response was forced to zero.

Figure 3.6 reflects the final probability that the combination of the two significant fluid bed drying CPPs will result in acceptable CQAs for all four response factors. Figure 3.6a reflects the overall probability when each of the 4 CQAs was weighed by their relative risk (lactam 90%, crushing strength 5%, cohesion 2.5%, and particles size 2.5%). For this reason, Figure 3.6a most closely resembles the tolerance surface of the gabapentin lactam knowledge space within the region that is acceptable for all CQAs. This figure is recommended as the most rigorous form of a design space. The user can

now make an informed decision regarding an acceptable combination of CPPs that results in an adequate probability that quality product will be produced in future batches.

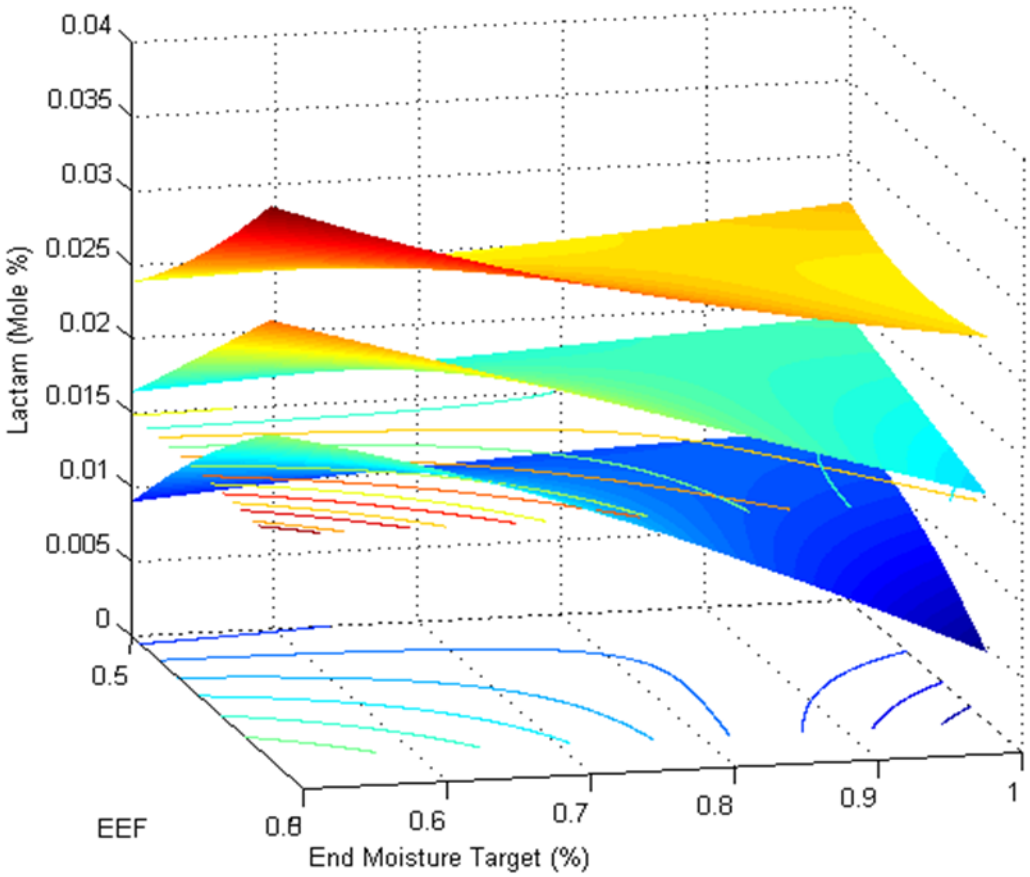

Figure 3.4. The process model (knowledge space) for the prediction of gabapentin lactam concentration with the 95% tolerance interval of 95% of the population displayed around the predictions.

Figure 3.6b reflects the overall probability surface if all CQAs were given equal weight. The overall probability of success goes down when the chance of any of the 4 CQAs being out of specifications are considered simultaneously. Therefore, the final probability surface or design space has a much lower probability of success. This calculation assumes that the four CQAs are orthogonal and completely independent, and therefore the probability of failure for each CQA does not overlap. It considers the

probability of success using four independent comparisons, or the Bonferoni method of multiple comparisons.[104] This is the most pessimistic measure of future success, so it may put overly restrictive limits on the manufacturing process. In reality, the four CQAs are correlated as shown in Figure 3.7, so the probability of a portion of the batch failing each CQA overlaps, and the probability of success is higher than considering four independent comparisons. As expected, granule median particle size was 50% correlated to tablet crushing strength, and tablet crushing strength is also 50% correlated to gabapentin lactam formation.

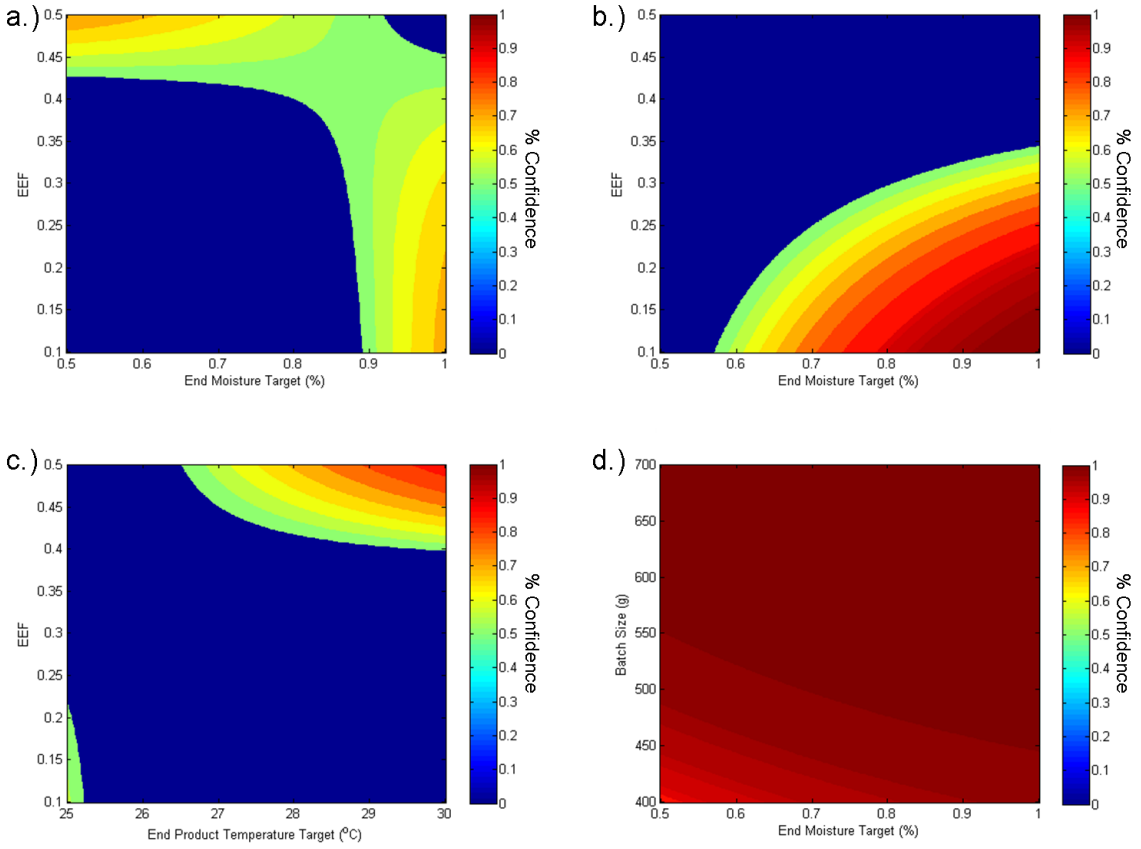

Figure 3.5. Tolerance surfaces (design spaces) that display the percent probability that the combination of CPPs will produce 95% of future batches within CQA specifications for **a.)** Gabapentin Lactam Concentration **b.)** Tablet Crushing Force **c.)** Blend Cohesion **d.)** Granule Median Particle Size.

It must be noted that Figure 3.6 represents the real probability of producing batches within specifications during future manufacturing under two different criteria. If the desired or necessary probability is not achieved with the optimum criterion, then the original calibration set must be augmented and the model regenerated to reduce model uncertainty within a local region of the knowledge space.

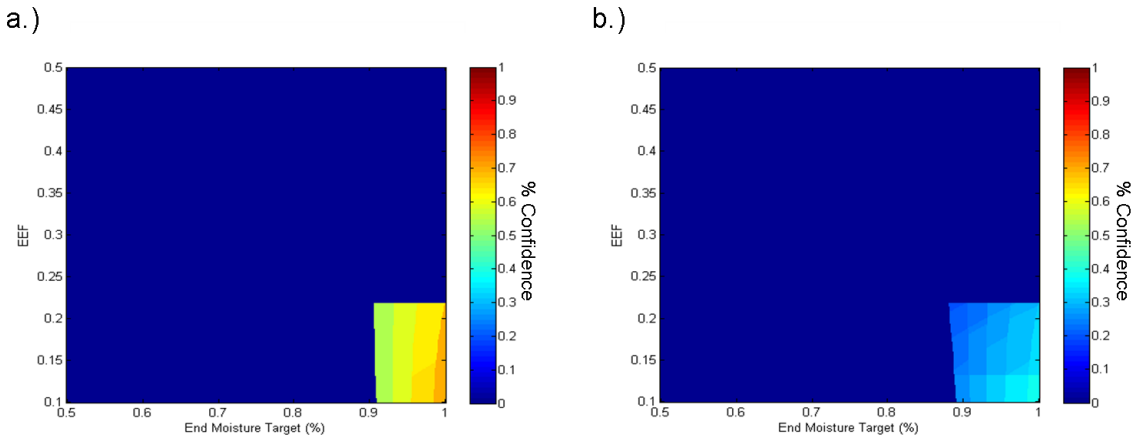

Figure 3.6. The final tolerance surface, which creates the final design space. It displays the probability that the combination of the 2 fluid bed drying CPPs (EEF & EMT) will produce 95% of future batches with all 4 CQAs within specifications: **a.)** Shows the probability weighed by the risk of each CQA (Lactam 90%, Crushing Strength 5%, Cohesion 2.5%, Particle Size 2.5%) **b.)** Shows the probability when the 4 CQAs are given equal weight.

When determining the final operating space, other factors such as manufacturing cost, efficiency, equipment constraints, and ease of processing may also be considered to reduce the final design space further into an operating target. Finally, the models that create a final design space, as with all models, must be continually maintained and updated as equipment ages, raw materials change, or new sources of variance are identified.

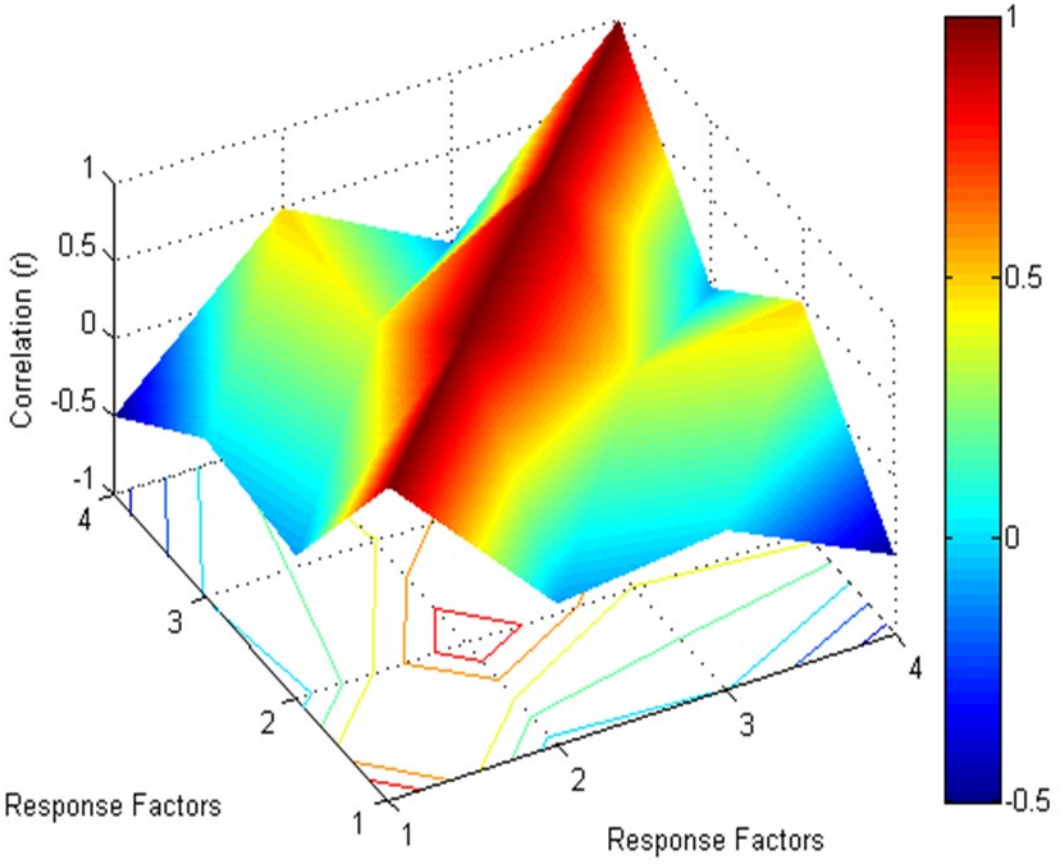

Figure 3.7. The correlation matrix, which displays the magnitude of the correlation between response factors (CQAs). Response Factor 1 = Median Particle Size; Response Factor 2 = Gabapentin Lactam %; Response Factor 3 = Cohesion; Response Factor 4 = Tablet Crushing Strength.

3.4 Conclusions

This chapter provided a demonstration of the development of a rigorous design space for a single pharmaceutical unit operation within the QbD paradigm. The hybrid controls and the design of experiments enabled four drying factors and all first order interaction terms to be investigated with a limited number of experiments. The results of the small scale experimentation allowed the number of drying factors identified during risk analysis (4) to be reduced by 50% for production control and future scale up

experimentation. The automation system allowed the drying process parameters to be modified in real time to control the drying rate in the presence of external environmental fluctuations. Further, the chapter has demonstrated reduced dimensionality of the DOE, reduced experimental variability that allowed identification of significant factors with fewer repeat experiments, eliminated the need for a preconditioned air system, and increased total process understanding.

The study also showed the importance of using statistics to appropriately implement the process models that create the knowledge space and final design space. Uncertainty must be understood throughout the knowledge space and reflected in its use. Thus, a rigorous design space can be identified using tolerance surfaces that maximizes the probability of future success and reduces the risk of process failure. All models must be continually maintained to ensure robustness throughout their use. These principles must be implemented to ensure product quality in a QbD pharmaceutical application.

Chapter 4: Efficient Scale-Up of a Fluid Bed Drying Laboratory Scale Design Space

4.1 Introduction

The benefits of automated control systems that are developed rigorously have been discussed in the previous chapters. They are the most efficient method for ensuring continuous improvement of a manufacturing process and for ensuring constant product quality. Without identifying and measuring variability in real-time and using that information to adjust the process accordingly, batch to batch and intrabatch variability increases significantly. Pharmaceutical companies are beginning to accept the benefits of these systems and provide the initial investment required. Quality by Design (QbD) and real-time release (RTR) applications are climbing significantly.[105]

Rigorous and well constructed design of experiments (DOE) are required to define and validate the relationship between drug product raw materials and manufacturing critical process parameters (CPPs) with drug product response factors known as critical quality attributes (CQAs). Developmental studies require a substantial investment by the pharmaceutical company, so it is imperative for the experimentation to be as efficient as possible while still providing the necessary information and statistical confidence. Leveraging the initial investment is important so that the maximum amount of information and monetary return can be realized.

Developing the raw material and manufacturing controls is most efficient at laboratory scale due to equipment and material costs, but the need to scale up the initial

controls for use at full production scale is a significant challenge that must be overcome to maximize the utility of initial laboratory scale studies. This challenge has been extensively studied in traditional batch manufacturing,[106, 107] but a universal solution has yet to be achieved. These issues continue to be studied in pharmaceutical development.

The fluid bed drying unit operation has several challenges that make scale-up difficult. Changes in equipment geometry can drastically change the fluid dynamics and mixing characteristics, while the size of the production scale equipment creates temperature gradients and hot spots than can impact product quality. If the challenges provided by process scale-up cannot be minimized, development in the quality by design (QbD) paradigm becomes exponentially more expensive and less feasible.

Chapter 2 developed an automated hybrid control system for the fluid bed granulation and drying unit operation that can be developed efficiently at laboratory scale and assures product quality. The control system used the environmental equivalency factor (EEF)[29] to control the rate of water addition/removal despite changes in the input air properties from batch to batch to control the major mechanism through which the fluid bed unit operation impacts product quality. Additionally, online near infrared spectroscopy (NIRS) was used to monitor the granule moisture content to provide immediate process feedback and define phase end points within the manufacturing process. The control system reduced the variability between replicate batches, allowing CPPs to be identified in fewer experiments, reduced the dimensionality of the DOE, enabled the calculation of process models with a minimum number of experiments, and rendered a pre-conditioned air system unnecessary.

In chapter 3, the hybrid control system was used in combination with DOE and rigorous statistical analyses to define a design space for the fluid bed drying of a gabapentin formulation at laboratory scale. The development process provided substantial process understanding, reduced the CPPs identified during risk analysis by 50%, and created a statistical tolerance surface so that an informed decision could be made regarding the design and/or operating space. These previous studies have provided a template for rigorous and efficient pharmaceutical development of unit operations, but the value of these advances is significantly reduced if the challenges of scale-up are not overcome.

The current chapter aims to demonstrate how the hybrid control system and laboratory scale design space can be efficiently scaled-up using the process understanding gained during development. The first principle controls within the hybrid system are directly scaleable, a substantial reason that first principle controls are universally desirable. The random fluctuations within a batch are wider at larger scale, resulting from larger environmental gradients within larger pieces of equipment, but median responses are statistically indistinguishable. The process data gained from online spectroscopy can also provide feedback, regardless of scale, to control the mechanisms of the manufacturing process. More importantly, however, is that the information gained from the empirical models gleaned from the laboratory scale DOE can be leveraged during scale-up. Half of the originally identified CPPs were eliminated at laboratory scale, and it is unlikely that a main effect would be significant at one scale and not at another. Therefore, the number of experiments that are needed at larger scales can be reduced by 75% when comparing full factorial designs (2^2 versus 2^4).

A stochastic approach to scale-up can also provide enhanced process understanding and more efficient development. An intermediate scale can be undertaken to inform the stakeholders how empirically derived predictors will have to be transferred as the scale increases without substantial material costs being incurred. The CPPs and their interactions identified at laboratory scale should still be significant predictors at all scales. However, the regression coefficients that describe their effect on the CQAs typically require adjustments. The shape of the transfer function is expected to be similar across substantial scale-up, with the magnitude of the transfer function being proportional to the magnitude of the scale-up. Therefore, much of the process understanding needed for a successful scale-up can be determined by performing an initial, intermediate scale-up study.

The range studied for each CPP can be significantly reduced upon scale-up. The statistical analysis performed to define the laboratory design space provides the necessary proof of the important region of the knowledge space. This area may shift upon scale-up, but the entire knowledge space studied at laboratory scale does not have to be replicated. Therefore, a local space that encompasses the initial design space can be studied during the initial scale-up, which can inform the stakeholders how the design space will shift and increases the statistical confidence within the local space. Upon scale-up to production scale, an even narrower region is expected to be probed using DOE. That region is defined by the initial design space and the transfer functions calculated during the initial scale-up.

This study was part of a project through the National Institute for Pharmaceutical Technology and Education (NIPTE) titled, “Development of Quality by Design (QbD)

Guidance Elements on Design Space Specifications across Scales with Stability Considerations." The research was originally published in the Journal of Pharmaceutical Innovation.[131] As part of the requirements of the project, the formulation was fixed, so the specifications on the CQAs had to be met through optimization of the CPPs of the manufacturing unit operations. The active pharmaceutical ingredient (API) for the formulation, gabapentin, was chosen due to its stability considerations,[89] so the CQAs for the product include stability indicators and manufacturing variables that include particle flow and tablet strength properties.

4.2 Materials and Methods

4.2.1 Pharmaceutical Formulation

The granule formulation for this project consisted of 93.75% gabapentin (Hangzhou Starshine Pharmaceutical Co., LTD, Hangzhou, China, Batch 0803023) as the API and 6.25% hydroxypropyl cellulose (HPC) (Klucel EF, Ashland Aqualon Functional Ingredients, Wilmington, DE, USA) as the binder. The granules, which comprise 71.99% of the final blend, were combined with the extragranular excipients - 11.25% microcrystalline cellulose (MCC) (Comprecel M102D+, Mingtai Chemical Company Ltd., Taoyuan Hsien, Taiwan), 6.75% starch (Lycatab C, Roquette America Inc., Geneva, IL, USA), 4.50% HPC, 2.47% crospovidone (Polyplasdone XL, ISP Chemicals, Wayne, NJ, USA), 1.23% Poloxamer 407 (WLS Enterprises, Indianapolis, IN, USA), 1.01% talc (IMI FABI LLC/Mutcher Inc., Benwood, WV, USA), and 0.79% magnesium stearate (Mg. St., Mallinckrodt, Hazelwood, MO, USA) - for powder blending. The final

concentration of Gabapentin in the blend was 67.49% and the final concentration of HPC (intra- and extra-granular) was 9.00%.

4.2.2 High Shear Granulation

4.2.2.1 Laboratory Scale (400-600 g batch size)

Gabapentin and HPC were granulated using a Collette MicroGral (GEA Pharma Systems, Columbia, MD, USA), a top driven high shear granulator with a 4 L glass bowl. The two powders were dry mixed in the granulator by the impeller at 500 rpm for five minutes. Water was sprayed onto the dry mixture using a six inch atomization nozzle (Spraying Systems Co., Wheaton, IL, USA) with a stainless steel, flat, fan spray pattern and peristaltic pump (323U/D, Watson-Marlow, Wilmington, MA, USA). The water addition rate was 16 mL/min with 15 psi atomization air pressure, and the total water amount was 5% by weight. The impeller speed and chopper speed during granulation were 500 and 1000 rpm, respectively. The impeller and chopper continued mixing after spray granulation completed for a 30 second wet massing period.

4.2.2.2 Intermediate Scale (1 kg batch size)

Gabapentin and HPC were granulated using a Collette High Shear Mixer Gral 10 (GEA Pharma Systems, Columbia, MD, USA), a top driven high shear granulator with a 10 L stainless steel bowl. The two powders were dry mixed in the granulator by the impeller at 420 rpm for five minutes. Water was sprayed onto the dry mixture using a six inch atomization nozzle with a stainless steel, flat, fan spray pattern and peristaltic pump (Spraying Systems Co., Wheaton, IL, USA). The water addition rate was 28.5 mL/min with 40 psi atomization air pressure, and the total water amount was 5% by weight. The

impeller speed and chopper speed during granulation were 420 and 1500 rpm, respectively. The impeller and chopper continued mixing after spray granulation completed for a 30 second wet massing period.

4.2.2.3 Pilot Scale (9.72 kg batch size)

Gabapentin and HPC were granulated using a Collette High UltimaGral 75 (GEA Pharma Systems, Columbia, MD, USA), a top driven high shear granulator with a 75 L stainless steel bowl. The two powders were dry mixed in the granulator by the impeller at 290 rpm for five minutes. Water was sprayed onto the dry mixture using a six inch atomization nozzle with a stainless steel, flat, fan spray pattern and peristaltic pump (Spraying Systems Co., Wheaton, IL, USA). The water addition rate was 277 mL/min with 50 psi atomization air pressure, and the total water amount was 5% by weight. The impeller speed and chopper speed during granulation were 290 and 1500 rpm, respectively. The impeller and chopper continued mixing after spray granulation completed for a 30 second wet massing period.

4.2.3 Fluid Bed Drying

4.2.3.1 Laboratory Scale (400-600 g batch size)

Fluid bed drying was performed using a Diosna Minilab (Dierks & Sohne GmbH, Osnabruck, Germany) fluid bed processor (FBP) fitted with an 11 L insert. The FBP contained an internal EGE-Electronik series LN/LG air flow sensor (Spezial-Sensoren GmbH, Gettorf, Germany) to measure volumetric airflow velocity in the inlet air pipe. Three internal thermocouples measured temperature of the heated air, product temperature, and outlet air. Two series RHL temperature/humidity transmitters (Dwyer

Instruments, Inc., Michigan City, IN, USA) were added to the system to measure the temperature and humidity of the inlet and exhaust air, respectively. A series 616 differential pressure transmitter (Dwyer Instruments, Inc, Michigan City, IN, USA) was added to the system to measure the pressure drop across the fluid bed. Near infrared spectra were collected through the front viewing window of the FBP using a model NIR256L-2.2T2 spectrometer (Control Development Inc., South Bend, IN, USA). It is a 256 element photodiode array spectrometer with an extended InGaAs detector (1,085-2,229 nm). An external halogen light source (Control Development Inc., South Bend, IN, USA; HL-2000) was used with a fiber optic probe (Control Development Inc., South Bend, IN, USA; 6 around 1 reflectance probe). The EEF value, drying end point (End Moisture Target (EMT)) (%w/w), end product temperature target (EPTT) (^{o}C), and batch size (g) were factors varied in a 2^4 full factorial design to study the drying factors identified during risk analysis. The drying DOE and major results are listed in Table 4.1. The inlet airflow velocity was optimized to maintain a constant bed height, and is constant for a given batch size after the initial constant rate drying period. The 450 g batch size required 5 m^3/hr, while the 650 gram batches required 10 m^3/hr. The filter bags were cleared using a backpressure pulse every 60 seconds at 30 psi for all experiments.

Table 4.1. Laboratory scale fluid bed drying DOE and selected response variables. (Yellow = Experiments pooled for error estimates).

Two-level 4-Factor Full-Factorial Design										
Combination	**Run Order**	**Factors**				**Responses**				
		EEF (a)	End Moisture Target (%w/w) (b)	Batch Size (g) (c)	End Prod. Temp Target (^{o}C) (d)	Median PS (µm)	Blend Lactam (mole %)	Cohesion (kPa)	Tablet Crushing Force (kP)	
									Compaction Force (lbs F)	(kP)
-	8	0.450	0.5	450	25	289				
a	7	0.175	0.5	450	25	296				
b	13	0.450	1.0	450	25	328	0.019	0.377		
ab	14	0.175	1.0	450	25	298				
c	16	0.450	0.5	650	25	334				
ac	2	0.175	0.5	650	25	310	0.028	0.439	2815	5.52
									2195	4.52
									1435	3.42
bc	1	0.450	1.0	650	25	330				
abc	3	0.175	1.0	650	25	353	0.016	0.352	3045	3.84
									2230	5.48
									1700	4.34
d	11	0.450	0.5	450	30	274	0.016	0.273	2675	5.06
									1930	4.14
ad	12	0.175	0.5	450	30	290				
bd	4	0.450	1.0	450	30	284	0.021	0.4	2955	5.48
									2230	4.42
abd	5	0.175	1.0	450	30	332				
cd	10	0.450	0.5	650	30	338	0.022	0.289	3030	5.56
									2425	4.9
									1560	3.56
acd	6	0.175	0.5	650	30	316	0.026	0.725		
bcd	9	0.450	1.0	650	30	329	0.016	0.373		
abcd	15	0.175	1.0	650	30	351				

Two-level 4-Factor Full-Factorial Design (Continued)										
Combination	**Run Order**	**Factors**				**Responses**				
		EEF (a)	End Moisture Target (%w/w) (b)	Batch Size (g) (c)	End Prod. Temp Target (^{o}C) (d)	Median PS (µm)	Blend Lactam (mole%)	Cohesion (kPa)	Tablet Crushing Force (kP)	
									Compaction Force (lbs F)	(kP)
Repeat	17	0.450	0.5	650	25		0.018	0.591	2655	4.4
									1840	3.9
									1540	3.3
Repeat	18	0.450	0.5	650	25		0.016	0.506	2870	5.6
									2160	4.4
									1540	3.4
Repeat	19	0.450	0.5	650	25		0.017	0.407		
Repeat	20	0.450	0.5	650	25		0.019	0.407		

4.2.3.2 Intermediate Scale (1 kg batch size)

Fluid bed drying for the 1 kg batch size was performed using a Versa Glatt Particle Coater (Glatt GmbH, Binzen, Germany) with a 1,251.05 in^3 conical insert on a 150 mesh screen (no additional distributor plate). The FBP did not contain an internal airflow sensor or an NIR sensor because the viewing window was not transparent to NIR radiation. A calibration predicting the airflow velocity at different flap % was created by measuring the linear velocity of the exhaust air using an Alnor Compuflow 8585 thermo-anemometer (FLW, Inc., Huntington Beach, CA, USA). A calibration to predict the granule moisture content using the outlet air temperature was created by sampling the FBD and recording loss on drying data using the Mark 3 Moisture Analyzer (Sartorious Mechatronics, Bohemia, NY, USA). Two internal thermocouples measured temperature of the heated air and outlet air. Two EasyLog temperature/humidity loggers (Lascar Electronics Ltd., Salisbury, UK; EL-USB-2) were added to the system to measure the temperature and humidity of the inlet and exhaust air, respectively. The airflow velocity was adjusted to maintain a constant bed height, but remained constant during the falling rate drying period with 25% of the airflow flap open. The EEF value and drying end point (End Moisture Target (EMT) by outlet air temperature) were factors varied in a 2^2 full factorial design to study the significant drying factors identified at laboratory scale. The drying DOE and major results are listed in Table 4.2. The filter bags were cleared by shaking once every 60 seconds for a five-second duration.

Table 4.2. Intermediate scale fluid bed drying DOE and selected response factors.

Two-Level, 2-Factor Full Factorial Design with 3 Repeats							
	Factors		Responses				
Exp	EEF	End Moisture Target	Median PS (µm)	Blend Lactam (Mole %)	Blend Cohesion (kPa)	Tablet Crushing Force (kP)	
						Compaction Force (lbs F)	
1	0.175	0.5%	277	0.026	0.304	4600	13.56
2	0.175	1.0%	283	0.024	0.487	4450	13.39
3	0.45	0.5%	302	0.015	0.271	4530	15.69
4	0.45	1.0%	297	0.016	0.227	4250	15.26
						3500	12.76
						2200	8.07
						1270	3.78
5	0.45	0.5%	280	0.016	0.252	4325	12.32
						3130	9.94
						1950	6.09
						950	1.82
6	0.45	0.5%	289	0.015	0.262	4725	15.48
7	0.45	0.5%	293	0.018	0.306	4515	15.84

4.2.3.3 Pilot Scale (9.72 kg batch size)

Fluid bed drying for the 9.72 kg batch size was performed using a Glatt GPCG-PRO-5 (Glatt GmbH, Binzen, Germany) on a 150 mesh screen with no additional distributor plate. The FBP control system contained an internal airflow sensor that output volumetric airflow velocity (f^3/m), five internal thermocouples that measured temperature of the inlet air, heated air, product, outlet air, and exhaust air, and two humidity sensors to measure the temperature and humidity of the inlet and exhaust air. The FBP did not contain an NIR sensor. A calibration to predict the granule moisture content using the

product temperature was created by sampling the FBP and recording loss on drying data using the Mark 3 Moisture Analyzer (Sartorious Mechatronics, Bohemia, NY, USA). The airflow velocity was adjusted to maintain a constant bed height, but remained constant during the falling rate drying period at 300 f^3/m. Only thee experiments were performed at the pilot scale. Two replicates of the target operating condition were performed to test the design space and transfer functions developed during the initial scales, while an additional experiment that varied the EEF variable was performed to validate that it was directly scaleable. The experiments and major results are listed in Table 4.3. The filter bags were cleared by shaking for a ten-second duration at 1 minute intervals.

Table 4.3. Pilot Scale fluid bed drying DOE and selected response factors.

Two-Level, 1-Factor Design of Experiments with 1 Repeat							
	Factors		Responses				
Exp.	EEF	End Moisture Target	Median PS (µm)	Blend Lactam (Mole %)	Blend Cohesion (kPa)	Tablet Crushing Force (kP)	
						Compaction Force (lbs F)	
1	0.175	0.5%	422	0.0229	0.347	3000	10
2	0.45	0.5%	272	0.0225	0.384	3200	10.5
3	0.45	0.5%	284	0.0214	0.334	4700	13.9
						3200	10.6
						2100	7.2
						1250	3.3

4.2.4 Fluid Bed Drying Control System

4.2.4.1 Laboratory Scale (400-600 g batch size)

The control system at laboratory scale was fully automated and was set to sample data and send commands at a set frequency of 5 seconds. The FBP internal measurements were collected by an onboard programmable logic controller (PLC) (Allen-Bradley, Rockwell Automation, Milwaukee, WI, USA). The PLC also communicated the process set points to the FBP and contained the necessary ladder logic to run the heater and airflow motor. The PLC sent the FBP process measurements and the previous set points to the DeltaVv.9 digital automation system (Emerson Process Management, Equipment & Controls, Inc., Lawrence, PA, USA) via open process control (OPC).

The DeltaV system received the process measurements from the PLC and the 4-20 mA analogue outputs from the temperature/humidity sensors and differential pressure transmitter and transformed the inputs into digital readings. The DeltaV software contained internal logic for safety switches, alarms, and unit conversions, and PID controllers. It also tagged readings from the FBP and input controls from the control software to organize the communication between these two systems.

The control software for the system was synTQ v. 3.5 (Optimal, Bristol, UK). This software synchronized all measurements on the FBP at a fixed cycle, so that all measurements within a cycle could be compared for a specific moment. The synTQ software received all process measurements from DeltaV via OPC and received NIR spectra directly from the spectrometer. It organized the raw data and sent the information to the necessary analytical models. All of the analytical and process models were compiled and input directly into the synTQ software. The analytical models output product or process property predictions, which were then passed within synTQ to the

control models. The control models took the property predictions and predicted the process parameters necessary to continue the process along the desired trajectory for the next cycle. These parameter predictions were then passed via OPC from synTQ to DeltaV, which translated the parameters for communication to the PLC, and the PLC finally adjusted the process parameters as directed. The automated, hybrid control system was described in detail in chapter 2.

4.2.4.2 Intermediate Scale (1 kg batch size)

The FBP at intermediate scale was not instrumented with an automated control system. A custom macro was created using Microsoft Excel 2007 (Microsoft Corporation, Redmond, WA, USA) to automatically calculate the EEF value at a given moment and the heated air temperature to maintain the EEF value at its set point. The process measurements were manually added to the Excel spreadsheet. The process measurements were recorded and the process factors adjusted at 30-second intervals. The airflow flap was manually adjusted to maintain a constant bed height and a univariate model was created to predict the granule moisture content using the outlet air temperature.

4.2.4.3 Pilot Scale (9.72 kg batch size)

The control system at pilot scale was semi-automated. All measurements were automated at a fixed frequency of 0.07 Hz (once every 15 seconds), but process adjustments had to be input manually. The system was controlled using the PITOPS Plus OPC control system (PiControl Solutions LLC, Katy, TX, USA). The automated measurements included inlet air temperature, inlet air humidity, heated air temperature,

product temperature, outlet air temperature, exhaust air temperature, exhaust air humidity, pressure drop across the fluid bed, and volumetric airflow velocity. The measurements were downloaded in real time into Microsoft Excel 2007 every 15 seconds, and a macro was created to automatically calculate the process set points for the next cycle, which were input manually by a technician. Near infrared spectroscopy was not available at pilot scale, so a univariate model was calculated to predict granule moisture content using the measured product temperature.

4.2.5 Blending

4.2.5.1 Laboratory Scale (400-600 g batch size)

A 3.5 quart, stainless steel, custom made V-blender was used to mix the dried granules with the extragranular excipients. Two SpectralProbe Process NIR spectrometers (Thermo Fisher Scientific, Wilmington, MA, USA; Serial numbers 1277 and 1502) were used to monitor the two arms of the V-blender in real time. The instruments collected 100 absorption values between 1,600 and 2,400 nm in reflection mode (interpolation from 8.71 to 7.31 nm) and were triggered by a light intensity sensor (intensity rises when powder falls against the sampling window, enabling collection). Measurements were made through a sapphire window in the top of either arm of the blender. Spectra were sent wirelessly to a computer and imported into a custom-made acquisition and analysis system. The system had a response time of less than two seconds to allow real-time, online monitoring of the blend homogeneity.

The Root Mean Squared Error from the Nominal Value (RMSNV) algorithm was used to monitor blending.[99] The RMSNV statistic is a weighted, cumulative, pooled

standard distance metric that takes into account the deviation of the predicted concentration of the major components (gabapentin, starch, MCC, and HPC) of a mixture from their target concentration, over a given number of rotations (1 minute of blending). The blend end point was determined by the trend of the pooled RMSNV of the two sensors and defined as the time at which the pooled RMSNV remained constant for a minimum of two minutes.

Models for predicting constituent concentration were developed using an efficient calibration approach (described in chapter 6) with the CLS/PLS algorithm for multivariate modeling.[100] All components except magnesium stearate were blended until the homogeneity criterion was reached. Finally, magnesium stearate was added and blended for five minutes in an additional lubrication blend that was not monitored by NIRS.

4.2.5.2 Intermediate Scale (1 kg batch size)

An IBC Bin Blender and Lifter – Mobile system (Servolift LLC, Wharton, NJ, USA) with a 5 L, stainless steel insert was used to mix the dried granules with the extragranular excipients. An ePAT 601 Blend Uniformity Monitoring System (NIR Spectrometer) (Expo Technologies, LLC., St. Louis, MO, USA) was used to monitor the blender in real time. The instrument collected 226 absorption values between 1,350-1,800 nm in reflection mode and was triggered by a light intensity sensor (intensity rises when powder falls against the sampling window, enabling collection). Measurements were made through a sapphire window on the top of the blender. Spectra were sent wirelessly to a computer and imported into a custom-made acquisition and analysis system. The

system had a response time of less than two seconds to allow real-time, online monitoring of the blend homogeneity.

The RMSNV algorithm was used to monitor blending. The four major components (gabapentin, starch, MCC, and HPC) of the mixture were used to determine the blend end point, which was defined as the time at which the RMSNV (one minute time window) remained constant for a minimum of two minutes.

Models for predicting constituent concentration were developed independently from the laboratory scale methods using the same efficient calibration approach and the partial least squares (PLS) algorithm. All components except magnesium stearate were blended until the homogeneity criterion was reached. Finally, magnesium stearate was added and blended for five minutes in an additional lubrication blend that was not monitored by NIRS.

4.2.5.3 Pilot Scale (9.72 kg batch size)

A 50 L insert was used with the IBC Bin Blender and Lifter – Mobile system (Servolift LLC, Wharton, NJ, USA) at the pilot scale. The spectrometer, calibration method, RMSNV parameters, and decision method was the same as the intermediate scale.

4.2.6 Tablet Compression

4.2.6.1 Laboratory Scale (400-600 g batch size)

The final blends were compressed on a 16-station, instrumented tablet press (B2 Stokes, Key Industries, Farmingdale, NJ, USA), fitted with load cells to measure the tablet compression forces. Only one set of 12.7 mm (0.5") flat faced, beveled edge,

round punches and a cylindrical die was used. The press speed was kept constant at 27 rpm. Each batch was compressed at 3 compression forces (Table 4.1). Each compression force was allowed to stabilize and then tablets were collected during the steady state into one minute time bins for each of the six minutes of compression. Tablets were randomly sampled from each time bin for the crushing strength measurements.

4.2.6.2 Intermediate Scale (1 kg batch size)

The final blends were compressed on a 10-station, Piccola Rotary Tablet Press (Model B, Knoll Pharmaceutical Co., Argentina), fitted with load cells to measure the tablet compression forces. Only one concave, oval (17.45 x 10.35 mm) punch and die set was used. The press speed was kept constant at 25 rpm, and the tablet target mass was 889 mg. Each batch was compressed at 3 compression forces (Table 4.2). Each compression force was allowed to stabilize and then tablets were collected during the steady state into one minute time bins for each of the six minutes of compression. Tablets were randomly sampled from each time bin for the crushing strength measurements.

4.2.6.3 Pilot Scale (9.72 kg batch size)

The final blends were compressed on a Manesty BB4 35 station Tablet Press (OYSTAR USA, NJ, USA). Seven concave, oval (17.45 x 10.35 mm) punch and die sets were used. The press speed was kept constant at 25 rpm, and the tablet target mass was 889 mg. Each batch was compressed at 3 compression forces that were adjusted to meet 3 tablet crushing strength targets (8, 10, and 12 kp) (Table 4.3). Each compression force

was allowed to stabilize and then tablets were collected during the steady state into one minute time bins for each of the six minutes of compression. Tablets were randomly sampled from each time bin for the crushing strength measurements.

4.2.7 Data Analysis

The analytical and process models that were included in each control system were created using MATLAB v. 7.1 R14 (The Mathworks, Natick, MA, USA) equipped with the PLS_Toolbox v. 3.0.4 (Eigenvector Research Inc., Wenatchee, WA, USA) and programs written in house. MATLAB code was compiled for laboratory scale automation using MATLAB Compiler (The Mathworks, Natick, MA, USA) for use by the synTQ software. The DOE results at each scale were analyzed using the statistical software, jmp 8 (SAS, Cary, NC, USA). All possible main effects and first order interactions were investigated, and variables were screened for significance using the p-value statistic at the α-level 0.10.

The NIR calibration for moisture content at laboratory scale was created by sampling granules from several trial drying batches. The reference moisture content was measured using loss on drying (LOD) on a Computrac Max-2000 moisture analyzer (Arizona Instruments, Chandler, AZ, USA). The predictive model was created using partial least-squares (PLS) regression on standard normal variate (SNV) corrected NIR spectra. The model required one PLS latent variable. Granule moisture content was measured via loss on drying at intermediate and pilot scale using the Mark 3 Moisture Analyzer (Sartorious Mechatronics, Bohemia, NY, USA).

Four response factors for each batch were selected during the initial risk analysis to represent the product CQAs. These properties included the median particle size of the

finished granules, the amount of gabapentin lactam in the final blend as a stability indicator, the cohesion of the final blend as a flow indicator, and the mean tablet crushing strength for each compression force within each batch. The median particle size was determined by sieve analysis of 100-g granule samples using U.S. standard test sieves (Fisher Scientific, Pittsburgh, PA, USA & VWR, West Chester, PA, USA). The samples were shaken using a sieve shaker (CSC Scientific, Fairfax, VA, USA) for five minutes at level five. Ten sieve cuts were collected for each sample (U.S. standard mesh #s: 18, 25, 35, 45, 60, 80, 120, 170, 230, and pan). A cumulative mass distribution was determined for each sample and the linear portion of the distribution was fit by linear least-squares to solve for the mass median (d_{m50}) value.

The chemical degradent for gabapentin is gabapentin lactam, so the gabapentin lactam concentration (mole %) in the final blends of these dried granule experiments was measured as the stability response. The lactam concentration was measured via reverse phase high pressure liquid chromatography (HPLC) with a SpectraSystem P4000 quaternary gradient pump, AS3000 variable-volume autosampler, and UV 6000 LP photodiode array detection system (Thermo Fisher Scientific Inc., Waltham, MA, USA) at the University of Iowa using a µBondpak CN-RP 3.9x300 mm column (Waters, Milford, MA, USA). The HPLC method used 5% acetonitrile in phosphate buffer as the mobile phase and a flow rate of 1.0 mL/mL and collected UV data at 210 nm.

Blend flow measurements were performed at Rutgers University. Cohesion, which is inversely proportional to flowability, was measured using the shear cell module of an FT4 powder rheometer (Freeman Technology, Malvern, UK) on 85 cm^3 samples. Cohesion is the shear strength at zero consolidation stress of a bulk powder.

Tablet crushing strength was determined using a diametric compression tester (Lab Scale - Model HT-300, Key International, Inc., Englishtown, NJ, USA; Intermediate and Pilot Scale – Model VK200, Varian, Inc., Santa Clara, CA, USA). During the test, the compressive force was applied at a constant rate. The oval tablets at intermediate and pilot scale were placed parallel to the longest axis. Fifteen tablets were randomly sampled across all time bins within each compression force for each batch and tested to determine the mean crushing strength.

4.3 Results and Discussion

The laboratory scale, intermediate scale, and pilot scale experiments and results are displayed in Tables 4.1, 4.2, and 4.3, respectively. Only two of the four laboratory scale drying factors (EEF and EMT) were identified as being CPPs during laboratory scale statistical analysis, which eliminated the EPTT and batch size variables from further study. The pilot scale was used to confirm success of the initial laboratory scale design space and scale-up transfer functions. While it was determined in subsequent analyses that a higher EMT was optimum, this data was not available when the larger scale experiments were identified, so the initial target operating conditions included EEF equal to 0.45 and EMT equal to 0.5%.

Gabapentin is an active ingredient with process induced chemical instability and the degradent, gabapentin lactam, has undesired biological activity, making it very dangerous at low concentrations.[89] Therefore, the gabapentin lactam concentration in the final blend was identified as the highest priority CQA during lab scale design space development, and was the highest priority process model to be scaled-up. It was expected that the effect from the EEF variable would be the same regardless of scale

because it is a variable based in first principles, while the EMT variable could require scale adjustments. The drying moisture target is similar between scales in traditional scale-up studies, however. There was no automation or online NIR monitoring of granule moisture content available at the intermediate or pilot scale, so the implementation of the target drying conditions was more difficult and less precise.

The results from the intermediate scale DOE showed that the lab scale process model for the lactam CQA was successful at predicting the intermediate scale results and did not need any adjustment. The 95% confidence intervals for the regression coefficients and intercepts if the lab scale model and intermediate scale model were developed independently are displayed in Figure 4.1. It can be seen that the regression coefficients are statistically indistinguishable. Therefore, no transfer function was needed to transfer the lab scale model to the intermediate scale.

The lactam prediction performance using the laboratory scale model on the intermediate and pilot scale is displayed in Figure 4.2. While the model performed adequately, there were several discrepancies. First, the sizes of the vessels at larger scales caused larger gradients within the process equipment, which contributed to the increase in variability and prediction error at larger scales. Additionally, the lack of automation at intermediate scale, the lack of online NIR moisture monitoring, and the reduced frequency of the command inputs at either larger scale contributed to the poorer prediction performance after transfer. These factors all contributed to the doubled prediction error upon scale-up to intermediate scale.

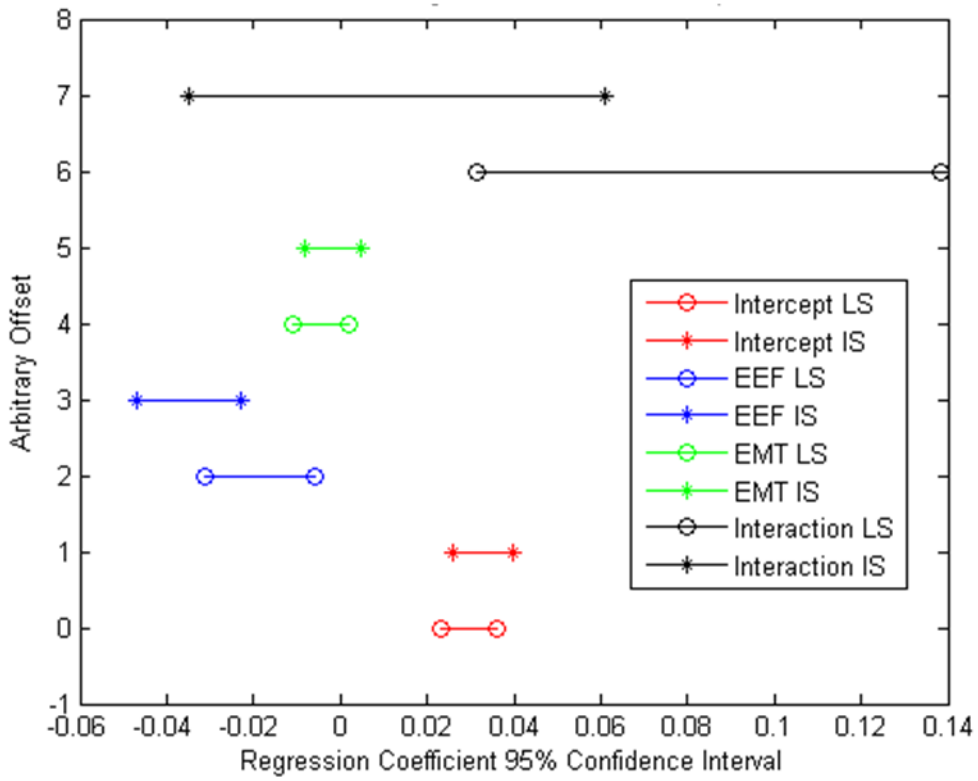

Figure 4.1. A comparison of the 95% confidence intervals for the regression coefficients for the blend lactam concentration process model between lab scale and intermediate scale. The regression coefficients are statistically indistinguishable. (LS = Lab Scale; IS = Intermediate Scale)

The results highlight the importance of online moisture monitoring using NIRS. When online spectroscopy was not used at larger scales, a less precise drying endpoint is introduced, which increases the risk of over drying. The tolerance surface that describes the probability that 95% of future batches will meet the lactam specification at the combination of CPPs for the intermediate scale is displayed in Figure 4.2b. It can be compared to the corresponding tolerance surface from the laboratory scale model in Figure 4.2a. The areas in the upper left of both figures are similar, which supports the success of the EEF variable being directly scaleable. The areas in the bottom right of each figure show the greatest difference, which resulted from the inaccuracy of the

intermediate scale controls with regards to meeting the drying end point. Online spectroscopy is substantially more accurate when predicting moisture content compared to an outlet temperature measurement, so the drying endpoint was more accurate at laboratory scale. Outlet temperatures are held down by the cooling effect of evaporation, so warming of the outlet temperature indicates that evaporation has slowed or ended. There is a lag time, however, until the temperature of the outlet air responds to the lower moisture content, so higher moisture targets are difficult to meet.

Loss on drying measurements confirmed that the moisture content of the 1.0% moisture end points were consistently over dried (data not shown), causing the increase in gabapentin lactam formation. This problem worsened at increased drying rates (lower EEF values), because the lag time resulted in increased over drying. Process analytical technology (PAT) and online spectroscopy substantially reduced this risk at laboratory scale. The other three design points from the 2^2 full factorial design at intermediate scale and the three experiments at pilot scale were all accurately predicted as meeting or not meeting lactam specifications by the lab scale process model.

The second highest priority of the four CQAs was tablet crushing strength. The laboratory process model was challenged because the shape of the tablets changed from laboratory scale to the larger scales. It was determined after completion of the laboratory scale DOE that the tablet mass (889 mg) was too large for patients to swallow using the round, flat-faced punches that were used during the initial studies. Capsule shaped tablets were used at the intermediate and pilot scales, which introduced a large magnitude of new variance to the process model that was not in the original calibration. An advantage of the capsule shaped tablet was that higher crushing strengths were observed

using similar compaction pressures, which allowed the tablet crushing strength specification (> 6 kP) to be satisfied with greater ease and no formulation adjustments. A transfer function had to be developed to accurately predict capsule shaped tablet crushing strength using fluid bed drying CPPs from the laboratory scale process model.

	Error (Mole %)
Lab Scale (Calibration)	**0.002**
Intermediate Scale (Prediction)	**0.004**
Pilot Scale (Prediction)	**0.004**

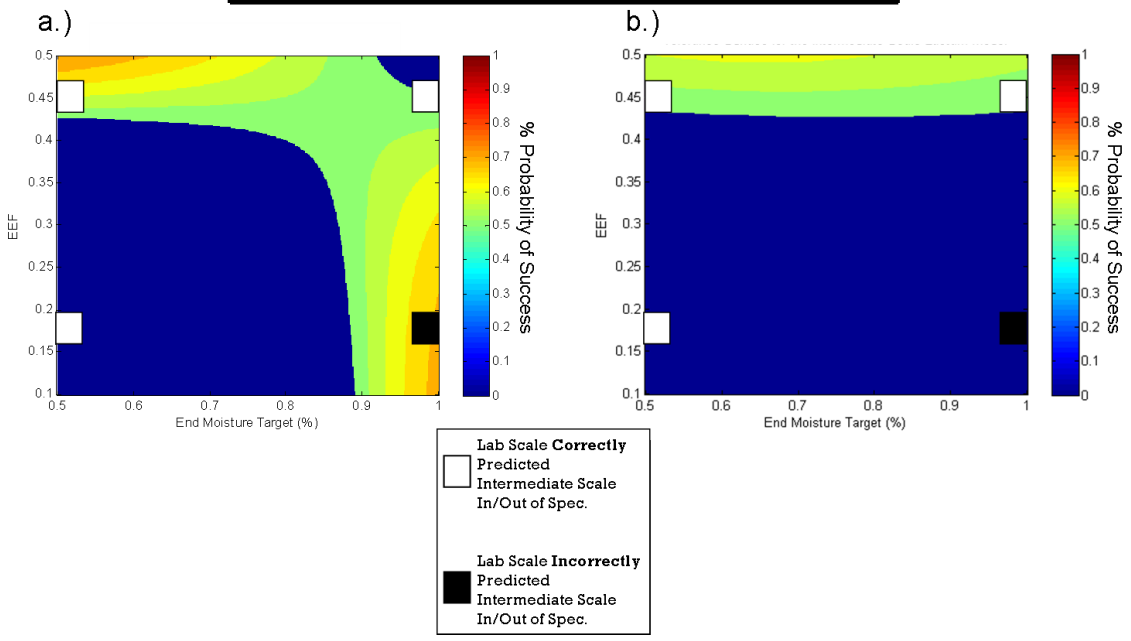

Figure 4.2. A comparison of the tolerance surface for the lactam concentration CQA process model between lab scale and intermediate scale. Three of the four locations of the 2^2 full factorial design were predicted correctly, and the incorrect prediction resulted from not having online NIR moisture measurements.

Figure 4.3 displays the process by which the transfer function was calculated. Figure 4.3a shows the prediction performance of the laboratory scale model applied directly to the larger scale data. It can be seen that the crushing strength of the capsule shaped tablets were significantly higher than predicted, which was hypothesized correctly. The intermediate scale data was used to calculate the necessary scale-up

transfer function, which was then applied to the pilot scale data with no additional adjustments. Plotting the intermediate scale predictions versus the measured responses (Figure 4.3b) shows that the relationship was linear (R^2 = 0.91). Therefore, a simple slope and bias correction was all that was necessary to transfer the predictions for the new tablet shape and scale-up. The transfer parameters are listed in Figure 4.3b and the corrected predictions are displayed in Figure 4.3c. The simple transfer function showed a significant improvement in prediction performance on both the intermediate scale data and the pilot scale data, demonstrating that the scale-up transfer function was consistent regardless of the magnitude of the scale change.

The larger scale prediction error was still significantly larger than at smaller scale, but the most significant errors were observed at the end of the model with larger tablet crushing strengths. These values were a great distance from the center of the laboratory scale model, so the increased prediction residuals were partially the results of a large degree of model extrapolation. The target tablet crushing strength was between 8-10 kP, where the model residuals were much lower. Therefore, the laboratory scale model in combination with the slope and bias correction was able to adequately predict tablet crushing strength in the target region.

The lowest priority process models were for the cohesion and granule median particle size CQAs. The EPTT variable for the cohesion model and the batch size variable for the particle size model were eliminated as CPPs during laboratory scale analysis, so these factors were not investigated upon scale up. Therefore, when calculating predictions for these models, the EPTT and batch size factors remained unchanged (EPTT = 25^{o}C; Batch Size = large group (650 g from lab scale)). When

calculating the effect of the EEF variable for the cohesion model and the EMT variable for the particle size model using the data from each scale independently, the regression coefficients were statistically indistinguishable (Figure 4.4). Therefore, both CPPs were directly scaleable and required no adjustment between scales.

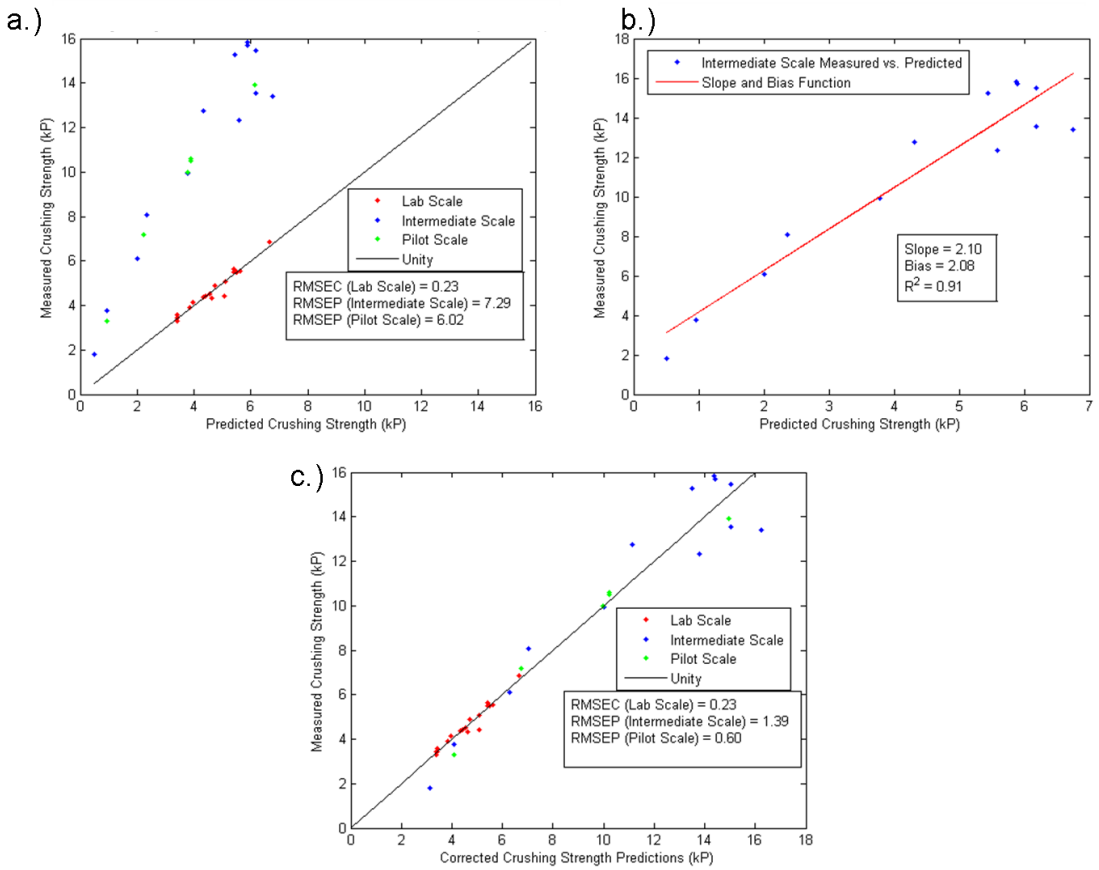

Figure 4.3. The calculation of the scale-up transfer function for the tablet crushing strength process model. **a.)** Tablet crushing strength predictions using the laboratory scale model directly; **b.)** The scale-up transfer function (slope and bias) calculation using the intermediate scale data; **c.)** The crushing strength prediction after applying the scale-up transfer function.

There was a significant bias between the granule median particle size predictions and measured responses at the larger scales, as highlighted by the difference between intercepts and increase in prediction error (Figure 4.4b). The measured particle size was consistently less than the predicted response. This was because granules produced at the

laboratory scale were used with no particle size adjustment for blending and compression. At the larger scales, granules that were greater than 750 µm were removed using a sieve because it was required for subsequent compression by the intermediate and pilot scale site managers. This caused a shift in the final particle size distribution as measured by sieve analysis, causing the consistent bias. A simple bias correction could have been used to address this change, but it was determined that the laboratory model could be used without adjustment due to its low priority and low risk.

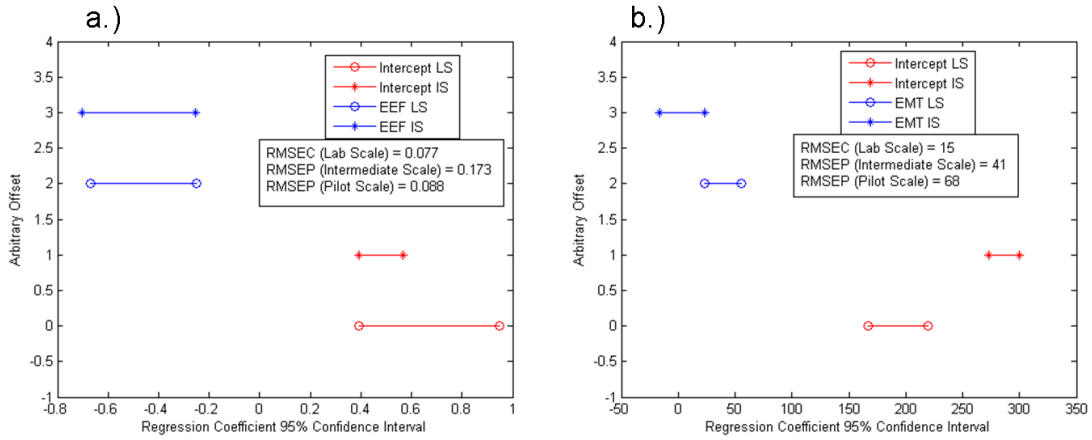

Figure 4.4. A comparison of the 95% confidence intervals for the regression coefficients for the **a.)** cohesion model and **b.)** granule median particle size model between lab scale and intermediate scale. The regression coefficients are statistically indistinguishable, except for the intercept in the particle size model. (LS = Lab Scale; IS = Intermediate Scale)

For the cohesion model, the prediction error at larger scales was approximately 2-2.5 times larger, which was consistent with the other models investigated. This was attributed to the larger magnitude of natural variability at larger scales and the decrease in precision of the controls at larger scales. Therefore, it was concluded that adjustable process parameters that accounted for environmental variability, a first principle variable, and a simple transfer function maximized the value of the laboratory scale studies. This

allowed the laboratory scale design space to be applied at larger scales. The importance of online spectroscopy for consistent production at all scales was also demonstrated.

4.4 Conclusion

A laboratory scale design space was efficiently scaled-up to a pilot scale by leveraging the laboratory scale DOE and applying effective transfer functions. In traditional scale-up methodology, DOEs are replicated at all scales. This study demonstrated that with the use of an automated control system that incorporates adjustable process parameters, first principle models, online spectroscopy, and an intermediate scale to calculate scale effects, scale-up development can be accomplished much more efficiently with no reduction in product quality and enhanced process understanding.

Half of the initially identified CPPs during risk analysis were eliminated as insignificant using the laboratory scale DOE. This significantly reduced the number of experiments necessary at larger scales and improved development efficiency. Additionally, the scale effects were investigated at an intermediate scale, which was approximately double from the laboratory scale, and about 1/10 of the pilot scale. One scale-up transfer function was needed due to a change in tablet shape at larger scales, and the slope and bias correction that was calculated for the intermediate scale performed well at the pilot scale. By reducing the number of pilot scale experiments to three, industrial efficiency was improved further.

Finally, the use of a first principle model in the initial process controls reduced the dimensionality of the DOEs needed at all scales, and made scale-up efforts significantly easier because first principle variables are insensitive to scale. This was

confirmed in the current study. The highest priority process model for gabapentin lactam was directly scaled-up and successfully predicted batch success or failure in 3 out of 4 design points. The incorrect design point resulted from over drying, which highlights the importance of PAT, online spectroscopy, and automated controls for quality production. There was increased variability in CQAs at larger scales due to larger equipment gradients and less precise controls. Scientifically rigorous development at early stages increased the value of all subsequent studies.

Chapter 5: Development of a Fluid Bed Granulation Design Space Using CQA Weighted Tolerance Intervals

5.1 Introduction

To this point, this dissertation has demonstrated an automated control system that provides quality and efficiency benefits for the fluid bed granulation and drying unit operation, developed a laboratory scale design space for fluid bed drying using DOE and advanced statistics to assure risk reduction, and demonstrated how the automated control system and laboratory scale design space could be scaled-up efficiently. Two weaknesses of the previous chapters are the limited evidence of the benefits of the automated controls for the granulation phase of a full fluid bed process and the lack of formulation or material factors in the DOE and design space development efforts. These shortcomings will be addressed in this chapter using an excipient platform and full 4-phase fluid bed experiments. The research was originally published in the Journal of Pharmaceutical Sciences.[132]

A major theme of this dissertation is that it is imperative that controls systems be efficient and robust so that their implementation over a long period of time is feasible. This requires well developed design of experiments (DOE), first principle calculations, and rigorous statistical modeling. Design of experiments is necessary to identify important factors, calculate their effects on the response factors, and identify interactions between factors. First principle controls are desirable because they describe the major mechanisms by which the manufacturing process impacts product properties, reduce the

dimensionality of subsequent DOEs, account for external variability that cannot be eliminated, and provide direct scale-up. Finally, statistical modeling is necessary to calculate the probability of success at all combinations within the measured knowledge space. This enables the analyst to make an informed design when defining the boundaries of the design space.

The control system that was used in the current chapter has been described in detail in chapter 2, and utilizes the environmental equivalency factor (EEF) as a first principle variable.[29] The calculation reduces four input variables (heated air temperature, airflow velocity, spray rate, and inlet air humidity) into a single factor, and calculates the heated air temperature needed to maintain a constant drying rate so that the water addition and removal rate can be maintained despite significant environmental fluctuations. This removes the need for a preconditioned air system, eliminating a substantial cost in large production facilities. Additionally, online spectroscopy was used in the control system to provide direct feedback on in-process material properties, identify process deviations immediately, and define meaningful phase end points. The potential for these controls to be efficiently implemented for the control of a pharmaceutical drying unit operation with a drug that has stability concerns was demonstrated in chapter 3, and the potential for simplified and robust scale-up was demonstrated in chapter 4.

The current chapter seeks to extend these principles to a full, four phase fluid bed process that includes powder mixing, spray granulation, heated drying, and cooling. The inclusion of the spray granulation phase is a significant step because it has a substantial impact on downstream physical properties including powder flow, packing efficiency,

and compactibility. The EEF controls have been shown to provide excellent control of the drying rate during fluid bed drying, and it is hypothesized that these same controls can be utilized during spraying to maintain a constant water addition rate, which is a major factor in controlling particle agglomeration during granulation. Small changes in the water content of the incoming airstream can significantly impact the water addition/removal rate, so controls are needed to account for this variability using feedforward control loops to reduce the variability in product properties between batches. Online monitoring of granule moisture content is hypothesized to provide a simple definition of the granulation and drying end points, removing another source of batch to batch variability.

It should be noted that the control system described herein does not consider the impact of the spray droplet size, which is another factor that can effect particle agglomeration during the granulation phase. Droplet size is highly variable in most spray systems, making it difficult to control. It is also very difficult to match droplet sizes when scaling-up because of the substantial differences in equipment size. Therefore, it is the goal of this chapter to demonstrate satisfactory controls of granule particle size without varying droplet size as part of the DOE. The droplet size variable could be used to remove another source of variability to control particle size in very sensitive formulations that require strict particle size specifications, however.

Also included in this chapter's DOE were two formulation factors (binder concentration and excipient ratio). The two excipients (lactose monohydrate and microcrystalline cellulose (MCC)) that were varied within the excipient ratio had substantially different wetting properties, which affect the amount of water available on

the particle surfaces per unit time, thus impacting particle agglomeration. The two formulation factors are known to affect the granulation process and final product properties, but they are often optimized independently during formulation studies. While this can be effective, there are often interactions between formulation and process parameters that are overlooked or never identified. These interaction effects can be extremely important and provide an additional degree of control that can be exploited by the analyst.

The inclusion of formulation and process factors within a single DOE required the use of the extended analysis of covariance (ANACOVA) model[64] to describe the interaction of these nominal and continuous variables. This model allowed the difference in the mean response between groups of a nominal factor to be measured while simultaneously describing effects of the continuous factors on the response variables within the nominal groups. This information substantially improved process understanding so that the most appropriate design space boundaries could be defined.

The final goal of the current study is to demonstrate a scientifically rigorous calculation of a design space for the fluid bed process, and specifically the granulation phase. The calculation will use statistical tolerance,[67] so that the probability of 95% of future batches meeting critical quality attribute (CQA) specifications can be defined for all combinations of critical process parameters (CPPs) and formulation factors. The necessity of statistical tolerance calculations for the definition of a pharmaceutical design space was described in chapter 3, but this is the first study that uses statistical tolerance in the definition of a granulation design space that includes both process and formulation factors.

5.2 Materials and Methods

5.2.1 Excipient Platform

An excipient platform was used to investigate formulation factors on the granulation and drying design space. Hydroxypropyl methylcellulose (HPMC) (Pharmacoat 606, Biddle Sawyer Corp., New York, NY, USA) was used as the polymeric binder. It was added to the fluid bed bowl with the other excipients as a dry powder. Water was used as the spray solution. Microcrystalline cellulose (MCC) (Avicel PH102, FMC BioPolymer, Philadelphia, PA, USA) and lactose monohydrate (Granulac 70, Meggle Excipients & Technology, Wasserburg, Germany) were the additional pharmaceutical excipients. The binder concentration and the ratio of lactose to MCC were factors varied as part of the DOE (Table 5.1). The batch size for all experiments was 650 grams.

5.2.2 Fluid Bed Processor (FBP)

Fluid bed granulation and drying was performed using a Diosna Minilab (Dierks & Sohne GmbH, Osnabruck, Germany) fitted with an 11 L insert. The FBP contained an internal EGE-Electronik series LN/LG air flow sensor (Spezial-Sensoren GmbH, Gettorf, Germany) to measure volumetric airflow velocity in the inlet air pipe. Three internal thermocouples measured temperature of the heated air, product temperature, and outlet air. Two series RHL temperature/humidity transmitters (Dwyer Instruments, Inc., Michigan City, IN, USA) were added to the system to measure the temperature and humidity of the inlet and exhaust air, respectively. A series 616 differential pressure transmitter (Dwyer Instruments, Inc, Michigan City, IN, USA) was added to the system to measure the pressure drop across the fluid bed. Near infrared spectra were collected

through the front viewing window of the FBP using a model NIR256L-2.2T2 spectrometer (Control Development Inc., South Bend, IN, USA). It is a 256 element photodiode array spectrometer with an extended InGaAs detector (1,085-2,229 nm). An external halogen light source (Control Development Inc., South Bend, IN, USA; HL-2000) was used with a fiber optic probe (Control Development Inc., South Bend, IN, USA; 6 around 1 reflectance probe).

The three powders were blended in the FBP at an airflow velocity of 8 m^3/hr for three minutes. The system was warmed to 30^oC during the blending phase. During spray granulation, deionized water was sprayed onto the fluidized powder mixture using a peristaltic pump (Watson-Marlow 323, Wilmington, MA, USA) at 10 mL/min. The standard, top spray nozzle for the Diosna Minilab was used with an atomization air pressure of 1.1 bar. The EEF set point for granulation and the end moisture target for granulation (EMT) were varied as part of the DOE (Table 5.1). The granule moisture content was measured via online near infrared (NIR) spectroscopy. The EEF set point during the drying phase was 0.7, which was optimized during trial experimentation, while the end of drying was defined when the NIR predicted moisture content was less than 3.0% and the standard deviation of moisture predictions over the previous minute was less than 0.05%. The inlet airflow velocity was adjusted to maintain a constant bed height during granulation and drying. The minimum airflow velocity was 10 m^3/hr and the maximum was 45 m^3/hr. After the drying end point was reached, the powders were fluidized at 8 m^3/hr until the product temperature and inlet air temperature were less than 30^oC. The filter bags were cleared during all phases using a backpressure pulse every 60 seconds at 30 psi for all experiments.

Table 5.1. The FBP DOE factor levels and response results. (*Yellow = Experiments pulled for error estimates)

Design of Experiments								
		Input Factors				Response Factors		
Run Order	Combination	HPMC Concentration (%w/w) (a)	Excipient Ratio (w/w) (b)	EEF (c)	End Moisture Target (Gran) (%w/w) (d)	Compressibility Index	Particle Size d10 (um)	Particle Size Span
4	(1)	5	1:2	1.1	6.0	25.5 26.0	48	1.4
13	a	15	1:2	1.1	6.0	23.4 24.5	46	1.7
15	b	5	2:1	1.1	6.0	21.2 19.8	53	1.9
11	ab	15	2:1	1.1	6.0	21.0 22.2	52	2.6
14	c	5	1:2	0.8	6.0	24.2 25.0	46	1.6
10	ac	15	1:2	0.8	6.0	23.8 24.7	51	1.5
12	bc	5	2:1	0.8	6.0	22.0 23.6	51	1.8
5	abc	15	2:1	0.8	6.0	27.0 25.8	48	2.8

Design of Experiments (Continued)								
		Input Factors				Response Factors		
Run Order	Combination	HPMC Concentration (%w/w) (a)	Excipient Ratio (%w/w) (b)	EEF (c)	End Moisture Target (Gran) (%w/w) (d)	Compressibility Index	Particle Size d10 (µm)	Particle Size Span
6	d	5	1:2	1.1	9.0	25.9 24.5	51	1.5
3	ad	15	1:2	1.1	9.0	25.5 26.2	49	2.2
9	bd	5	2:1	1.1	9.0	23.0 22.4	59	1.4
7	abd	15	2:1	1.1	9.0	26.3 26.3	49	3.5
2	cd	5	1:2	0.8	9.0	23.4 25.3	56	1.8
16	acd	15	1:2	0.8	9.0	23.2 25.3	42	2.3
8	bcd	5	2:1	0.8	9.0	25.9 29.7	55	2.1
1	abcd	15	2:1	0.8	9.0	22.3 22.0	60	3.4

5.2.3 Fluid Bed Processor Control System

The control system was set to sample data and send commands at a set frequency of 0.075 Hz (one measurement every 15 seconds). The FBP internal measurements, which included airflow velocity, heated air temperature, product temperature, and outlet temperature, were collected by an onboard programmable logic controller (PLC) (Allen-Bradley, Rockwell Automation, Milwaukee, WI, USA). The PLC also communicated the process set points to the FBP and contained the necessary ladder logic to run the heater and airflow motor. The PLC sent the FBP process measurements and the previous set points to the DeltaV v.9 digital automation system (Emerson Process Management, Equipment & Controls, Inc., Lawrence, PA, USA) via open process control (OPC).

DeltaV received the process measurements from the PLC and the 4-20 mA analogue outputs from the temperature/humidity sensors and differential pressure transmitter and transformed the inputs into digital readings. The DeltaV software contained internal logic for safety switches, alarms, and unit conversions, as well as PID controllers. It also tagged readings from the FBP and input controls from the control software to organize the communication between these two systems.

The control software for the system was synTQ version 3.5 (Optimal, Bristol, UK). This software synchronized all measurements on the FBP at a fixed cycle, so that all measurements within a cycle could be compared for a specific moment. SynTQ received all process measurements from DeltaV via OPC and received NIR spectra directly from the spectrometer. SynTQ organized the raw data and sent the information to the necessary analytical models. All of the analytical and process models were compiled and input directly into the synTQ software. The analytical models output

product or process property predictions, which were then passed within synTQ to the control models. The control models took the property predictions and predicted the process parameters necessary to continue the process along the desired trajectory for the next cycle. These parameter predictions were then passed via OPC from synTQ to DeltaV, which translated the parameters for communication to the PLC, and the PLC finally adjusted the process parameters as directed. The automated, hybrid control system was described in detail in a chapter 2.

5.2.4 Data Analysis

The analytical and process models that were included in the control system were created using MATLAB v.7.1 R14 (The Mathworks, Natick, MA, USA) equipped with the PLS_Toolbox v.3.0.4 (Eigenvector Research Inc., Wenatchee, WA, USA) and programs written in house. MATLAB code was compiled using MATLAB Compiler (The Mathworks, Natick, MA, USA) for use by the synTQ software. The DOE results were analyzed using the statistical software, jmp 8 (SAS, Cary, NC, USA). All possible main effects and first order interactions were investigated, and variables were screened for significance using the p-value statistic at the α-level 0.10.

The NIR calibration for moisture content was created by sampling granules from five trial batches, which also varied in their excipient concentrations. The reference moisture content was measured using loss on drying (LOD) on a Computrac Max-2000 moisture analyzer (Arizona Instruments, Chandler, AZ, USA). The predictive model was created using partial least-squares (PLS) regression on standard normal variate (SNV) corrected NIR spectra. The model required three PLS latent variables.

A 2^4 full factorial design was created to study the 4 input factors (Table 5.1). The input factors included a nominal formulation factor (excipient ratio), a continuous formulation factor (binder (HPMC) concentration), and two continuous process factors (EEF, EMT). It was assumed prior to experimentation that all interactions above first order would not be significant, so the experiments to discover these effects were pooled for error estimates.

Three response factors for each batch were selected to represent the product CQAs. These properties included a powder flow indicator (compressibility index), the fraction of fines in the finished granules (d_m10), and a metric for the width of the granule particle size distribution (span). The compressibility index[108, 109] is a measure of the ratio of the dried granules tapped density to their bulk density.

$$Compressibility\_Index = 100 * \left[\frac{\rho_{tapped} - \rho_{bulk}}{\rho_{tapped}} \right] \tag{5.1}$$

The bulk density of the final granule samples were measured by pouring granules through a baffle system into 100 mL graduated cylinders. Approximately 90 mL samples were collected and their masses were measured using an electronic scale (Mettler PM16K, Mettler-Toledo Inc., Columbus, OH, USA). Tapped density was measured by tapping the filled graduated cylinders 525 times using a tap densitometer (Vanderkamp 10705, LABEQUIP LTD, Markham, Ontario, Canada) and recording the tapped volume. Two bulk and tapped density measurements were measured for each granule batch.

The other two CQAs were determined by sieve analysis of 100 g granule samples using U.S. standard test sieves (Fisher Scientific, Pittsburgh, PA, USA & VWR, West Chester, PA, USA). The samples were shaken using a sieve shaker (CSC Scientific, Fairfax, VA, USA) for five minutes at level five. Ten sieve cuts were collected for each

sample (U.S. standard mesh #s: 18, 25, 35, 45, 60, 80, 120, 170, 230, and pan). A cumulative mass distribution was determined for each sample and three portions of the distribution were fit by linear least-squares to solve for the particle size that included 10% (d_m10), 50% (d_m50), and 90% (d_m90) of the cumulative mass distribution. The width of the particle size distribution was described by using the metric, span,[110] which has traditionally been used to describe the width of the size distribution of droplets, suspensions, and inhalants.

$$Span = \left[\frac{d_m 90 - d_m 10}{d_m 50} \right] \tag{5.2}$$

5.3 Results and Discussion

The measured response variables (CQAs) are listed in Table 5.1, and a summary of each models' performance are listed in Table 5.2. The CQAs represent the properties that are most significantly affected by a wet granulation operation. Ideally, the formulation and process factors would have been related to final tablet properties or biological performance attributes because they are more relevant, but taking the granulation batches through the compression unit operation was beyond the scope of this study. Additionally, the design space that was calculated for the current study only considered formulation and process factors related to the spray granulation phase of the fluid bed process. A comprehensive design space for the fluid bed unit operation would include process factors from the drying phase as well, but the expansion of the dimensionality of the DOE was unnecessary for the aims of the current chapter. A demonstration of the drying effects on product CQAs and the calculation of a design space using a similar control system has been reported in chapter 3.

A major tenet of this study was the inclusion of nominal, formulation factors and continuous process factors within the same DOE. Many traditional product development efforts have proceeded stepwise through formulation optimization and then process optimization. Stepwise methods overlook possible interactions between formulation factors and manufacturing parameters which often substantially affect product CQAs and could result in a lack of control. While it is not typical to have this degree of flexibility with regards to the pharmaceutical formulation within a design space of a batch process, the knowledge gained by identifying interactions between formulation and process factors leads to improved process understanding. This in turn, facilitates development of optimal formulations and the location of design space boundaries.

Table 5.2. Model statistics for the three process models that predict the granule CQAs

Model Statistics			
	Compressibility Index	**d_m10**	**Span**
Samples	32	16	16
Number of Model Parameters	5	4	5
R^2	0.33	0.47	0.95
RMSE*	1.85	3.93 µm	0.19
P-Value	0.0513	0.0491	<0.0001

There are two types of possible interactions between nominal and continuous variables that significantly impact the model and require the use of the extended analysis of covariance (ANACOVA) model.[64] Each interaction type was identified in different models within the current study and are displayed in Figure 5.1. The model to predict the particle size d_m10 (Figure 1b) had an effect from the EMT variable that was parallel between the two excipient ratios. The effect satisfied the assumption of parallelism within ANACOVA, which means the main effect from the EMT variable was adjusted by

the difference in mean particle size d_m10 between excipient ratio groups, and an interaction effect was not required.

The model to predict compressibility index (Figure 5.1a) had a reverse interaction[111] between excipient ratio and EEF, which did not satisfy the parallelism assumption and required the use of the extended ANACOVA model with an interaction term. This means that the effect of the EEF variable on compressibility index changed directions between excipient ratio groups, which was crucial information for identifying an optimum formulation and appropriate design space.

Finally, the model to predict particle size span (Figure 5.1c) had a same-direction interaction[111] between excipient ratio and HPMC concentration. This also did not satisfy the parallelism assumption and required the use of the extended ANACOVA model with an interaction term. The effect of the HPMC concentration variable on particle size span was in the same direction between excipient ratio groups, but the effect was much greater in the high lactose (2:1 ratio of lactose:MCC) excipient ratio group.

The compressibility index was determined to be the CQA with the highest priority. While it has traditionally been used in the pharmaceutical industry as a measurement of particle flow, it is more appropriately a measure of packing efficiency. If the granule or powder bulk density was similar to the tapped density (low compressibility index), then the powder system packed efficiently under low stress. This correlates to efficiency with respect to filling dies in a rotary tablet press, resulting in desirable tablet properties (low mass variability, increased strength, etc.) Therefore, lower compressibility index values correlate to better downstream manufacturability. The U.S. Pharmacopeia (USP) has seven levels of the compressibility index, with values

less than or equal to 25 referred to as passable, and values greater than 25 considered poor.[108] Thus, the specification threshold for the compressibility index CQA was 25.

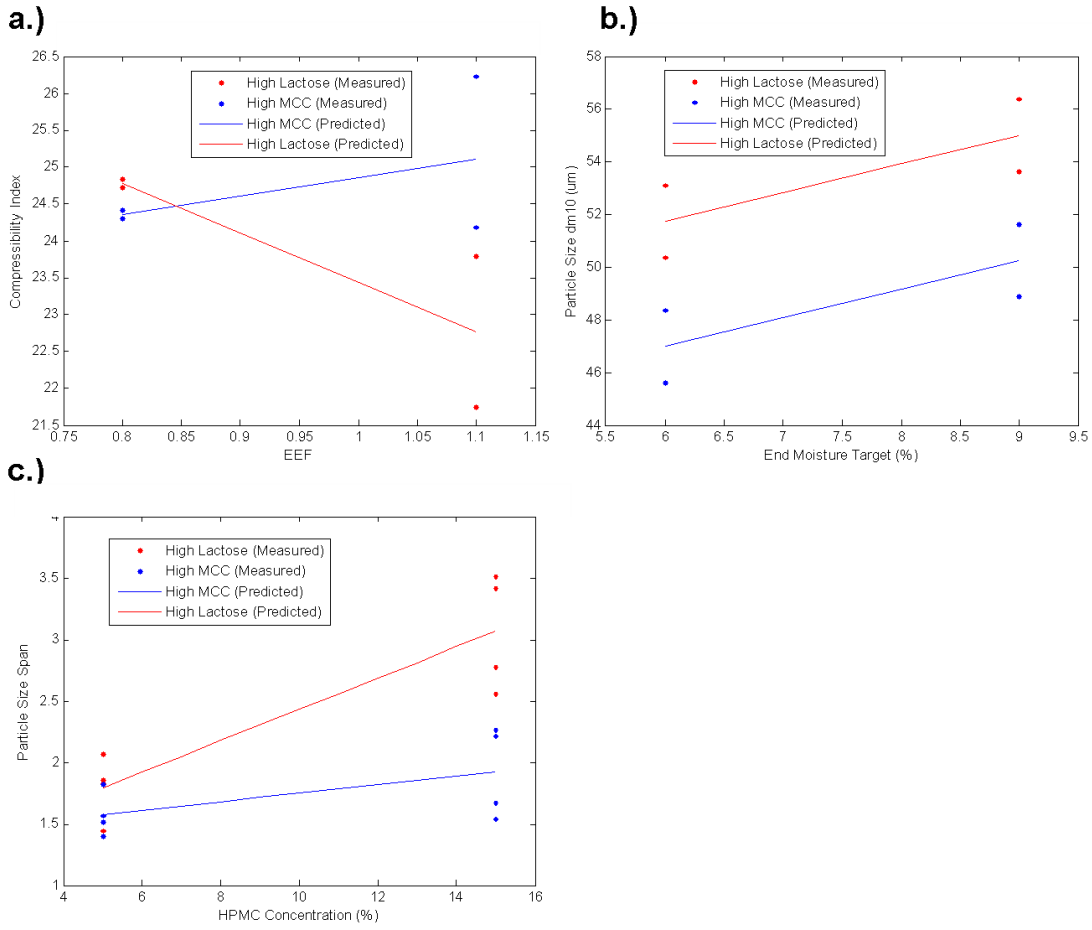

Figure 5.1. The different interaction effects between nominal variables and continuous variables. **a.)** The reverse interaction effect of the EEF variable on compressibility index between different excipient ratios. **b.)** The parallel effect of the EMT variable on the particle size d_m10 between different excipient ratios. **c.)** The same direction interaction effect of the HPMC concentration variable on particle size span between different excipient ratios.

The model that predicted compressibility index included three main effects (excipient ratio, EEF, EMT) and two interaction effects (excipient ratio*EEF, EEF*EMT). The significance of the nominal variable (excipient ratio) meant that there was a significant difference between the mean compressibility index of the two excipient ratio groups, so a knowledge space that displays the process model predictions is

displayed separately for each excipient ratio (Figures 5.2a and 5.3a). As noted previously, the interaction between excipient ratio and EEF was a reverse interaction. Therefore, the mean difference of compressibility index between groups was not as large, but the effect of the EEF variable was reversed. This can be observed in the difference along the EEF dimension in Figures 5.2a and 5.3a. There was no interaction between the excipient ratio and the EMT variable, so the effect along the EMT dimension in Figures 5.2a and 5.3a was similar. The interaction between EEF and EMT caused the curvature that was observed in the knowledge space of the two figures.

The EMT defined the end point of the spray granulation phase, so a high EMT allowed for more water to be added to the fluidized powders and increased particle agglomeration. This additional agglomeration caused an increase in the number of large particles (>500 μm) and a reduction in the fraction of fines, which reduced the packing efficiency (increased compressibility index). It was expected that the EMT variable would have a similar effect on the different excipient ratio groups, which was proven to be true.

The high lactose excipient ratio group had substantially better wetting properties than the high MCC group. Lactose is a disaccharide sugar with 8 hydroxyl groups per molecule, making it polar and increasing its affinity for water molecules. Microcrystalline cellulose is a naturally occurring polymer derived from wood pulp with a high degree of internal bonding in the crystalline structure, reducing its affinity for water molecules. Water interacted with lactose much more easily than MCC, which allowed liquid bridges to form between lactose particles with a higher probability. Therefore, the granulation process was more efficient with respect to the amount of water

added in the high lactose excipient ratio, resulting in larger and more spherical particles. These properties, combined with favorable flow properties of pure lactose compared to MCC, caused an increase in the packing efficiency over the range encountered.

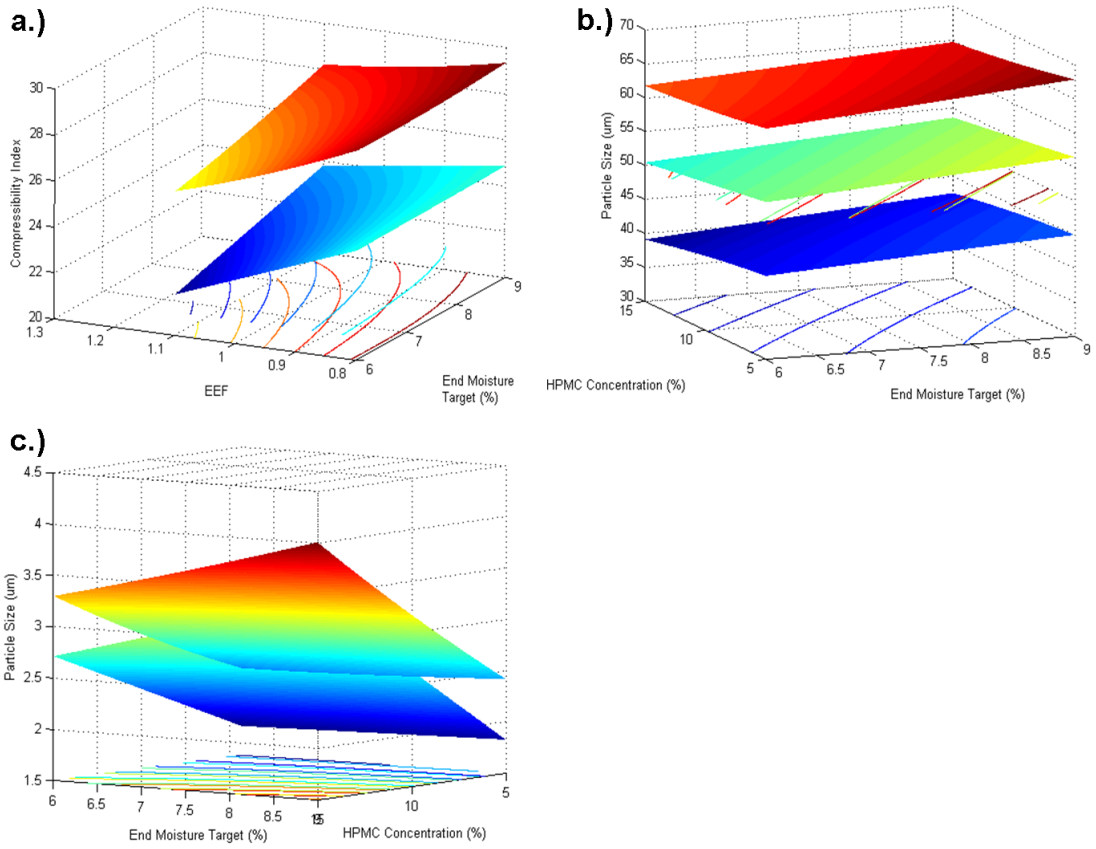

Figure 5.2. The process model predictions (knowledge space) for the three CQAs of the high lactose excipient ratio batches. The predictions of **a.)** compressibility index, **b.)** particle size d_m10, and **c.)** particle size space also include the 95% tolerance surfaces that include the space where there is a 95% probability that 95% of future batches will reside. The particle size d_m10 CQA includes both the low and high tolerance surfaces because it is a two sided specification, while the compressibility index and particle size span CQAs only include the high tolerance surface.

Reduced EEF values resulted in improved compressibility index in the high MCC group. The EEF variable controlled the energy of the input air stream during the spray granulation phase. A low EEF corresponded to a higher energy input, which was primarily achieved through an increase in the heated air temperature. Therefore, at low EEF, water was removed from the system at a higher rate. The spray rate remained the

same for all experiments, so the length of the spray granulation phase and the amount of water added were increased to achieve a similar granule moisture content at the endpoint. This extra time allowed batches with higher MCC ratios (which granulated with reduced efficiency) to grow particles to a more ideal size. As a result, packing efficiency increased at low EEF in the high MCC excipient ratio batches.

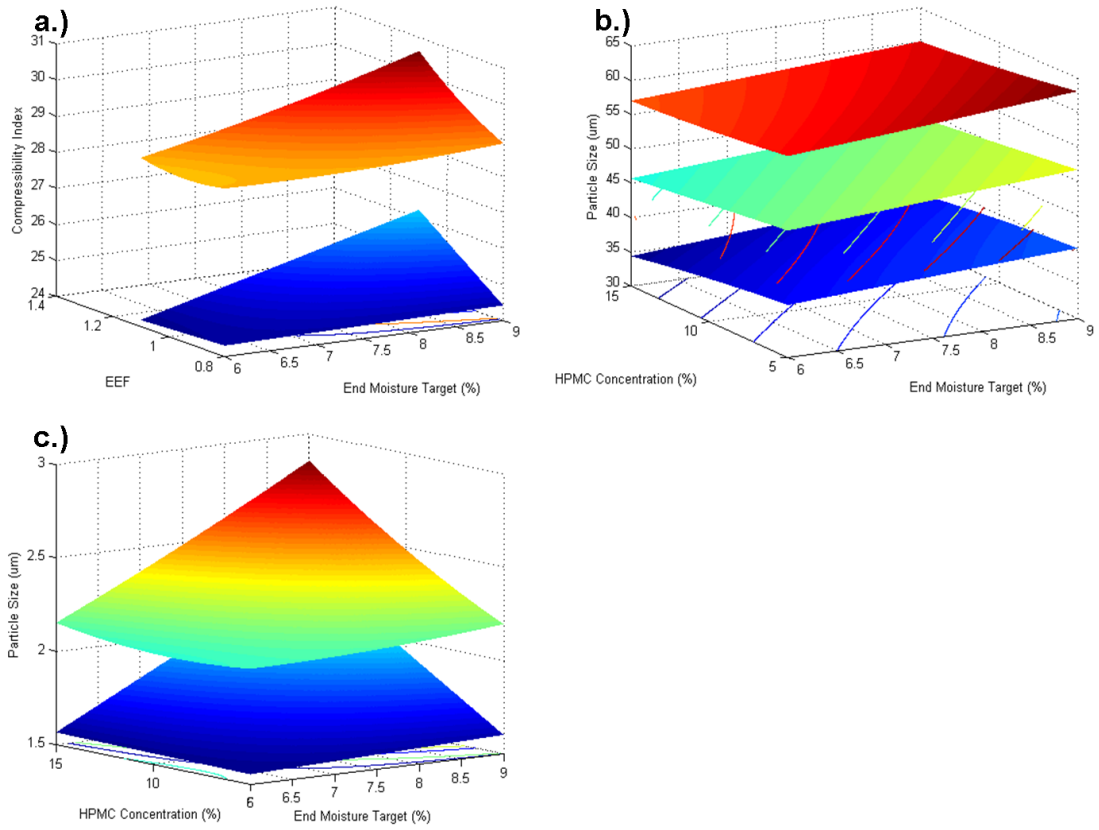

Figure 5.3. The process model predictions (knowledge space) for the three CQAs of the high MCC excipient ratio batches. The predictions of **a.)** compressibility index, **b.)** particle size d_m10, and **c.)** particle size span also include the 95% tolerance surfaces that include the space where there is a 95% probability that 95% of future batches will reside. The particle size d_m10 CQA includes both the low and high tolerance surfaces because it is a two sided specification, while the compressibility index and particle size span CQAs only include the high tolerance surface.

Conversely, the increased energy input and time in the granulation phase was not favorable for the high lactose excipient ratio batches. This was the result of the high efficiency with which lactose granulated, which caused an increase in the number of

particles greater than 500 μm at extended times, widened the particle size distribution, and reduced the packing efficiency. This effect was exacerbated at high moisture targets because the change in the duration of spraying was greater. These factors created the interaction between EEF and EMT.

The compressibility index predictions from the model are displayed in the lower surfaces of Figures 5.2a and 5.3a. All models contain uncertainty due to random error or experimental errors, and this uncertainty was not constant throughout the entire modeled space. Uncertainty was dependent on distances from the center of the model and the location of calibration samples. Therefore, it was inappropriate to use the model predictions themselves to define a design space. For this reason, a tolerance interval[67] was calculated that described a range of response values that contained a 95% probability that 95% of all future responses will be included. Because the specification for the compressibility index CQA was one-tailed (<= 25), only the high tolerance threshold was calculated. It is displayed as the upper surface in Figures 5.2a and 5.3a. This surface was used to determine a design space that reduced the risk of future batch failure.

Figures 5.4a and 5.5a display tolerance surfaces for the compressibility index process model of the high lactose and high MCC excipient ratio batches, respectively. The probability of each combination of CPPs producing future product that passes the compressibility index specification is shown in these figures. They are used to define the single factor design space. The high lactose excipient ratio provides an increase in the probability of meeting the compressibility index specification at all locations, and within these batches, high EEF and low EMT give the optimum combinations for this CQA.

The second highest priority CQA was the particle size that included 10% of the cumulative mass distribution (d_m10) of a batch from the sieve analysis. This was used as a measure of the fraction of fines. A low d_m10 indicated a large fraction of fines. The d_m10 CQA has a two-tailed specification ($45 <= d_m10 <= 60$) because a low fraction of fines resulted in poor packing efficiency and poor tablet quality, but a large fraction of fines resulted in poor flow properties and increased the probability of segregation. The specification thresholds were optimized for this specific formulation.

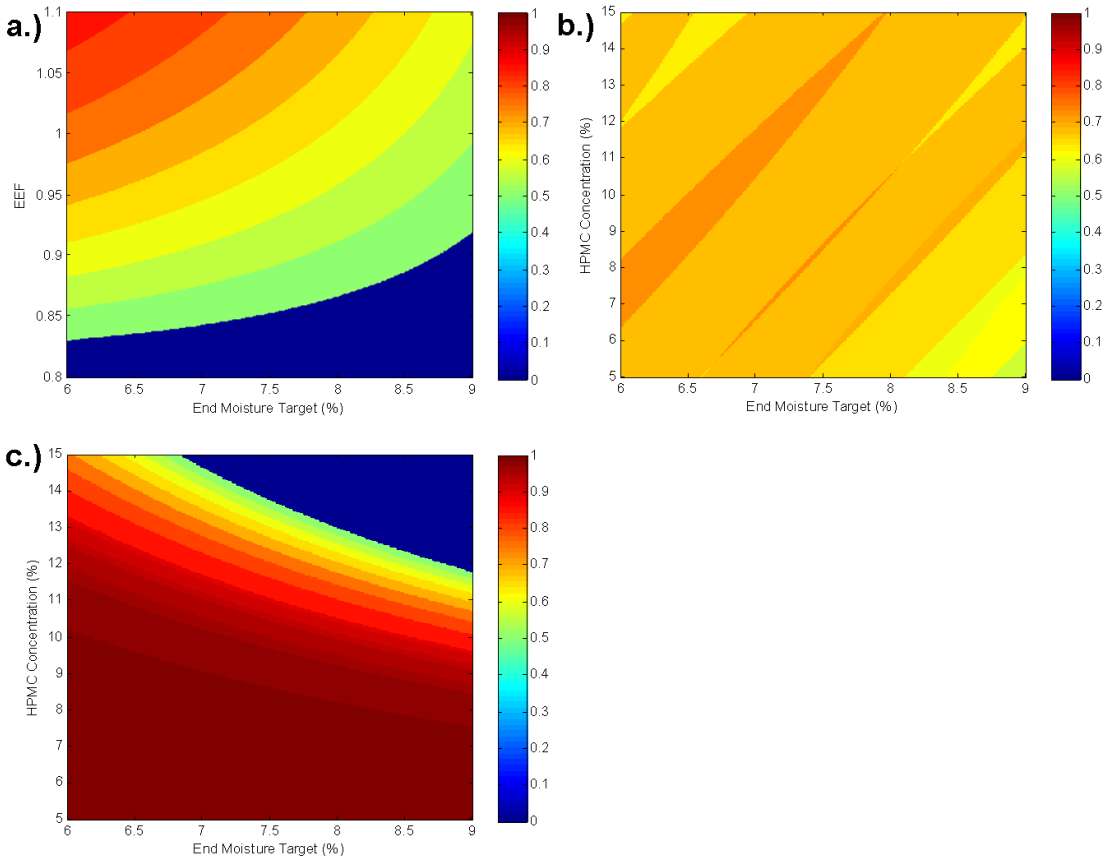

Figure 5.4. The single CQA tolerance surfaces (design spaces) for the high lactose excipient ratio that displays the probability that 95% of future batches will meet the CQA specification at the given location: **a.)** Compressibility Index; **b.)** Particle Size d_m10; **c.)** Particle Size Span.

The model to predict d_m10 contained three main effects (excipient ratio, HPMC concentration, EMT). The prediction results, low tolerance surfaces, and high tolerance

surfaces are displayed in Figures 5.2b and 5.3b. Not surprisingly, the excipient ratio again had the strongest effect on d_m10. The high MCC batches did not granulate efficiently and therefore have a larger fraction of fines (low d_m10). The EMT variable was directly proportional to d_m10, which was expected because increased spraying allowed for more particle agglomeration and a smaller fraction of fines. Conversely, the HPMC concentration was inversely proportional to d_m10. This was unexpected because it would seem that an increase in the binder concentration would reduce the number of fines. The high HPMC concentration (15%) was still a minor component of the batch, however, so it is hypothesized that while there was additional particle agglomeration in the bulk of the batch, the fraction of fines was not reduced by higher binder concentrations.

The tolerance surface (single factor design space) for the d_m10 process model is depicted in Figures 5.4b and 5.5b for the high lactose and high MCC batches, respectively. The optimum space within the high lactose batches (Figure 5.4b) was in the middle of the investigated space. Locations where d_m10 was predicted to be high (high EEF, low HPMC) had an increased probability of failing the high specification, while locations where d_m10 was predicted to be low had an increased probability of failing the low specification. For the high MCC batches, there was a much greater probability of failing the low specification, so the optimum region was in the bottom right of Figure 5.5b. Overall, there was a greater probability of successfully meeting the d_m10 specifications within the high lactose batches, so the optimum process space was at intermediate EMT and HPMC concentration values with the high lactose excipient ratio.

The final CQA for this project was the particle size span, which was an indicator of the width of the particle size distribution. A narrow particle size distribution (low span) was desirable because it significantly reduces the risk of future batch segregation, while maintaining adequate flow, packing efficiency, and compaction properties. Therefore, the span specification was one-tailed (<= 3), and defined the magnitude of the width of the distribution as being no more than 3 times the median particle size.

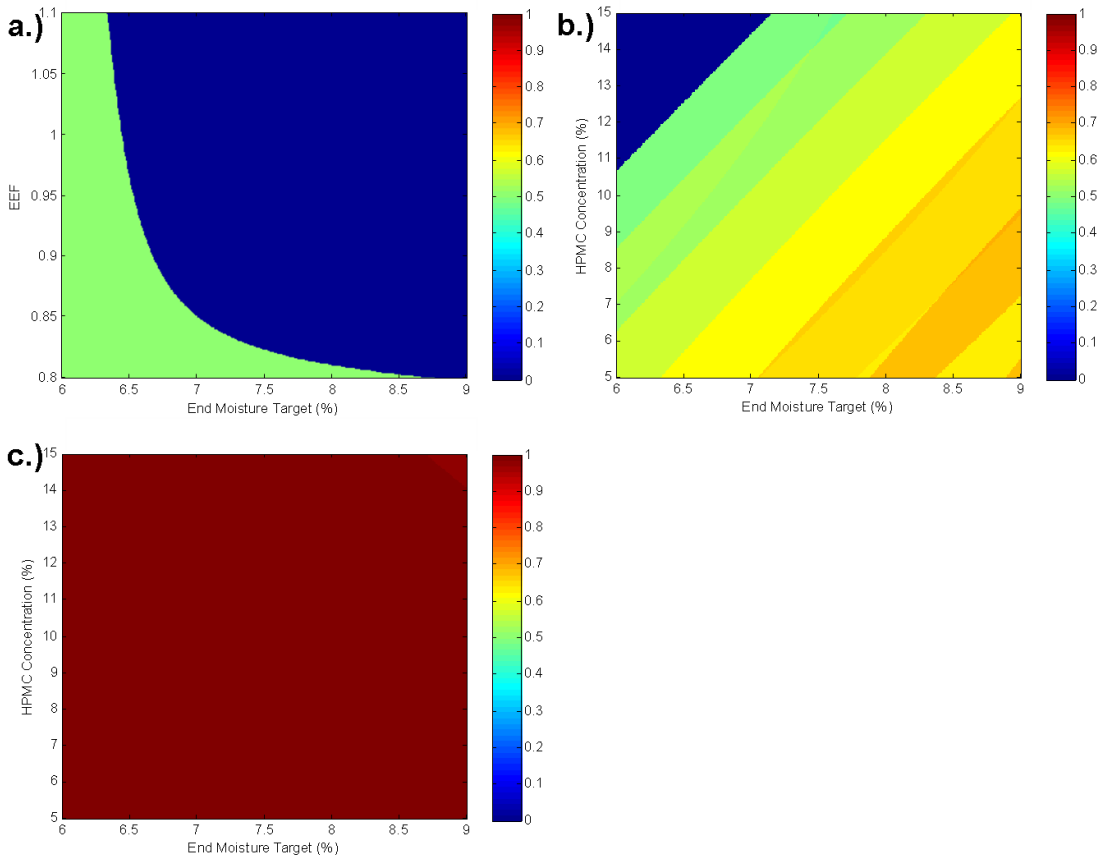

Figure 5.5. The single CQA tolerance surfaces (design spaces) for the high MCC excipient ratio that displays the probability that 95% of future batches will meet the CQA specification at the given location: **a.)** Compressibility Index; **b.)** Particle Size d_m10; **c.)** Particle Size Span.

The model that predicted the span of the particle size distribution included three main effects (excipient ratio, HPMC concentration, EMT) and two interaction effects (excipient ratio*HPMC, HPMC*EMT). The predictions and the high tolerance surfaces

are presented in Figures 5.2c and 5.3c. The main effects were all intuitive. Generally, any effect that caused more particle agglomeration widened the particle size distribution because the starting particle size distribution for all batches was narrow at small particle sizes. There was very little particle size growth in the high MCC batches, so the span of the particle size distribution remained small. Higher HPMC concentrations created more particle agglomeration, so the span of the particle size distribution at higher HPMC concentration was larger. This same effect was observed for the EMT variable.

The interaction effect between the HPMC concentration variable and the EMT variable was in the same direction as the main effects, but the combined effect of high HPMC and EMT or low HPMC and low EMT was greater than the predicted effect when they were considered independently. The HPMC effect on the span of the distribution was in the same direction for both excipient ratios (Figure 5.1c), but the magnitude of the effect was much greater in the high lactose batches. This violates the assumption of parallelism in ANACOVA, which necessitated the excipient ratio*HPMC concentration interaction term in an extended ANACOVA model. The high MCC batches granulated inefficiently regardless of the HPMC concentration, so the change in HPMC concentration did not impact the high MCC batches as substantially.

The tolerance surfaces (single factor design spaces) for the particle size span CQA for the high lactose and high MCC batches are depicted in Figures 5.4c and 5.5c, respectively. There is a very high probability of meeting the span specification at all points of the knowledge space within future high MCC batches. The same high probability of success exists with future high lactose batches, but only at combinations at low HPMC concentration and low EMT. All of these locations are at points where

particle agglomeration was reduced, the number of large particles (>500 µm) was reduced, and the span of the distribution was narrow.

To create the final design space the tolerance surfaces for the three CQAs were combined and decisions on optimum formulation parameters were made. As stated previously, it is impractical to include variability with respect to formulation concentrations in a design space for a batch process. Therefore, the knowledge gained from the DOE was used to choose an optimum excipient ratio and an optimum HPMC concentration, and the combination of the EEF and EMT variables at these optimum points created the design space.

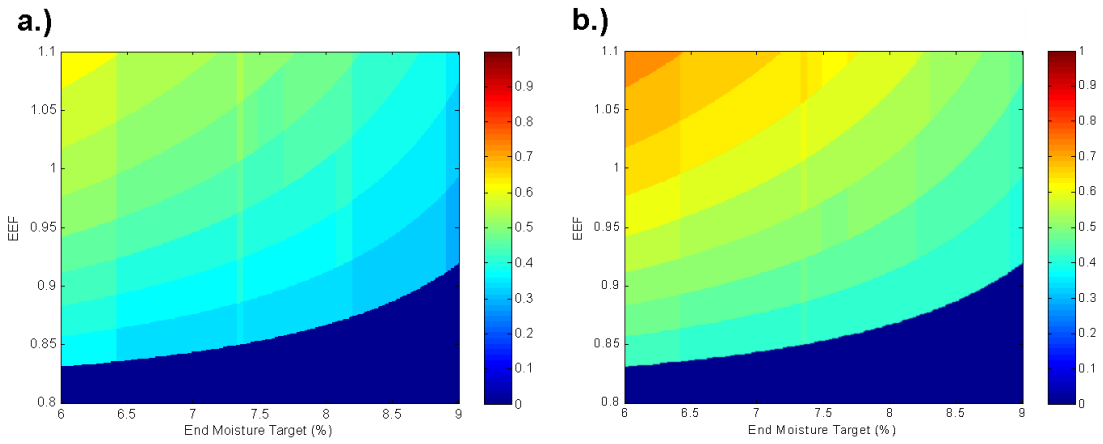

Figure 5.6. The final design space for the high lactose excipient ratio that displays the probability that 95% of future batches will meet all CQA specifications at the given location: **a.)** CQAs are given equal weight; **b.)** CQAs are weighed by risk.

There was a much higher probability of passing the compressibility index and d_m10 specifications at the high lactose excipient ratio, and the probability of passing the particle size span specification was also high at certain locations in the high lactose excipient ratio. Therefore, the 2:1 ratio of lactose to MCC was identified as the optimum excipient ratio. It was determined that 8% was the optimum HPMC concentration by analyzing the tolerance surfaces for the d_m10 and particle size span models (Figures 5.4b

and 5.4c). Therefore, the probabilities of passing the d_m10 and particle size span specifications for all EMT values at the optimum formulation were multiplied with the probabilities of passing the compressibility index specification at all EMT and EEF values. The result was the probability of passing all three CQA specifications in 95% of future batches. This combined tolerance surface created the final design space and is displayed in Figure 5.6a.

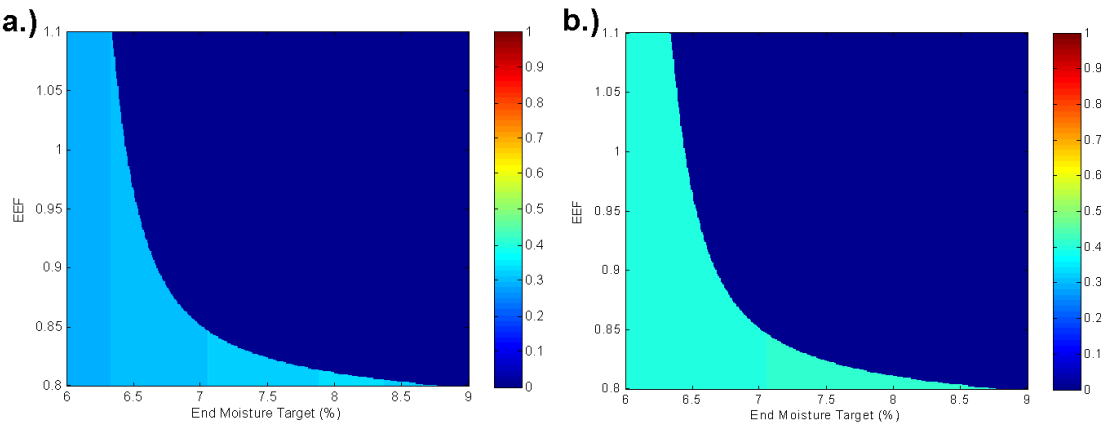

Figure 5.7. The final design space for the high MCC excipient ratio that displays the probability that 95% of future batches will meet all CQA specifications at the given location: **a.)** CQAs are given equal weight; **b.)** CQAs are weighed by risk.

The direct combination of probabilities via multiplication gave equal weight to all CQAs, which may not be appropriate for some formulations. The compressibility index was identified as being the most significant CQA, followed by d_m10 and particle size span. Therefore, an additional tolerance surface was calculated and displayed in Figure 5.6b, which gives 50% of the total weight to the compressibility index CQA, and 25% to each of the other CQAs. This figure more closely resembles the compressibility index tolerance surface, and more adequately describes the risk of the process. For both figures (5.6a and 5.6b), the optimum region that maximized the probability of future success is

located at high EEF and low EMT values. This local region would be where the operating space would be identified, and the total area of the operating space would depend on the degree of risk associated with a failure mode. The combined tolerance surfaces for the high MCC batches are displayed in Figures 5.7a and 5.7b, and the low probabilities of success prove again that the high lactose excipient ratio was optimal.

Table 5.3. The correlation matrix for the three response factors

Response Factor Correlation Matrix			
	Compressibility Index	**d_m10**	**Particle Size Span**
Compressibility Index	1.00	-0.30	0.05
dm10	-0.30	1.00	0.11
Particle Size Span	0.05	0.11	1.00

Conservative methods for calculating the combined tolerance surfaces are described here because it was assumed that all CQAs were independent and uncorrelated. Therefore, it considered the risk of failure for each CQA specification independently, and lowered the overall probability of success. Most manufacturing response variables have some degree of correlation, which was the case for this particular example (Table 5.3). Therefore, there is at least a 30% probability that failure of one CQA will have simultaneous failures of other CQAs, which reduces the number of future batches that have at least 1 failure mode. The probabilities within the combined tolerance surface could be adjusted accordingly, but reporting the most conservative results will reduce greatly the risk of underestimating future failures. If the desired probability of success

was not met, additional experiments must be augmented to the original DOE at the local region where a high probability of success is necessary (operating space). This would reduce the model error in the operating space and shift the center of the model toward the operating space, both of which would lower uncertainty.

5.4 Conclusion

The quality by design (QbD) paradigm in the pharmaceutical industry is moving product development in a much more rigorously scientific direction that requires well designed experiments and control systems, but results in higher degrees of product quality and substantial economic incentives over time. The current chapter described a hybrid control system that was developed efficiently and was able to control the fluid bed granulation and drying unit operation through four manufacturing phases. The control system made use of a first principle relationship to control the major mechanism of the manufacturing process using a single variable. Online spectroscopy provided increased process understanding and immediate feedback for control of phase end points. Combined, these controls resulted in reduced variability with respect to manufacturing quality using a limited number of experiments.

The DOE that was developed to optimize the manufacturing process for the given combination of materials included both formulation and process factors. The subsequent analysis of the data identified significant interactions between variables including a nominal formulation factor and continuous process factors. This information would not have been identified in traditional stepwise developmental efforts, which could have resulted in misidentifying the optimum combination of formulation and process factors in the final design space. Additionally, a rigorous statistical analysis that utilized extended

ANACOVA models and tolerance intervals around the response factor predictions was used to define the optimum design space that reduced the risk of future batch failure to a specified level.

Chapter 6: Efficient Near Infrared Spectroscopic Calibration Methods for Pharmaceutical Blend Monitoring

6.1 Introduction

The benefits of a hybrid control system that combines first principle calculations and empirical modeling for the fluid bed granulation and drying unit operation have been well established in the previous chapters. The described control systems were designed specifically for the needs of the unit operation and were ideal for the complexities associated with fluid bed granulation and drying. The level of complexity, the type of online measurements, and the control strategy may not be necessary for all formulations, systems, or unit operations, however. A control system must be designed for each system to meet all of the quality requirements while incurring the smallest possible costs.

The powder blending unit operation for most pharmaceutical formulations is a system that lacks the level of complexity associated with fluid bed granulation and drying. It is a unit operation that is required for almost all solid formulations in the pharmaceutical industry, and inputs mechanical stress to charged powders via vessel rotation to assure a homogeneous distribution of solid components throughout the batch for further processing. Powder mixing is never the same from batch to batch, so a control system is needed to simply monitoring the homogeneity of the blend in real-time so that the blend can be stopped when a satisfactory and consistent level of homogeneity is reached for every batch. This chapter will discuss a method for efficient and robust

development of a multivariate spectral calibration, the most challenging and cost consuming step in the development of a control system for powder blending.

The use of near infrared (NIR) spectroscopy in the pharmaceutical industry has become increasingly popular over the past several decades.[112] Little or no sample preparation is needed, which allows for efficient data collection and the ability to monitor processes online. However, there can be a substantial cost in generating and maintaining robust quantitative multivariate NIR calibrations. This chapter seeks to demonstrate efficient means of generating calibrations and maintaining them through the life-cycle of the method.

Large sample sets are typically created using experimental design techniques.[113] These sets contain enough samples to span the expected variance of chemical and physical characteristics, while also including several replicate samples. In a system that has four chemical components and two physical components, a calibration set with only two levels of each component would require a minimum of 70 independent samples. The sample size increases exponentially when additional component levels are added (as is frequently necessary for more sensitive calibrations). Additionally, it is necessary to generate a validation set and calibration transfer samples (for update or transfer). Considering all of the samples required, the development and maintenance of a robust NIR calibration can be an expensive undertaking.

A potential advantage that a pharmaceutical analyst has for reducing the required number of design points is access to pure components samples. The highest concentration point for all chemical components is available by scanning pure components, thereby requiring minimal preparation. Similarly, scans of all other pure

components serve as zero concentration points for the analyte(s) of interest. The concentration for constituents that is the point of interest (e.g. the final formulation for a pharmaceutical blend or tablet) for each component is typically available during process development. Therefore, three concentration levels are available for all chemical components without creating new samples. Utilizing these available samples is the basis of this efficient calibration study. This technique is intended to be a low cost effort during research and development to provide satisfactory predictions during process development. It is not intended to be a final method used for product testing or process optimization, but the initial models can be updated with additional samples created by design to improve model sensitivity over a specific concentration range.

This chapter demonstrates the development and performance of efficient NIR calibrations for pharmaceutical blend monitoring. It addresses the performance of several popular multivariate calibration algorithms including partial least-squares (PLS) regression, classical least-squares (CLS) regression, augmented classical least-squares (ACLS) regression, classical least-squares/partial least-squares (CLS/PLS) regression, artificial neural networks (ANN), and least-squares support vector machines (LSSVM). Due to the differences in the calculation of the regression vectors for each algorithm, some are more appropriate for the creation of robust calibrations with reduced sample sets. A critical analysis of the performance of each algorithm is provided, as well as a discussion of the blend end point determination.

The transfer ability of the two best performing models is presented as an additional indication of model robustness. Calibration transfer is a vital portion of any online spectroscopic method because multiple NIR instruments are necessary and each

instrument drifts over time, requiring a change or update in the calibration. The ease at which this transfer process is successful is a major contributor to the success of the method and is a strong indicator of the original calibration's robustness.

This study was part of a major research project through The National Institute for Pharmaceutical Technology and Education (NIPTE) funded by the U.S. Food and Drug Administration. The project title is "Development of Quality by Design (QbD) Guidance Elements on Design Space Specifications Across Scales with Stability Considerations." It is focused on improving pharmaceutical product quality and maximizing process innovation and continuous quality improvements by developing control systems and process design spaces across several unit operations and several scales. The research was originally published in the Journal of Pharmaceutical Innovation.[133]

6.2 Theory

6.2.1. Multivariate Calibration Algorithms

The PLS algorithm is the most widely used calibration algorithm for quantitative predictions using spectral data because of its data reduction capabilities and its performance in prediction statistics. Partial least-squares regression is a bilinear modeling algorithm based on Herman Wold's general PLS principle.[114] A thorough review of the PLS algorithm is provided by Bjorsvik and Martens.[115]

The PLS algorithm calculates the regression vector by maximizing the covariance between the spectral data matrix and the reference data. Therefore, a PLS calibration is only as good as its reference data. An accurate and robust PLS calibration must have reference samples covering the entire concentration range that will be encountered in future predictions. The greater the number of concentration levels and replicates over the

range, the better the prediction statistics. Therefore, the PLS algorithm was hypothesized to be less effective for efficient calibrations using reduced samples sets.

The CLS algorithm has not been widely applied for NIR calibrations in the pharmaceutical industry because it is very difficult to estimate the pure component contribution for all spectrally active components in the sample matrix. Spectral shapes imparted by an instrument, light source, sample particle size, etc. are very difficult to determine when creating a calibration model, and thus CLS calibrations typically result in reduced accuracy statistics. Classical least-squares regression assumes that the Y variable(s) is a random variable with a distribution that depends on the X variable(s), which is considered non-random and controlled by the experimenter. The CLS algorithm is based upon explicit linear additive models (Beer's Law) that require quantitative knowledge of all spectrally active components in the calibration set,[75] and the regression vector becomes the portion of each components' pure component spectra that is orthogonal to the other pure components.

The ACLS technique, developed by Haaland and Melgaard,[75, 116, 117] is a method intended to enhance the CLS algorithm. The calibration procedure and calculation of the pure component matrix is the same as with the CLS algorithm, but ACLS allows the user to augment the predicted pure component matrix with empirically derived spectral shapes. For example, if a user determines that a difference between two lots of an excipient is causing prediction errors, samples of each lot can be collected and the difference spectrum or loading(s) from a principal component analysis (PCA) can be added to the predicted pure component matrix, $\hat{\mathbf{K}}$. This effectively orthogonalizes the regression vector for all other components to the newly derived spectral interference

shape. This can be repeated for all known interferences during calibration or prediction (prediction augmented CLS: PACLS).

The ACLS and PACLS techniques make calibrations more robust, but often lower prediction accuracy statistics because more of the measured pure component signal is removed from the regression vector due to orthogonalization. Therefore, the major drawback with the CLS algorithm is not solved, but a very intuitive calibration transfer and/or update method is introduced. A calibration transfer or update can be accomplished with a reduced sample set by simply deriving the spectral shape of the new instrument or interference and adding it to the pure component matrix.

Another simple improvement aimed at utilizing the advantages of CLS and PLS together is the hybrid (CLS/PLS) algorithm, also developed by Haaland and Melgaard.[100, 118, 119] In this method, a CLS, ACLS, or PACLS model is developed as discussed previously. A subsequent PLS model is calculated to relate the spectral residuals from the initial CLS model to the concentration residuals for each component. The predicted concentration residuals are then added to the original CLS predictions.

The PLS step of the hybrid algorithm models the structured noise remaining in the spectral data matrix, **X**, after the CLS model is calculated. This structured noise is affecting predictions and results from additional spectrally active components (particle size, instrument, etc.) that are not included in the predicted pure component matrix. The hybrid algorithm is hypothesized to be the ideal candidate for the creation of efficient calibrations using reduced sample sets. The inclusion of measured pure component scans in the CLS step allows the model to be specific for each component, while the PLS step can reduce prediction errors for better accuracy and precision. The ability to augment the

CLS portion of the hybrid algorithm makes it ideal for efficient calibration transfer or update, which is especially important for reduced sample set calibrations where significant spectral interference shapes may be encountered during prediction.

Artificial neural networks are pattern recognition methods that have been adapted to solve regression problems. It is a nonlinear modeling technique that may be more appropriate for complex data matrices. As stated in its name, ANN mimic the function of biological neural networks by being constituted of individual neurons positioned on interconnected layers. A typical ANN has an input layer, one or more hidden layer(s), and an output layer. The number of neurons on the input and the hidden layers can vary. Compared to PLS and CLS based methods, ANN do not assume linearity between inputs and outputs and can successfully be deployed in situations where the distribution of the residuals is not normal. Numerous publications show cases where ANNs provided more accurate and precise results than linear techniques.[120-123]

Artificial neural networks are particularly subject to overfitting and a good validation strategy must be developed. They perform poorly when trying to predict values outside of the training range, while linear methods can extrapolate quite well. Finally, due to the large number of elements to estimate during the development of an ANN, the number of samples must be large.[124] However, its ability to model non-linear relationships can be highly beneficial in efficient calibrations where it is highly hypothetical that the relationship between spectral data and sample concentration is linear between 0 and 100%.

Support vector machines (SVM) were originally developed for binary classification situations.[125] The idea behind SVM is to determine samples that define the

most appropriate cluster limits (support vectors) as well as reduce the misclassification rate. In regression situations, support vector regression (SVR) and least-squares support vector machines (LSSVM) try to find the best fit of the data by limiting the number of samples outside an error range set by the user.

Least-squares support vector machines has been developed to perform on data presenting non-linear relationships with a limited number of observations. The main advantage of LSSVM is that only two parameters need to be determined. Its main drawback is the computation time; it is exponentially proportional to the size of the dataset and can take several hours to perform on a set of several hundred samples. This problem is minimized using reduced sample sets. Cogdill and Dardenne[126] provided a good overview of LSSVM. Shawe-Taylor et al.[127] and Suykens et al.[128] are references for theoretical aspects of support vector machines.

6.2.1 Blend End Point Determination

The Root Mean Squared Error from the Nominal Value (RMSNV) statistic for blend end point determination is a moving window, weighted error statistic.[99] It is calculated by:

$$\text{RMSNV} = \sqrt{\frac{\sum_{t-i}^{t} W_1(\hat{Y}_1 - Y_1)^2 + \sum_{t-i}^{t} W_2(\hat{Y}_2 - Y_2)^2 + \ldots \sum_{t-i}^{t} W_n(\hat{Y}_n - Y_n)^2}{i(W_1 + W_w + \ldots W_n)}} \qquad (6.1)$$

where W is the weight given to a component and i is the number of data points used in a single window. The reference concentration for a given component (Y_n) is the nominal concentration of the component in the final blend and is compared to the predicted concentration value for that species ($\hat{Y}$). The weight for a given component can be adjusted based on the requirements and/or performance of the measurement. The

blending end point is reached when the RMSNV statistic reaches a pre-determined minimum threshold over the previous window. The adjustable parameters make the RMSNV statistic ideal for meeting the needs of a specific blending operation.

6.3 Materials and Methods

6.3.1. Pharmaceutical Formulation

The formulation contained eight components, and Gabapentin (Hangzhou Starshine Pharmaceutical Co., LTD, Hangzhou, China, Batch 0803023) was the active pharmaceutical ingredient (API). Granules comprising 93.75% API and 6.25% hydroxypropyl cellulose (HPC) (Klucel EXF, Ashland Aqualon Functional Ingredients, Wilmington, DE, USA) were manufactured using a bottom driven, high shear granulator (Diosna P1-6, Dierks & Söhne GmbH, Osnabruck, Germany, 6 L bowl) and tray dried at Purdue University. The granules were created as part of a design of experiments to optimize the wet granulation unit operation for this formulation. Three granulation batches of 1.2 Kg were granulated with 1.0%, 2.0%, and 2.5% water by weight, respectively. All three batches were dried to 0.5% moisture by weight. The median particle size for the three batches were 233 μm, 450 μm, and 590 μm, respectively. These batches were then sampled for the small scale blend experiments.

The granules, which comprise 71.99% of the blend, were combined with the extragranular excipients: 1.23% Poloxamer 407 (WLS Enterprises, Indianapolis, IN, USA), 2.47% crospovidone (Polyplasdone XL, ISP Chemicals, Wayne, NJ, USA), 6.75% starch (Lycatab C, Roquette America Inc., Geneva, IL, USA), 11.25% microcrystalline cellulose (MCC) (Comprecel M102D+, Mingtai Chemical Company Ltd., Taoyuan Hsien, Taiwan), 1.01% talc (IMI FABI LLC/Mutcher Inc., Benwood, WV, USA), 4.50%

HPC, 0.79% magnesium stearate (Mg. St., Mallinckrodt, Hazelwood, MO, USA) - for powder blending. The final concentration of Gabapentin in the blend was 67.49% and the final concentration of HPC (intra- and extra-granular) was 9.00%.

6.3.2 Blending, Sampling, and Instrumentation

Blending was performed at the Duquesne University Center for Pharmaceutical Technology (DCPT) with a 5.5 L bin blender (L.B. Bohle LLC, Warminster, PA, USA) with DeltaV (Emerson Process Management, Equipment & Controls, Inc., Lawrence, PA, USA) controls. The blender was run at 15 rpm for 15 minutes with all components except Mg. St. to ensure that each blend was completely homogenous. Magnesium stearate was then added to the blender and an additional 5 minute lubrication blend was performed. The lubrication blend was not considered in any of the following data analysis.

6.3.2.1 Side Sensor

Blends that were performed for data collection by the side sensor were completed using a small scale blend simulator that was mounted inside the 5.5 L bin blender against the side axis window. The small scale blends had a total mass of 30 grams, with an approximate fill volume of 85%. The system was designed to make the calibration processes as efficient, with respect to raw materials, as possible.

Pure component scans of each material and the pharmaceutical granules were collected by filling the blend simulator with 30 grams of a given component. Granule scans for each granulation batch were collected by filling the blend simulator with 30 grams of granules. Data were collected with the same procedure as the blends. This

procedure allowed for the pure component and granule scans to be similar in terms of physical properties and noise as compared to the dynamic or tumbling blends. The calibration curves for gabapentin and HPC had four concentration points (other components (0%), blend concentration (67.49% API, 9.00% HPC), granule concentration (93.75% API, 6.25% HPC), pure component (100%)), while the calibration curves for all other excipients had three concentration points (other components (0%), blend concentration (nominal %), pure component (100%)).

Diffuse reflectance NIR spectral data were collected using a model NIR256L-2.2T2 spectrometer from Control Development Inc. (South Bend, IN, USA). It is a 256 element photodiode array spectrometer with an extended InGaAs detector (1085-2229 nm). An external halogen light source (Control Development Inc., HL-2000) was used with a fiber optic probe (Control Development Inc., South Bend, IN, USA, 6 around 1 reflectance probe). The side sensor was stationary, with the fiber optic probe placed against a sapphire window on the rotation axis of the blender. The spot size for this system was approximately 400 μm. Spectra were collected with 16 coadditions averaged for a single scan with an integration time of 0.028 seconds. A single scan was collected every five seconds. A dark reference was collected by disconnecting the lamp from the fiber optic probe and a light reference was collected by measuring the diffuse reflectance from a 99% Spectralon Reflectance Standard (Labsphere Inc., North Sutton, NH, USA). Reference scans were collected once daily.

6.3.2.2 Top Sensor

Blends that were performed for data collection by the top sensor were lab scale blends with a total mass of approximately 800 g. The fill ratio of these blends in the 5.5

L bin blender was less than 50%. The top sensor was set to collect spectra when inverted to assure that each scan had powder directly in front of the sensor. At 15 rpm, the scans were collected at four second intervals. Pure component and granules scans were collected by filling the blender and spinning at 15 rpm in the same procedure that was performed on the small scale blend simulator. The calibration curves for the top sensor had the same concentration levels for each component as the side sensor calibrations.

Diffuse reflectance NIR spectral data was collected using the Blend Uniformity Analyzer from Control Development Inc. (South Bend, IN, USA). It is a 256 element photodiode array wireless spectrometer with an InGaAs detector (910-1680 nm) and an internal dual tungsten halogen lamp. This spectrometer was attached to the lid of the blender and rotated with the blender. The spot size for this system was 25 mm. Spectra were collected with 16 coadditions averaged for a single scan with an integration time of 0.033 seconds. The dark and light reference scans are internal for the top sensor and were collected once daily.

6.3.3 Data Analysis

All of the data analysis was performed using MATLAB v. 7.1 R14 (The Mathworks, Natick, MA, USA) equipped with the PLS_Toolbox v. 3.0.4 (Eigenvector Research Inc., Wenatchee, WA, USA), LSSVM Lab v1.5 (Katholieke Universiteit Leuven, Belgium),[128] the neural network toolbox v5.1 (The Mathworks, Natick, MA, USA), and programs written in house.

Table 6.1. The number of spectra and independent samples for the calibration set, test set, and prediction set for the top and side sensor.

	Top Sensor Data Sets										
	Calibration Set									Test Set	Prediction Set
	Pure Component Scans							Blend Scans	Granule Scans	Blend Scans	Full Blend Profile
	API	HPC	MCC	Starch	Poloxamer	Crospovidone	Talc				
Number of Spectra	19	23	18	16	12	16	15	68	53	30	227
Number of Independent Samples	1	1	1	1	1	1	1	4	3	2	1
	Side Sensor Data Sets										
	Calibration Set									Test Set	Prediction Set
	Pure Component Scans							Blend Scans	Granule Scans	Blend Scans	Full Blend Profile
	API	HPC	MCC	Starch	Poloxamer	Crospovidone	Talc				
Number of Spectra	28	30	30	30	30	30	30	30	133	35	367
Number of Independent Samples	1	1	1	1	1	1	1	2	3	3	1

The calibration set for the side sensor consisted of 371 spectra from 12 independent samples. The wavelength range was truncated to the 1151-2229 nm range to eliminate the noisy portion of the detector at shorter wavelengths. Further information on the calibration set, test set, and prediction set are included in Table 6.1. The blend scans in the calibration set represent the final minute of 2 independent blends. The 1.0% and 2.0% moisture content granulation batches supplied the granules for these 2 blends, respectively.

The calibration set for the top sensor contained 240 spectra from 14 independent samples. The wavelength range was truncated to the 924-1656 nm range to remove the noisy ends of the spectrometer. Further information on the top sensor data sets can be found in Table 6.1. The blend scans in the calibration set represent the final minute of four independent blends. Each granulation batch was represented in one of the four independent blends, with the 2.0% moisture content batch represented twice.

Calibrations for both instruments were created using the algorithms described previously to predict each of the concentrations of the four major blend components (Gabapentin, MCC, HPC, and Starch), which comprise 94.49% of the final blend. The other minor components were present in concentrations less than 2.5%, which is too low for consideration in this context. The prediction performances for the reported efficient calibrations are of magnitudes that would constitute a significant portion of these low concentrations.

The calibrations for each of the four major components were optimized for the minimum cross-validation error independently by preprocessing methods, augmentation, number of modeling factors, etc.; even calibrations using the same algorithm. For

example, the spectral preprocessing and number of latent variables were optimized for the gabapentin PLS calibration; similarly, the same parameters were independently optimized for the starch PLS calibration. For ANN and LSSVM, a randomly selected stop set of 20% of the calibration was used to tune the parameters. The stop set acted like a 1-block cross validation approach and allowed model parameters to be tuned. Both non-linear approaches were developed based on principal component scores. For ANN, 10 independent generations were created to ensure that results were not based on a local minimum. All parameters (for ANN: network structure, momentum, learning factor, transfer function, etc.; for LSSVM: kernel and regularization factor) were independently tuned for each parameter and each material.

The calibration performance was reported with multiple statistics including the coefficient of determination (R^2), root mean squared error of the calibration (RMSEC), standard error of the calibration (SEC), bias, slope, and offset. The test performance was reported using the R^2, root mean squared error of prediction (RMSEP), standard error of prediction (SEP), bias, slope and offset statistics. Finally, the spectra collected from a separate full blend that is not in the calibration or test sets was used for prediction purposes to study the effect of the blend end point determination using different algorithms.

For all calibration algorithms studied in this manuscript, the RMSNV statistic was determined using the four major components of the pharmaceutical blend with each component receiving an equal weight (1/4). The moving window contained enough samples to comprise one minute of blending (12 samples for the side sensor; 15 samples for the top sensor).

Different test sets were used for the side and top sensor. The side sensor utilized the final 15 scans of two additional independent, small scale blends created using granules from the 1.0% and 2.0% moisture granulation batches and the final five scans of a third independent blend with granules form the 2.0% moisture granulation batch (35 total spectra) as an independent test set. An additional independent blend using granules from the 2.0% moisture granulation batch was used as a prediction set for determining blend homogeneity. For the top sensor, the final 15 spectra from two separate blends using granules from the 1.0% and 2.0% moisture granulation batches, respectively, were used as an independent test set and a third independent blend using granules from the 2.0% moisture granulation batch was used for prediction of the blend end point.

6.3.4 Calibration Transfer

The two best performing algorithms from the calibration study were studied further in a calibration transfer study. The common wavelength range (1151-1680 nm) between the two sensors' truncated calibration sets were used so that the calibrations could be applied to both instruments. Calibration transfer was attempted from the side sensor to the top sensor (S-T) and from the top sensor to the side sensor (T-S) for all transfer techniques. The same test and prediction sets were used to evaluate the performance of the transferred calibrations with the RMSEP, SEP, and bias statistics reported.

Each calibration was applied directly to the other spectrometer data as the simplest possible prediction scenario. Robust calibrations were created using different numbers of spectra from both instruments' calibration sets (100%, 50%, and 25%) as a baseline to compare the performance of the transfer techniques. For each transfer

technique, the 10 samples from the calibration set having the lowest residuals were removed to create the transfer set. Each calibration was then transferred using bias correction, direct standardization (DS), and piecewise direct standardization (PDS),[73, 74] and the results were compared for performance. Standardization samples were removed prior to developing calibrations. Thus, all calibration models were developed without the 10 best samples.

6.4 Results and Discussion

6.4.1. Calibration Study

Performance results from the calibration study can be found in Table 6.2, which contains the pooled calibration statistics for the four major components for both sensors. The top sensor data contained less noise than the side sensor data; as a result, the calibration statistics were generally better for the top sensor. There were exceptions, and the differences between the two instruments depended on the multivariate algorithm employed.

In all models, the error statistics were notably lower for nonlinear methods (ANN and LSSVM) than for the linear multivariate algorithms. The ANN models had the lowest error statistics, but these models lacked sensitivity, which was observed when predicting full blend profiles (Figures 6.1 and 6.2). The ANN models predicted all samples in a range around the blend point as having the nominal blend concentration, so blends that were not homogenous would have been predicted to be homogenous by the ANN method. The ANN algorithm has many more parameters to optimize than linear methods, which are not intuitive and require an extensive validation method. The number of independent samples that were available in this efficient calibration setting did

not allow for a rigorous ANN optimization. The ANN algorithm was not considered further.

Table 6.2. The pooled calibration performance statistics across the 4 major blend components for both sensors using multiple calibration algorithms.

		Top Sensor Calibration Statistics						
		Pooled Statistics for 4 Major Components						
		PLS	CLS	Aug-CLS	CLS/PLS	Aug CLS/PLS	LSSVM	ANN
Calibration	R^2	0.9869	0.9853	0.9850	0.9945	0.9936	0.9999	0.9999
	RMSEC	0.0399	0.0426	0.0431	0.0261	0.0279	0.0042	0.0036
	SEC	0.0399	0.0427	0.0431	0.0261	0.0279	0.0042	0.0036
	Bias	0.0000	0.0000	0.0000	0.0000	0.0000	0.0000	0.0005
	Slope	1.0000	0.9585	0.9850	0.9945	0.9936	1.0001	1.0030
	Offset	0.0000	0.0030	0.0030	0.0011	0.0013	0.0000	0.0000
Test	R^2	0.9893	0.9875	0.9892	0.9689	0.9701	0.9999	1.0000
	RMSEP	0.0323	0.0397	0.0379	0.0455	0.0448	0.0080	0.0004
	SEP	0.0322	0.0385	0.0366	0.0457	0.0449	0.0078	0.0004
	Bias	0.0021	-0.0104	-0.0103	0.0006	0.0026	0.0016	0.0000
	Slope	0.9337	0.9089	0.9109	0.9772	0.9747	0.9967	1.0000
	Offset	0.0177	0.0122	0.0118	0.006	0.0086	0.0024	-0.0004
		Side Sensor Calibration Statistics						
		Pooled Statistics for 4 Major Components						
		PLS	CLS	Aug-CLS	CLS/PLS	Aug CLS/PLS	LSSVM	ANN
Calibration	R^2	0.9700	0.9844	0.9843	0.9927	0.9953	0.9999	0.9996
	RMSEC	0.0632	0.0458	0.0461	0.0313	0.0252	0.0034	0.0074
	SEC	0.0632	0.0459	0.0461	0.0313	0.0252	0.0034	0.0074
	Bias	0.0000	0.0000	0.0000	0.0000	0.0000	0.0000	0.0000
	Slope	1.0000	0.9844	0.9843	0.9927	0.9953	1.0000	1.0002
	Offset	0.0000	0.0029	0.0030	0.0014	0.0009	0.0000	-0.0001
Test	R^2	0.9756	0.9179	0.9778	0.9795	0.9843	0.9972	0.9998
	RMSEP	0.0416	0.0738	0.0408	0.0383	0.0339	0.0180	0.0035
	SEP	0.0412	0.0741	0.0392	0.0384	0.0336	0.0180	0.0034
	Bias	0.0054	0.0016	-0.0116	0.0017	0.0055	0.0009	0.0008
	Slope	0.9641	0.9660	0.9672	1.0460	1.0403	0.9563	1.0007
	Offset	0.0137	0.0096	-0.0034	-0.0092	-0.0039	0.0113	0.0006

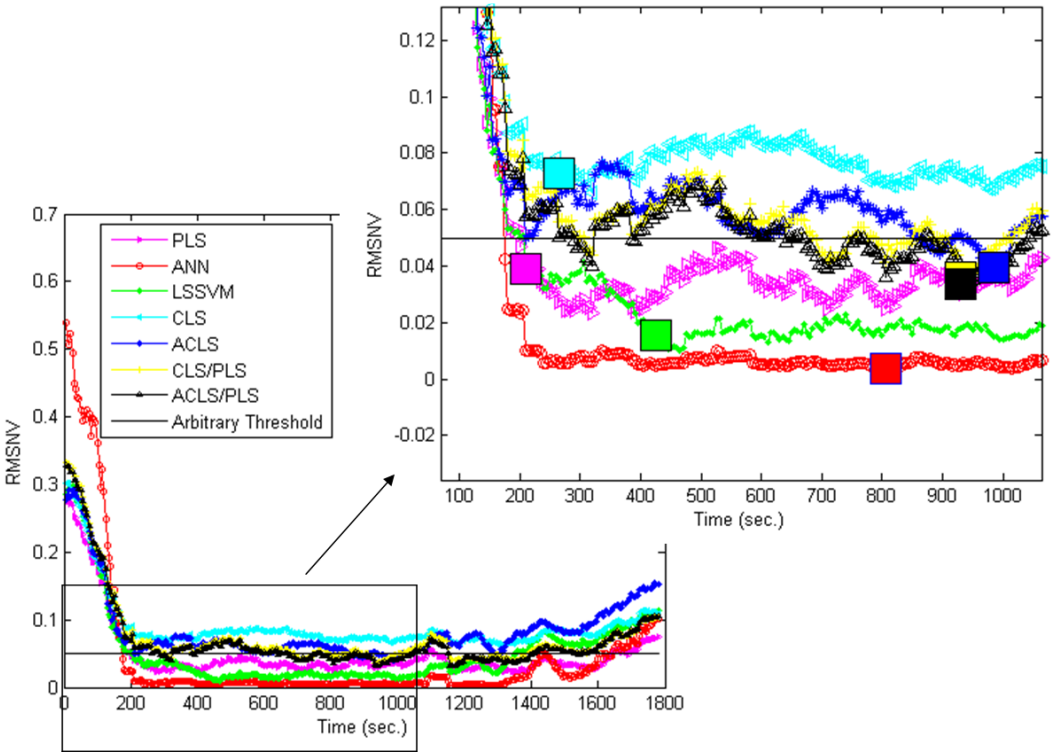

Figure 6.1. RMSNV trends of a single independent blend using multiple calibration algorithms on side sensor data. The solid boxes in the zoomed portion of the figure represent the blend end point as determined by each algorithm. The end point is defined when the RMSNV over the previous minute is less than or equal to the test error for the respective calibration. The solid line represents a strictly arbitrary threshold for RMSNV.

The performance of the CLS algorithm was comparable to that of PLS. This demonstrates the advantage that CLS based algorithms have over PLS with reduced sample sets and pure component spectra. Even without spectral shapes in the $\hat{\mathbf{K}}$ matrix that represent physical effects such as particle size and density, the prediction results were acceptable.

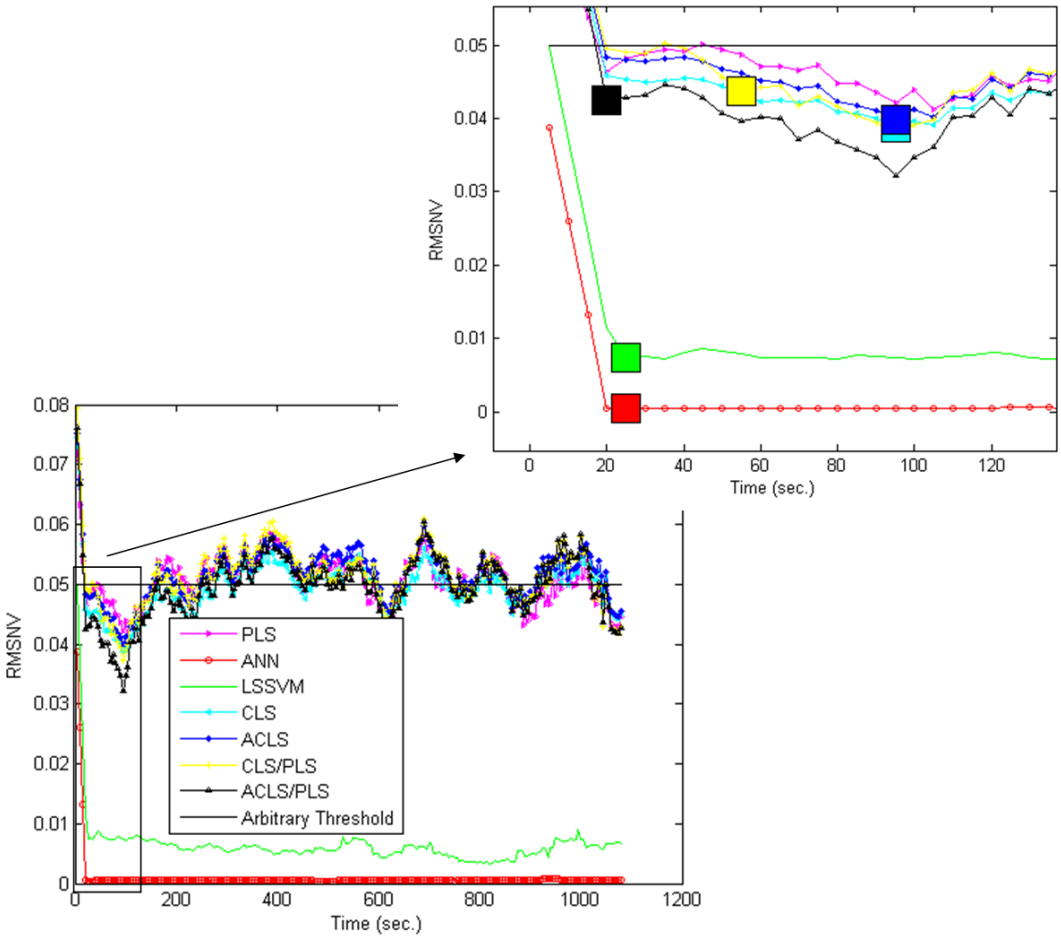

Figure 6.2. RMSNV trends of a single independent blend using multiple calibration algorithms on top sensor data. The solid boxes in the zoomed portion of the figure represent the blend end point as determined by each algorithm. The end point is defined when the RMSNV over the previous minute is less than or equal to the test error for the respective calibration. The solid line represents a strictly arbitrary threshold for RMSNV.

Test and prediction results for CLS were improved by augmenting additional spectral shapes from other spectrally active factors, but the effects were different for each component. Calibration performance was improved further by adding the PLS step to the ACLS calibrations for the ACLS/PLS hybrid algorithm. The PLS step made minor corrections to the original ACLS predictions to account for errors caused by the regression vector still containing spectral variation from other components that were not

represented in the $\hat{\mathbf{K}}$ matrix. These components included spectral baseline effects from different blend runs, changes in the residual moisture between blends, and changes in the physical properties of the component powders, most notably the granules. The improvements were greater when dealing with the noisier data from the side sensor. It should be noted that all models showed acceptable prediction performance for blend homogeneity monitoring, even with as few as 12 and 14 independent samples. Using the CLS based methods and taking care in calibration optimization, combined with the use of pure component scans, led to useful calibrations based on a minimal number of samples (efficient calibration).

6.4.1.1 Side Sensor Analysis

For the side sensor, the starch, MCC, and HPC CLS calibrations were improved by augmenting the spectral shapes extracted from the differences between blends derived by a PCA. An additional spectral shape derived from a PCA on different sieve cuts of the granules was added to the MCC calibration to represent the scattering effects from particle size differences. The improvements by these ACLS calibrations for both sensors demonstrate the power of the method. This was particularly noticeable when using small sample sets. The improvements over PLS were more substantial using the side sensor data. These data were noisier, which lead to spurious correlations between the **X** and **Y** data that were observed in the PLS predictions. The utility of the CLS based models was not diminished by these noise effects to the same degree because the pure component scans forced correlation between the regression vector and appropriate spectral variation.

Error statistics of LSSVM were approximately ten-fold lower than other algorithms in calibration, but were five times greater from calibration to test results. The

other algorithms did not show this magnitude of error increase. This was a sign of overfitting due to the side sensor having a higher noise magnitude, and LSSVM extracted spurious correlations as useful information.

6.4.1.2 Top Sensor Analysis

The starch and HPC calibrations were improved by augmenting the spectral shapes that represented the mean difference among the four independent blends that were included in the calibration set for data from the top sensor. The spectral difference between independent blends resulted from differences in the baseline of the spectra on a given day and differences in scattering properties from particles size and bulk density differences, especially because some blends differed in mass by 200 grams. These shapes were derived by concatenating the spectra from these blends into a matrix and performing PCA on the data. The blends have the same nominal concentrations, but were clearly separated in score space in the first two principal components. When the loadings for these two components were added to the $\hat{\mathbf{K}}$ matrix the calibration statistics were similar or slightly worse because of the removal of pure component signal from the regression vector. However, the calibrations were more robust, showing better prediction and test results.

In contrast with the side sensor, LSSVM on the top sensor displayed limited overfitting because calibration and test error were much closer than on the side sensor. While still providing lower error statistics, LSSVM was much more sensitive to spectral noise than most of the other modeling techniques.

6.4.2 Blend End Point Determination

The performance of the calibration significantly effected the determination of the blending end point using the RMSNV statistic. The RMSNV profiles resulting from the predictions on the blend monitored using the side sensor are displayed in Figure 6.1, while the RMSNV profiles using the top sensor data are displayed in Figure 6.2.

The ending criterion, or RMSNV threshold, should reflect the model's test statistics, an empirically derived relationship with future product variability, and/or the necessary performance of the blend in subsequent unit operations. An arbitrary error threshold used for all blends is insufficient. The side sensor blend profiles (Figure 6.1) show that differences in model error can lead to substantial differences in the blend end point determination using an arbitrary threshold such as 5% (see the solid line in Figure 6.1). The PLS, LSSVM, and ANN algorithms would have stopped the blends before the blend was homogenous, while the CLS based algorithms would have never stopped the blends because the error in the models was always greater than the threshold. Figure 6.2 displays the effect an arbitrary threshold had using the top sensor data. All algorithms would have stopped the blend prematurely because the lower noise of the top sensor instrument allowed all of the algorithms to reach the 5% threshold quickly.

Without having tablet variability data to train a blend variability model, a more appropriate ending criterion was the test error for a given model. When a RMSNV point, which pools the error over the four major components and one minute worth of data collection, was less than or equal to the test error of the calibration, the blend was determined to be homogenous. This indicates that the blend had reached a maximum discernable homogeneity, based on the analytical method employed. Figures 6.1 and 6.2

demonstrate the blend end point as determined by each algorithm with this criterion by the solid squares.

6.4.2.1 Side Sensor Performance

The side sensor calibrations demonstrated how increases in the amount of noise present in the data matrix can affect the performance of the multivariate algorithms. The presence of significant noise caused all of the algorithms to perform similarly, with all RMSNV trends correlated at greater than 91.8% (Table 6.3). The small, subtle variations associated with minor components diffusing throughout the blend were masked and as a result, the multivariate algorithms were only able to correlate the larger sources of variation to the reference values. The only major differences between RMSNV profiles were differences in prediction bias (Figure 6.1), which created offsets in the trends while the features remained similar.

The CLS algorithm produced the highest error statistics while the nonlinear methods had the lowest. Both augmenting the CLS algorithm and using the secondary PLS step improved the error statistics for CLS, but the CLS/PLS hybrid algorithm did a better job of monitoring the minor blend fluctuations throughout the process. The ACLS algorithm had the lowest correlations with other algorithms, while PLS, CLS/PLS, and ACLS/PLS were highly correlated. The PLS algorithm modestly outperformed the other linear algorithms when comparing overall error.

There was a significant difference in the blend end points as determined by each algorithm that was the result of differences in prediction bias and the determination of the ending error threshold. While all algorithms showed similar trends, the valleys or local minima in the RMSNV trends met the ending threshold at different times because of the

differences in the test performance and the blend prediction bias. The CLS algorithm determined that blend homogeneity had been achieved quickly because the test error for CLS was highest, which defined a higher error threshold. The PLS and LSSVM algorithms indicated the ending criterion had been reached quickly because there was a low prediction bias for this blend. The ACLS, CLS/PLS, ACLS/PLS, and ANN algorithms analyzed the blend as requiring longer to reach homogeneity.

Table 6.3. Correlations between RMSNV trends using a single blend and multiple calibration algorithms for both sensors.

Top Sensor RMSNV Correlations Between Algorithms							
	PLS	**CLS**	**ACLS**	**CLS/PLS**	**ACLS/PLS**	**LSSVM**	**ANN**
PLS	1.0000	0.8303	0.8851	0.8957	0.8183	0.3556	0.4203
CLS	0.8303	1.0000	0.9838	0.9232	0.9456	0.4336	0.5167
ACLS	0.8851	0.9838	1.0000	0.9446	0.9441	0.3906	0.4650
CLS/PLS	0.8957	0.9232	0.9446	1.0000	0.9540	0.4090	0.4809
ACLS/PLS	0.8183	0.9456	0.9441	0.9540	1.0000	0.2972	0.4026
LSSVM	0.3556	0.4336	0.3906	0.4090	0.2972	1.0000	0.9470
ANN	0.4203	0.5167	0.4650	0.4809	0.4026	0.9470	1.0000
Side Sensor RMSNV Correlations Between Algorithms							
	PLS	**CLS**	**ACLS**	**CLS/PLS**	**ACLS/PLS**	**LSSVM**	**ANN**
PLS	1.0000	0.9912	0.9183	0.9936	0.9923	0.9294	0.9867
CLS	0.9912	1.0000	0.9352	0.9920	0.9927	0.9383	0.9807
ACLS	0.9183	0.9352	1.0000	0.9280	0.9375	0.9817	0.9406
CLS/PLS	0.9936	0.9920	0.9280	1.0000	0.9990	0.9329	0.9801
ACLS/PLS	0.9923	0.9927	0.9375	0.9990	1.0000	0.9406	0.9820
LSSVM	0.9294	0.9383	0.9817	0.9329	0.9406	1.0000	0.9550
ANN	0.9867	0.9807	0.9406	0.9801	0.9820	0.9550	1.0000

A more rigorous validation procedure that included more than 2 independent samples at the blend point would have provided a more accurate model performance metric, which would have allowed the algorithms to determine blend end points over a narrow time range. Adding a concentration standard deviation statistic over each one

minute time window as an additional minimum end point criterion would also make the end points for each algorithm more precise.

6.4.2.2 Top Sensor Performance

The top sensor data (Figure 6.2) show that all of the multivariate algorithms performed adequately when using data with a lower magnitude of noise and a larger spot size. Reduced noise resulted in fewer spurious correlations to the reference data, while a larger spot size reduced the inherent variation observed between measurements. The linear multivariate algorithms predicted blending trends that were highly correlated (Table 6.3), while the nonlinear methods showed fewer trends and had lower correlations. The PLS algorithm did not determine a blend end point, however, due to a prediction bias for the entire blend run that never allowed the RMSNV statistic to get within 1% of the test error. All other algorithms established the blend end point within a 75 second range (20-95 sec.). The short blending times were not surprising for these blends because the fill ratio of the powder in the blender was less than 50% and the larger spot size resulted in a larger scale of scrutiny.

The nonlinear methods determined the end point criterion was reached quickly because the models lacked adequate sensitivity in the concentration range around the nominal blend end point. The problem with simple, three-level calibrations over the entire concentration range (0%-100%) is that they traditionally have low prediction accuracy and sensitivity, with biases in predictions being common. For the nonlinear methods, the subtle spectral changes associated with small changes in chemical concentrations in NIR spectra did not produce a proportional response in the predictions because the calibrations were not trained to recognize these changes appropriately. The

algorithms recognized samples with a high concentration of a single component as being very similar to the pure component, and therefore output predictions that were close to 100%. This resulted in an over-prediction bias for one component and an under-prediction bias for other components. The same problem was observed near the nominal concentration point. The nonlinear methods suffered from this problem more severely. These models no longer showed any trends after the blends had begun to approach the nominal concentration. Due to the number of parameters that need to be optimized for the nonlinear methods, reduced sample set calibrations are not appropriate.

Efficient calibration typically is improved by creating a small number of independent samples around the concentration point of interest. This allows the calibration to more accurately predict samples close to this concentration level. The range of these samples is a function of users' need. For accurate and precise predictions of all new samples, the range of concentrations in the calibration set around the point of interest must encompass all anticipated new sample concentrations. This approach will result in robust calibrations that are selective, accurate, and precise with a reduced number of samples. While all of the multivariate algorithms can benefit from additional samples, the present chapter demonstrates that the ACLS/PLS algorithm's performance was satisfactory without requiring additional samples.

All of the linear multivariate algorithms in Figure 6.2 showed a one minute period of decreasing blend variability after the initial concentration change. The CLS based algorithms, which used the pure component scans as a significant advantage in the efficient calibration setting, were most sensitive to the slight concentration changes around the blend end point and would stop the bed at the more appropriate end point of

95 seconds. If the blend was stopped before this point, some of the minor excipients would not have had the opportunity to fully diffuse throughout the blend, resulting in homogeneity problems that could create problems with the final dosage forms.

The differences among the blend end points determined by the linear algorithms were strictly the results of prediction biases as proven by the high overall correlations between these trends (Table 6.3). As stated previously, a more rigorous validation process, the inclusion of a prediction standard deviation metric, and the addition of samples to the calibration set would cause these predicted end points to converge.

This calibration performance study demonstrated the utility of efficient calibrations while highlighting the importance of understanding the instruments' noise characteristics, scale of scrutiny, and resulting capabilities. When using an instrument with increased noise, reduced sample set calibrations were more appropriate because the instrument limited the performance of the component predictions. All of the algorithms presented using the side sensor data performed adequately, and additional expenses used in model building would be wasted. When an instrument (top sensor) with a higher signal to noise ratio was used, the calibration process and multivariate algorithm became more critical. The CLS based algorithms took advantage of pure component scans to create sensitive models with reduced sample sets. Like all quality by design (QbD) projects, an adequate risk analysis must be completed prior to performing an experimental design, so that the user knows the performance level required of the analytical models that inform the process.

6.4.3 Calibration Transfer Study

The two best performing algorithms (ACLS/PLS and LSSVM) from the calibration study were investigated further in a calibration transfer setting. This is an additional indicator of model robustness. Ease of transfer is an important property for an NIR model in the pharmaceutical industry. If a new calibration must be created at each instance that an instrument fails, requires maintenance or a calibration update, or a different instrument must be utilized, the costs become prohibitive.

For this study, several calibration transfer techniques were compared against robust calibration designs (calibrations including data from both sensors) to determine which of the two algorithms were easier to transfer. Transfers were created for predicting side sensor data using the top sensor calibrations (T-S) and for predicting top sensor data using side sensor calibrations (S-T). Due to the differences in noise patterns, the S-T transfers were not successful (data not shown). The failure of the S-T transfer was anticipated, because a transfer of a calibration created on a poorer instrument to an instrument of higher quality will inherently be limited by the lower quality instrument.

The T-S transfer results are listed in Table 6.4 and the resulting RMSNV trends for the independent blend are displayed in Figure 6.3. Table 6.4 shows that most of the errors incurred by the transfer process were in the Gabapentin predictions. The errors were mostly the result of a large prediction bias. There were minimal increases in the prediction variability when transferring the calibrations. This result was confirmed in Figure 6.3 because the RMSNV profiles resulting from the direct prediction of side sensor data from the top sensor calibrations showed the same trends as the prediction results using the side sensor calibration. Only an offset due to a prediction bias was observed. The results for the transfer of the ACLS/PLS algorithm using PDS 3 and PDS

5 and for the transfer of the LSSVM algorithm using DS and all PDS parameters showed low error statistics; however, it is important to note that the low error was due to a lack of sensitivity, which is visualized in Figure 6.3. Only the PDS 5 error statistics are provided in Table 6.4. Other iterations of the optical standardization methods provided similar error statistics.

When data from the side sensor were added to the top sensor calibration set to create robust calibrations, the blend predictions showed all of the same fluctuations, but with slight increases in error resulting from an increase in noise in the calibration matrix. There was very little difference when adding all of the side sensor calibration data, half of the data, or a quarter of the data. This showed that both the ACLS/PLS and LSSVM calibrations could be efficiently updated with additional information.

The ideal solution was to simply transfer the original calibration using mathematical techniques, so a small number of spectra from only the blend concentration level could be used to train the transfer. The 10 samples having the lowest prediction residuals from the side sensor calibration set were used to train each method. A simple bias correction of the predictions was all that was necessary to create transferred RMSNV trends that were highly correlated with the robust calibration trends. The optical standardization methods (DS and PDS) were not as successful for transferring these calibrations. Due to the differences in instrument noise and band broadening between instruments, these techniques smoothed away the spectral information containing the subtle concentration changes that created the blending profiles.

Table 6.4. Calibration transfer performance for the ACLS/PLS and LSSVM algorithms using several transfer techniques. Calibrations created using top sensor data are used to predict component concentrations in side sensor data.

Top To Side Sensor Transfer Performance										
API										
	Direct Prediction		**Robust (all)**		**Robust (Quarter)**		**Bias Correction**		**PDS 5**	
	ACLS/PLS	**LSSVM**	**ACLS/PLS**	**LSSVM**	**ACLS/PLS**	**LSSVM**	**ACLS/PLS**	**LSSVM**	**ACLS/PLS**	**LSSVM**
RMSEP	0.25	0.08	0.06	0.02	0.07	0.03	0.06	0.04	0.02	0.01
SEP	0.06	0.04	0.06	0.02	0.07	0.02	0.06	0.04	0.01	0.00
Bias	0.24	-0.07	0.01	-0.01	0.01	0.02	0.00	-0.01	0.02	0.00
MCC										
	ACLS/PLS	**LSSVM**	**ACLS/PLS**	**LSSVM**	**ACLS/PLS**	**LSSVM**	**ACLS/PLS**	**LSSVM**	**ACLS/PLS**	**LSSVM**
RMSEP	0.05	0.03	0.04	0.01	0.03	0.01	0.03	0.03	0.01	0.00
SEP	0.03	0.03	0.03	0.01	0.03	0.01	0.03	0.03	0.01	0.00
Bias	0.04	0.00	-0.02	0.00	-0.01	0.01	0.00	0.01	0.01	0.00
HPC										
	ACLS/PLS	**LSSVM**	**ACLS/PLS**	**LSSVM**	**ACLS/PLS**	**LSSVM**	**ACLS/PLS**	**LSSVM**	**ACLS/PLS**	**LSSVM**
RMSEP	0.14	0.03	0.06	0.01	0.06	0.01	0.05	0.04	0.04	0.00
SEP	0.05	0.03	0.06	0.01	0.06	0.00	0.05	0.03	0.03	0.00
Bias	-0.13	0.01	0.03	-0.01	0.02	0.00	0.01	-0.02	0.02	0.00
Starch										
	ACLS/PLS	**LSSVM**	**ACLS/PLS**	**LSSVM**	**ACLS/PLS**	**LSSVM**	**ACLS/PLS**	**LSSVM**	**ACLS/PLS**	**LSSVM**
RMSEP	0.04	0.03	0.09	0.01	0.10	0.00	0.03	0.03	0.03	0.00
SEP	0.03	0.02	0.07	0.01	0.07	0.00	0.03	0.02	0.03	0.00
Bias	-0.02	0.01	-0.06	0.00	-0.07	0.00	0.00	0.01	-0.01	0.00

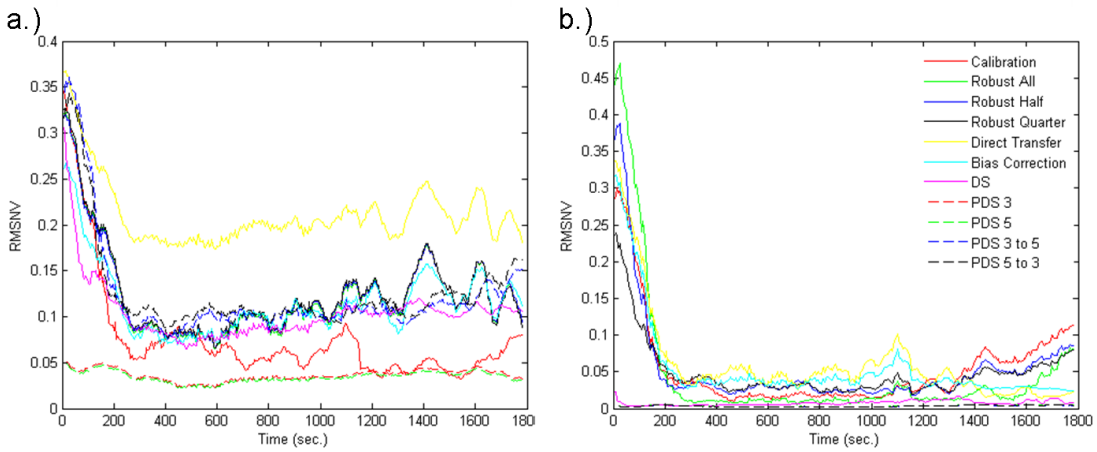

Figure 6.3. The RMSNV trends generated by transferring calibrations created using top sensor data to data collected on the side sensor using several transfer techniques. **a.)** The transfer prediction results for the ACLS/PLS calibration. **b.)** The transfer prediction results for the LSSVM calibration.

The transfer results showed that both the ACLS/PLS and LSSVM calibrations were robust and easily transferred. The success of the simple bias correction method demonstrated that both calibrations were correlated strongly to the net analyte signal (NAS) of each component because new spectral variation encountered by different instrumental data merely resulted in a prediction bias. All of the relevant (with respect to the analyte of interest) spectral variation was still recognized by the models.

The LSSVM transfer results were more similar to the original predictions because the original predictions using LSSVM lacked sensitivity to subtle concentration variation. The major spectral variations that the LSSVM algorithm was trained to model were similar between instruments. The ACLS/PLS transfer results showed that the models retained their original sensitivity to subtle concentration changes, which is an important property in blend monitoring because it is the trend information that is important. To

mitigate the problem of a prediction bias, the absolute RMSNV threshold can be scaled to account for the offsets in blend trends.

These results support the conclusion that sensitive and robust calibrations can be created efficiently with a limited number of independent samples if pure components are available and the proper modeling algorithms are used. Classical least-squares based algorithms were most appropriate for the efficient calibration setting, while nonlinear algorithms were limited for this application. Modest improvements to the results are noted with additional calibration samples.

6.5 Conclusion

Sensitivity is the most important model property in blend process monitoring so that subtle concentration changes caused by the distribution of blend constituents can be recognized. Depending upon the algorithm, accuracy is also an important feature of a calibration. Specifically, the RMSNV algorithm requires both sensitivity and accuracy to achieve an optimum end point calculation. However, the trend information gathered by a blend monitoring system is most important so that the end point can be determined when the blend stops changing.

This chapter demonstrates that sensitive and robust multivariate spectral calibrations can be created from limited sample sets when pure component scans are available. Classical least-squares based methods produced the most sensitive calibrations using an efficient calibration strategy. The accuracy of CLS calibrations were further improved when using the ACLS/PLS algorithm. Nonlinear methods produced low error statistics based on the samples available in an efficient calibration approach, but lacked adequate sensitivity without additional samples.

The chapter also highlighted the need to understand the capabilities of the instrumentation and the requirements of a given product or system. Efficient calibrations are ideal for a scenario in which the precision of a calibration is limited by the hardware (including the sampling system). This study demonstrates that following an efficient calibration effort, accuracy and precision are improved in diminishing returns through additional calibration samples. Efficient calibration offers a means of reducing the resources required to generate a quantitative calibration. This is particularly important for the long term success of quantitative spectral analysis in the pharmaceutical industry.

Finally, this chapter demonstrates that the investment incurred for an optimum control system is process dependent. In pharmaceutical powder blending, a robust method for monitoring blend homogeneity is required to reduce the variability between batches and assure content uniformity in the final dosage forms. This can be developed using online NIRS, rigorous model development, a rigorous end point criterion, and a blend-stop communication system. Any additional complexities that are built into the control system are unnecessary, and do not justify the additional expense.

Chapter 7: Summary

The pharmaceutical industry has shown significant progress in recent years with regards to the discovery of new drug molecules, dosage systems, biological targeting methods, and advanced disease treatments. Despite these advances, the industry continues to lag behind comparable industries in terms of manufacturing innovation, quality production, and industrial efficiency. In the past, restrictions put on manufacturers by the FDA and comparable regulatory agencies to "lock in" validated systems did not enable companies to implement production line improvements. The regulatory agencies have acknowledged this shortcoming and are currently encouraging the use of the ICH guidelines that allow flexibility within a validated design space. It is now the responsibility of pharmaceutical manufactures to design rigorous and efficient manufacturing systems to meet the standards of current industrial practice while also realizing a financial return.

In the current QbD paradigm as part of the Critical Path Initiative, the amount of regulatory flexibility offered to companies is directly proportional to the risk associated with the given process. The manufacturer must demonstrate that an adequate level of process understanding has been reached throughout development, and that this understanding has led to a quantitative description of the relationships between raw material, process, and product factors, which are then related to clinical performance. This understanding requires rigorous planning of measurement systems, control systems, and DOE from initial stages so that the complex relationships between all of the aforementioned factors can be described clearly.

This dissertation has demonstrated the importance of rigorous scientific design and understanding at all levels of process or product development. A system should be developed to meet the needs of the product or the operation. In chapter 6, a simple control system that was based on maximizing the information available through multiple online NIR sensors using a limited number of samples was developed for pharmaceutical blending. By understanding the information that was available to the pharmaceutical analysts with no additional effort and comprehending the differences between multivariate modeling algorithms, a robust and sensitive homogeneity monitoring system was able to be developed with a minimal investment. This would allow different batches to be stopped at precisely the same level of homogeneity even when there were substantial differences between powder properties and blend times. A greater degree of production quality and process understanding was enabled.

More complex operations require control systems with increased complexity. A formulation for the delivery of gabapentin is an example of a system with an API that is sensitive to manufacturing conditions because gabapentin has process induced chemical instability that is directly related to its physical stability. Complicating matters, the chemical impurity, gabapentin lactam, has reversed biological activity and is required to be less than 0.4 mole % in the final dosage form for a two year shelf life. Therefore, rigorous DOE was necessary to quantify the relationships between unit operations and gabapentin stability to assure product safety.

A hybrid control system that is the first of its kind was developed in chapter 2 for the fluid bed drying of a model gabapentin formulation. Fluid bed processing is a complex unit operation with a large degree of energy input that requires care during

development, but offers significant advantages in the process of commercial scale batches. The hybrid control system combined first principle calculations with empirical modeling, data management, and online sensing that allowed for strict control of the drying process. The first principle calculations provided control of the major mechanism by which the process impacted product quality, while offering substantial economic benefits by reducing the dimensionality of the DOE and eliminating the need for preconditioned air systems. The empirical controls allowed the process set points to be optimized with a limited number of experiments, and the online sensing provided additional process understanding, immediate feedback, and precise definitions of process end points between batches. The control system maximized the advantages of traditional control strategies, while eliminating the major drawbacks, and provided a significant improvement in production quality with minimal developmental costs.

This dissertation also demonstrated the importance of rigorous statistical analyses for the calculation of process models, the definitions of design space boundaries, and the assurance of future product quality. Even with the most extensive DOE and development efforts, models contain uncertainty that must be accounted for when making decisions regarding future production. Statistical tolerance calculations can provide the analyst with information about the probability of meeting specifications in future batches, which is crucial in making informed decisions. Without this information, design space boundaries could be too lenient and lead to an increase number of failed batches.

Due to the care and rigor required during development, a substantial financial investment is required. For this reason, failure during scale-up or commercialization can have dire financial consequences for a pharmaceutical company. This dissertation

demonstrated that the hybrid control system also offers advantages for scale-up development with a limited financial investment. The first principle calculations are directly scalable, and a stochastic approach can be used to do a small magnitude scale-up that trains all of the transfer functions for scale-up regardless of magnitude. This provided substantial material and cost savings.

The benefits of the hybrid control system extended to the spray granulation phase, where particle agglomeration was controlled using the same EEF calculations and online measurements. Additionally, this dissertation demonstrated the importance of material properties in the processing behavior of spray granulation, which necessitates material factors being included in developmental DOE. Material properties often have strong interactions with processing factors, which significantly impact final product quality and necessitate the use of extended ANACOVA modeling. Understanding these relationships and how they are quantified provides benefits for the production of pharmaceutical products in a QbD setting, and provides the evidence that is required by regulatory agencies for allowing flexibility and the constant improvement of production lines.

The use of PAT in QbD development efforts is critical so that process or product variability can be identified and addressed appropriately. Without measurements that are implemented at strategic locations, this variability can go undetected, which then magnifies the variability in final products and reduces product quality. Online measurements of the production stream are absolutely necessary for any feedback or feedforward control to be implemented. Thus, PAT is absolutely necessary for the development of control systems for continued product improvement, and any development effort in the QbD paradigm.

The work demonstrated in this dissertation facilitates the movement of the pharmaceutical industry toward the desired state, as defined by the FDA's Critical Path Initiative and the ICH. It is a demonstration of the next step in manufacturing innovation so that the pharmaceutical industry can compete in terms of quality and efficiency with other industries. The rigor that is necessary in the development of control systems requires extensive work, but the potential rewards are substantial. Continued use of systems like those described in this dissertation offer great promise to the pharmaceutical industry.

References

1. Cogdill RP, Knight TP, Anderson CA, Drennen III JK 2007. The financial returns on investments in process analytical technology and lean manufacturing: Benchmarks and case study. Journal of Pharmaceutical Innovation 2:38-50.

2. Q8(R2) Pharmaceutical Development. 2009. In Anonymous Internation Conference on Harmonisation of Technical Requirements for Registration of Pharmaceuticals for Human Use.

3. Guidance for Industry: Quality Systems Approach to Pharmaceutical CGMP Regulations 2006. , Rockville: U.S. Department of Health and Human Services, Food and Drug Administration.

4. Kunii D, Levenspiel O. 1991. Fluidization Engineering., 2nd ed., London: Wiley.

5. Iveson SM, Litster JD, Hapgood K, Ennis BJ 2001. Nucleation, growth and breakage phenomena in agitated wet granulation processes: a review. Powder Technology 117:3-39.

6. Kunii D, Levenspiel O. 1991. Introduction. In Anonymous Fluidization Engineering: Second Edition, Boston, MA: Butterworth-Heinemann. p 1-13.

7. Kunii D, Levenspiel O. 1991. Fluidization and Mapping of Regimes. In Anonymous Fluidization Engineering: Second Edition, Boston, MA: Butterworth-Heinemann. p 61-92.

8. Grace JR 1986. Contacting modes and behaviour classification of gas-solid and other two-phase suspensions. Can J Chem Eng 64:353-528.

9. Geldart D 1973. Types of gas fluidization. Powder Technology 7:285-292.

10. Geldart D, Abrahamsen AR 1978. Homogeneous fluidization of fine powders using various gases and pressures. Powder Technology 19:133-136.

11. Kunii D, Levenspiel O. 1991. Solid Movement: Mixing, Segregation, and Staging. In Anonymous Fluidization Engineering: Second Edition, Boston, MA: Butterworth-Heinemann. p 211-233.

12. Kunii D, Levenspiel O. 1991. Industrial Applications of Fluidized Beds. In Anonymous Fluidization Engineering: Second Edition, Boston, MA: Butterworth-Heinemann. p 15-58.

13. Kunii D, Levenspiel O. 1991. Bubbles in Dense Beds. In Anonymous Fluidization Engineering: Second Edition, Boston, MA: Butterworth-Heinemann. p 115-134.

14. Davidson JF, Harrison D. 1963. Fluidized Particles, New York: Cambridge Univ. Press.

15. Kunii D, Levenspiel O. 1991. Bubbling Fluidized Beds. In Anonymous Fluidization Engineering: Second Edition, Boston, MA: Butterworth-Heinemann. p 137-164.

16. Horio M, et al. 1986. In Ostergaard K, Sorensen A, editors. Fluidization V, New York: Engineering Foundation. p 151.

17. Fitzgerald TJ, Crane SD 1980. Proc 6th Int Conf on Fluidized Bed Combustion 3:815.

18. Fitzgerald TJ. 1985. In Davidson JF, et al., editors. Fluidization, New York: Academic Press. p 413.

19. Kunii D, Levenspiel O. 1991. The Dense Bed: Distributors, Gas Jets, and Pumping Power. In Anonymous Fluidization Engineering: Second Edition, Boston, MA: Butterworth-Heinemann. p 95-112.

20. Kunii D, Levenspiel O. 1991. Particle-to-Gas Mass and Heat Transfer. In Anonymous Fluidization Engineering: Second Edition, Boston, MA: Butterworth-Heinemann. p 257-276.

21. Wildfong PLD, Samy A-, Corfa J, Peck GE, Morris KR 2002. Accelerated Fluid Bed Drying Using NIR Monitoring and Phenomenological Modeling: Method Assessment and Formulation Suitability. J Pharm Sci 91:631-639.

22. Kunii D, Levenspiel O. 1991. Heat Transfer between Fluidized Beds and Surfaces. In Anonymous Fluidization Engineering: Second Edition, Boston, MA: Butterworth-Heinemann. p 313-335.

23. Kunii D, Levenspiel O. 1991. Design for Physical Operations. In Anonymous Fluidization Engineering: Second Edition, Boston, MA: Butterworth-Heinemann. p 397-427.

24. Faure A, York P, Rowe RC 2001. Process control and scale-up of pharmaceutical wet granulation processes: a review. European Journal of Pharmaceutics and Biopharmaceutics 52:269-277.

25. Rambali B, Baert L, Massart DL 2003. Scaling up of the fluidized bed granulation process. Int J Pharm 252:197-206.

26. Harbert FC 1973. Moisture measurement and control in industrial processes. case studies carried out by Sira Institute Report R505:1-24.

27. Harbert FC 1974. Automatic control of industrial drying processes. Manufact Chem Aerosol News 45:23-24.

28. Alden M, Torkington P, Strutt ACR 1988. Control and Instrumentation of a Fluidized-Bed Drier Using the Temperature-Difference Technique. Powder Technology 54:15-25.

29. Ebey GC 1987. A thermodynamic model for aqueous film-coating. Pharmaceutical Technology 11:40-50.

30. Walter K 2007. Introduction to Real Time Process Determination. Pharmaceutical Engineering 27:40-53.

31. Strong JC 2009. Psychrometric analysis of the environmental equivalency factor for aqueous tablet coating. AAPS PharmSciTech 10:303-309.

32. Behjat Y, Shahhosseini S, Hashemabadi SH 2008. CFD modeling of hydrodynamic and heat transfer in fluidized bed reactors. International Communications in Heat and Mass Transfer 35:357-368.

33. Arastoopour H, Strumendo M, Ahmadzadeh A 2008. Numerical Simulation of Poly-dispersed Systems, Circulating Fluidized Bed Technology IX. Proceedings of the 9th International Conference on Circulating Fluidized Beds :313-318.

34. Szafran RG, Kmiec A 2004. CFD modeling of heat and mass transfer in a spouted bed dryer. Ind Eng Chem Res 78:1025-1031.

35. Wachem BGM, Shouten JC, Bleek CM, Krishna R, Sinclair JL 2001. CFD modeling of gas-fluidized beds with a bimodal particle mixture. AIChE J 47:1292-1302.

36. Wang HG, Yang WQ, Senior P, Raghavan RS, Duncan SR 2008. Investigation of batch fluidized bed drying by mathematical modeling, CFD simulation and ECT measurement. AIChE J 54:427-444.

37. Groenewold H, Tsotsas E 1997. A new model for fluid bed drying. Drying Technology 15:1687-1698.

38. Peglow M, Heinrich S, Tsotsas E, Morl L 2004. Fluidized bed drying: Influence of dispersion and transport phenomena. Drying A:129-136.

39. United States Food and Drug Administration, Department of Health and Human Services 2003. Current Good Manufacturing Practice in Manufacturing, Processing, Packing, or Holding of Drugs; General. Code of Federal Regulations 21(4).

40. Abberger T, Seo A, Schæfer T 2002. The effect of droplet size and powder particle size on the mechanisms of nucleation and growth in fluid bed melt agglomeration. Int J Pharm 249:185-197.

41. PAT - A Framework for Innovative Pharmaceutical Pharmaceutical Development, Manufacturing, and Quality Assurance. 2004. FDA Guidance for Industry .

42. Rambali B, Baert L, Massart DL 2001. Using Experimental Design to Optimize the Process Parameters in fluidized Bed Granulation on a Semi-full Scale. Int J Pharm 220:149-160.

43. Schinzinger O, Schmidt PC 2005. Comparison of the Granulation Behavior of Three Different Excipients in a Laboratory Fluidized Bed Granulator Using Statistical Methods. Pharmaceutical Development and Technology 10:175-188.

44. Niskanen T, Yliruusi J, Niskanen M, Kontro O 1990. Granulation of Potassium Chloride in Instrumented Fluidized Bed Granulator-Part 2: Evaluation of the Effects of Two Independent Process Variables Using 3^2-Factorial Design. Acta Pharmaceutica Fennica 99:23-30.

45. Rajniak P, Mancinelli C, Chern RT, Stepanek F, Farber L, Hill BT 2007. Experimental study of wet granulation in fluidized bed: Impact of the binder properties on the granule morphology. Int J Pharm 334:92-102.

46. Frake P, Greenhalgh D, Grierson SM, Hempenstall JM, Rudd DR 1997. Process control and end-point determination of a fluid bed granulation by application of near infra-red spectroscopy. International journal of pharmaceutics 151:75-80.

47. Rantanen J, Lehtola S, Ramet P, Mannermaa J, Yliruusi J 1998. Online monitoring of moisture content in an instrumental fluidized bed granulator with a multi-channel NIR moisture sensor. Powder Technology 99:163-170.

48. Rantanen J, Antikainen O, Mannermaa J, Yliruusi J 2000. Use of the Near-Infrared Reflectance Method for Measurement of Moisture Content During Granulation. Pharmaceutical Development and Technology 5:209-217.

49. Rantanen J, Wikstrom H, Turner R, Taylor LS 2005. Use of In-Line Near-Infrared Spectroscopy in Combination with Chemometrics for Improved Understanding of Pharmaceutical Processes. Anal Chem 77:556-563.

50. Watano S, Miyanami K 1995. Image processing for on-line monitoring of granule size distribution and shape in fluidized bed granulation. Powder Technology 83:55-60.

51. Watano S 2001. Direct control of wet granulation processes by image processing system. Powder Technology 117:163-172.

52. Hu X, Cunningham JC, Winstead D 2008. Study growth kinetics in fluidized bed granulation with at-line FBRM. Internation Journal of Pharmaceutics 347:54-61.

53. Portoghese F, Berruti F, Briens C 2008. Continuous on-line measurement of solid moisture content during fluidized bed drying using triboelectric probes. Powder Technology 181:169-177.

54. Rantanen J, Kansakoski M, Suhonen J, Tenhunen J, Lehtonen S, Rajalahti T, Mannermaa J, Yliruusi J 2000. Next Generation Fluidized Bed Granulator Automation. AAPS PharmSciTech 1:article 10.

55. Rantanen J, Jorgensen A, Rasanen E, Luukkonen P, Airaksinen S, Raiman J, Hanninen K, Antikainen O, Yliruusi J 2001. Process Analysis of Fluidized Bed Granulation. AAPS PharmSciTech 2:article 21.

56. Plackett RL, Burman JP 1946. The Design of Optimum Multifactorial Experiments. Biometrika 33:305-325.

57. Box GEP, Hunter WG, Hunter JS. 2005. Statistics for Experimenters: Design, Innovation, and Discovery, Second ed., New York, NY: John Wiley & Sons, Inc.

58. NIST/SEMATECH 2010. e-Handbook of Statistical Methods: Response surface designs. 2011. http://itl.nist.gov/div898/handbook/pri/section3/pri336.htm

59. NIST/SEMATECH 2010. What is a mixture design? 2011. http://itl.nist.gov/div898/handbook/pri/section5/pri54.htm

60. Lunney PD, Cogdill RP, Drennen III JK 2008. Innovation in Pharmaceutical Experimentation Part 1: Review of Experimental Designs Used in Industrial Pharmaceutics Research and Introduction to Bayesian D-Optimal Experimental Design. Journof Pharmaceutical Innovation 3:188-203.

61. Chaloner K, Verdinelli I 1995. Bayesian Experimental Design: A Review. Statistical Science 10:273-304.

62. NIST/SEMATECH 2010. What is a computer-aided design? 2011. http://itl.nist.gov/div898/handbook/pri/section5/pri52.htm

63. Kleinbaum DG, Kupper LL, Nizam, Muller KE. 2008. Applied regression analysis and other multivariate methods, Fourth ed., Belmont, CA: Brooks/Cole.

64. Kleinbaum DG, Kupper LL, Nizam A, Muller KE. 2008. Analysis of Covariance and Other Methods for Adjusting Continuous Data. In Anonymous Applied Regression Analysis and Other Multivariate Methods: Fourth Edition, Belmont, CA, USA: Thomson: Brooks/Cole. p 264-274.

65. Seber GAF, Wild CJ. 1989. Nonlinear Regression, New York, NY: John Wiley & Sons, Inc.

66. Box GEP, Draper N. 2007. Response Surfaces, Mixtures, and Ridge Analyses, Second ed., New York, NY: John Wiley & Sons, Inc.

67. NIST 2010. Tolerance intervals for a normal distribution. 2011. http://itl.nist.gov/div898/handbook/prc/section2/prc263.htm

68. Rantanen J, Yliruusi J 1998. Determination of Particle Size in a Fluidized Bed Granulator With a Near Infrared Set-up. Pharm Pharmacol Commun 4:73-75.

69. Shi Z, Cogdill RP, Short SM, Anderson CA 2008. Process characterization of powder blending by near-infrared spectroscopy: Blend end-points and beyond. Journal of Pharmaceutical and Biomedical Analysis 47:738-745.

70. Rasanen E, Rantanen J, Jorgensen A, Karjalainen M, Paakkari T, Yliruusi J 2001. Novel Identification of Pseudopolymorphic Changes of Theophylline During Wet Granulation Using Near Infrared Spectroscopy. Journal of Pharmaceutical Sciences 90:389-396.

71. Jorgensen A, Rantanen J, Karjalainen M, Khriachtchev L, Rasanen E, Yliruusi J 2002. Hydrate Formation during Wet Granulation Studied by Spectroscopic Methods and Multivariate Analysis. Pharmaceutical Research 19:1285-1291.

72. Hausman DS, Cambron RT, Sakr A 2005. Application of on-line Raman spectroscopy for characterizing relationships between drug hydration state and tablet physical stability. International journal of pharmaceutics 299:19-33.

73. Igne B, Hurburgh Jr. CR 2008. Standardisation of near infrared spectrometers: evaluation of some common techniques for intra- and inter-brand calibration transfer. Journal of Near Infrared Spectroscopy 16:539-550.

74. Igne B, Roger J, Roussel S, Bellon-Maurel V, Hurburgh CR 2009. Improving the transfer of near infrared prediction models by orthogonal methods. Chemometrics and Intelligent Laboratory Systems 99:57-65.

75. Haaland DM, Melgaard DK 2000. New Prediction-Augmented Classical Least-Squares (PACLS) Methods: Application to Unmodeled Interferents. Applied Spectroscopy 54:1303-1312.

76. Engell S 2007. Feedback control for optimal process operation. Journal of Process Control 17:203-219.

77. Davis B, Lundsberg L, Cook G 2008. PQLI Control Strategy Model and Concepts. Journal of Pharmaceutical Innovation 3:95-104.

78. Muske KR 2003. Estimating the Economic Benefit from Improved Process Control. Ind Eng Chem Res 42:4535-4544.

79. Bauer M, Craig IK, Tolsma E, de Beer H 2007. A Profit Index for Assessing the Benefits of Process Controls. Ind Eng Chem Res 46:5614-5623.

80. Edgar TF 2004. Control and operations: when does controllability equal profitability? Computers and Chemical Engineering 29:41-49.

81. Bolton R, Tyler S 2008. PQLI Engineering Controls and Automation Strategy. Journal of Pharmaceutical Innovation 3:88-94.

82. Franklin GF, Powell JD, Amami-Naeini A. 2010. Feedback Control of Dynamic Systems, 6th ed., New Jersey: Prentice Hall.

83. Doyle J, Francis B, Tannenbaum A. 1990. Feedback Control Theory: Mac.

84. Seborg DE, Edgar TF, Mellichamp DA. 1989. Process Dynamics and Control, NY: John Wiley & Sons.

85. Montgomery D, C., Keats JB, Runger GC, Messina WS 1994. Integrating Statistical Process Control and Engineering Process Control. Journal of Quality Technology 26:79-87.

86. Cogdill RP, Anderson CA, Drennen III JK 2005. Process Analytical Technology Case Study, Part III: Calibration Monitory and Transfer. AAPS PharmSciTech 6:E284-E297.

87. Gabapentin. September 1, 2009. PubMed Health July 7, 2011:1. http://www.ncbi.nlm.nih.gov.authenticate.library.duq.edu/pubmedhealth/PMH0000940/

88. Neurontin. April 28, 2009. FDA Drug Label July 7, 2011:29. http://www.accessdata.fda.gov.authenticate.library.duq.edu/drugsatfda_docs/label/2009/020235s041,020882s028,021129s027lbl.pdf

89. Potschka H, Feuerstein TJ, Loscher W 2000. Gabapentin-lactam, a close analogue of the anticonvulsant gabapentin, exerts convulsant activity in amygdala kindled rats. Naunyn-Schmiedeberg's Arch Pharmacol 361:200-205.

90. U.S. Department of Health and Human Services, Food and Drug Administration, Center for Drug Evaluation and Research (CDER) 2000. Waiver of In Vivo Bioavailability and Bioequivalence Studies for Immediate-Release Solid Oral Dosage Forms Based on a Biopharmaceutics Classification System. Guidance for Industry .

91. Gabapentin. 2011. 2011. FDA. www.drugs.com/pro/gabapentin.html

92. Lin S, Hsu C, Ke W 2010. Solid-state transformation of different gabapentin polymorphs upon milling and co-milling. Int J Pharm 396:83-90.

93. FDA 2007. Generic Firm Commences Gabapentin Recall Due to Excessive Impurities. FDAnews Drug Daily Bulletin 4(226).

94. Gabapentin Tablets. December 1, 2009. USP Revision Bulletin July 7, 2011:2. http://www.usp.org.authenticate.library.duq.edu/pdf/EN/USPNF/gabapentinTablets.pdf

95. Zour E, Lodhi SA, Nesbitt RU, Silbering SB, Chaturvedi PR 1992. Stability Studies of Gabapentin in Aqueous Solutions. Pharmaceutical Research 9:595-600.

96. Ciavarella AB, Gupta A, Sayeed V, Khan MA, Faustino PJ 2007. Development and application of a validated HPLC method for the determination of gabapentin and its major degradation impurity in drug products. Journal of Pharmaceutical and Biomedical Analysis 43:1647-1653.

97. Hsu C, Lin S 2009. Rapid examination of the kinetic process of intramolecular lactamization of gabapentin using DSC–FTIR. Thermochimica Acta 486:5-10.

98. Igne B, Shi Z, Talwar S, Drennen III JK, Anderson CA 2012. Dynamic Design Space as an Integrated Component of Quality by Design. Journal of Pharmaceutical Innovation Under Review.

99. Shi Z, Cogdill RP, Short SM, Anderson CA 2008. Process characterization of powder blending by near-infrared spectroscopy: Blend end-points and beyond. Journal of Pharmaceutical and Biomedical Analysis 47:738-745.

100. Haaland DM, Melgaard DK 2001. New Classical Least-Squares/Partial Least-Squares Hybrid Algorithm for Spectral Analyses. Applied Spectroscopy 55:1-8.

101. Short SM, Cogdill RP, Drennen III JK, Anderson CA 2011. Performance-based quality specifications: The relationship between process critical control parameters, critical quality attributes, and clinical performance. J Pharm Sci 100:1566-1575.

102. Kirsch LE 2010. Linking Drug Stability to Manufacturing Physical Chemical Foundations Gabapentin. 2011. PharmaHUB. http://pharmahub.org/resources/409

103. Kleinbaum DG, Kupper LL, Nizam A, Muller KE. 2008. Statistical Inference: Estimation. In Anonymous Applied Regression Analysis and Other Multivariate Methods, Belmont, CA: Thomson Brooks/Cole. p 23-26.

104. Kleinbaum DG, Kupper LL, Nizam A, Muller KE. 2008. The Bonferroni Approach. In Anonymous Applied Regression Analysis and Other Multivariate Methods, Belmont, CA: Thomson Brooks/Cole. p 442-444.

105. Liscinsky M 2011. FDA, EMA announce pilot for parallel assessment of Quality by Design applications. FDA News Release :March 16, 2011.

106. Leuenberger H, Betz G 2007. Granulation process control - production of pharmaceutical granules: the classical batch concept and the problem of scale-up. Handbook of Powder Technology 11:705-733.

107. Leuenberger H, Betz G, Jones DM 2006. Scale-up in the field of granulation and drying. Drugs and the Pharmaceutical Sciences 157:199-236.

108. Sheehan C 2011. <1174> Powder Flow. United States Pharmacopeia 28:618.

109. Carr RL 1965. Evaluating Flow Properties of Solids. Chem Eng 72:163-168.

110. U.S. Department of Health and Human Services, Food and Drug Administration, Center for Drug Evaluation and Research (CDER) 2002. Guidance for Industry: Nasal Spray and Inhalation Solution, Suspension, and Spray Drug Products - Chemistry, Manufacturing, and Controls Documentation.

111. Kleinbaum DG, Kupper LL, Nizam A, Muller KE. 2008. Two-way ANOVA with Equal Cell Numbers. In Anonymous Applied Regression Analysis and Other Multivariate Methods: Fourth Edition, Belmont, CA, USA: Thomson: Brook/Cole. p 513-541.

112. Anderson CA, Drennen III JK, Ciurczak EW. 2008. Pharmaceutical Applications of Near-Infrared Spectroscopy. In Burns DA, Ciurczak EW, editors. Handbook of Near-Infrared Analysis, Third Edition ed., New York, NY: CRC Press: Taylor & Francis Group. p 585-611.

113. Cogdill RP, Anderson CA, Delgado-Lopez M, Chisholm R, Bolton R, Herkert T, Afnan AM, Drennen III JK 2005. Process Analytical Technology Case Study: Part II. Development and Validation of Quantitative Near-Infrared Calibrations in Support of a Process Analytical Technology Application for Real-Time Release. AAPS PharmSciTech 6:E273-E283.

114. Joreskog KG, Wold H. 1983. Systems Under Indirect Observations, Causality/Structure/Prediction, Vols. I and II ed., Amsterdam: North-Holland.

115. Bjorsvik H, Martens H. 2008. Data Analysis: Calibration of NIR Instruments by PLS Regression. In Burns DA, Ciurczak EW, editors. Handbook of Near-Infrared Analysis, Third Edition ed., New York, NY: CRC Press: Taylor & Francis Group. p 189-205.

116. Haaland DM, Melgaard DK 2002. New augmented classical least squares methods for improved quantitative spectral analyses. Vibrational Spectroscopy 29:171-175.

117. Melgaard DK, Haaland DM, Wehlburg CM 2002. Concentration Residual Augmented Classical Least Squares (CRACLS): A Multivariate Calibration Method with Advantages over Partial Least Squares. Applied Spectroscopy 56:615-624.

118. Wehlburg CM, Haaland DM, Melgaard DK, Martin LE 2002. New Hybrid Algorithm for Maintaining Multivariate Quantitative Calibrations of a Near-Infrared Spectrometer. Applied Spectroscopy 56:605-614.

119. Wehlburg CM, Haaland DM, Melgaard DK 2002. New Hybrid Algorithm for Transferring Multivariate Quantitative Calibrations of Intra-vendor Near-Infrared Spectrometers. Applied Spectroscopy 56:877-886.

120. Wu W, Walczak B, Massart DL, Heuerding S, Erin F, Last IR, Prebble KA 1996. Artificial neural networks in classification of NIR spectral data: Design of the training set. Chemometrics and Intelligent Laboratory Systems 33:35-46.

121. Dou Y, Sun Y, Ren Y, Ren Y 2005. Artificial neural network for simultaneous determination of two components of compound paracetamol and diphenhydramine hydrochloride powder on NIR spectroscopy. Analytica Chimica Acta 528:55-61.

122. Kovalenko IV, Rippke GR, Hurburgh Jr. CR 2006. Measurement of Soybean Fatty Acids by Near-Infrared Spectroscopy: Linear and Nonlinear Calibration Methods. Journal of American Oil Chemist's Society 83:421-427.

123. Igne B, Rippke GR, Hurburgh Jr. CR 2008. Measurement of Whole Soybean Fatty Acids by Near Infrared Spectroscopy. American Oil Chemist's Society 85:1105-1113.

124. Borggaard C. 2001. Neural Networks in Near-Infrared Spectroscopy. In Williams P, Norris K, editors. Near-Infrared Technology in Agricultural and Food Industries, 2nd ed., St. Paul, Minnesota: AACC.

125. Vapnik V. 1995. The Nature of Statistical Learning Theory, New York, NY: Springer-Verlag New York, Inc.

126. Cogdill RP, Dardenne P 2004. Least-squares support vector machines for chemometrics: an introduction and evaluation. Journal of Near Infrared Spectroscopy 12:93-100.

127. Shawe-Taylor J, Cristianini N. 2000. Support Vector Machines and other kernel-based learning methods, UK: Cambridge University Press.

128. Suykens JAK, Van Gestel T, De Brabanter J, De Moor B, Vandewalle J. 2002. Least Squares Support Vector Machines, Singapore: World Scientific.

129. Zacour BM, Drennen III JK, Anderson CA. 2012. Hybrid Controls Combining First Principle Calculations with Empirical Modeling for Fully Automated Fluid Bed Processing. Journal of Pharmaceutical Innovation. In Review.

130. Zacour BM, Drennen III JK, Anderson CA. 2012. Development of a Statistical Tolerance Based Fluid Bed Drying Design Space. Journal of Pharmaceutical Innovation. In Review.

131. Zacour BM, Drennen III JK, Anderson CA. 2012. Efficient Scale-Up of a Fluid Bed Drying Laboratory Scale Design Space. Journal of Pharmaceutical Innovation. In Review.

132. Zacour BM, Drennen III JK, Anderson CA. 2012. Development of a Fluid Bed Granulation Design Space Using CQA Weighted Tolerance Intervals. Journal of Pharmaceutical Sciences. In Review.

133. Zacour BM, Igne B, Drennen III JK, Anderson CA. 2011. Efficient Near Infrared Spectroscopic Calibration Methods for Pharmaceutical Blend Monitoring. Journal of Pharmaceutical Innovation 6:10-23.